BNL--38869

DE87 003215

OPTIMIZED GROUND COUPLED HEAT PUMP DESIGN
PHASE I FINAL REPORT

J.W. Andrews, M. Catan, P. Le Doux, P.D. Metz, J.H. Saunders

Prepared for the
OFFICE OF BUILDINGS AND COMMUNITY SYSTEMS
U.S. DEPARTMENT OF ENERGY

DEPARTMENT OF APPLIED SCIENCE

BROOKHAVEN NATIONAL LABORATORY
UPTON, LONG ISLAND, NEW YORK 11973

BNL 38869
INFORMAL REPORT

OPTIMIZED GROUND COUPLED HEAT PUMP DESIGN
PHASE I FINAL REPORT

J.W. Andrews, M. Catan, P. Le Doux, P.D. Metz, J.H. Saunders

October 1985

Prepared for the
OFFICE OF BUILDINGS AND COMMUNITY SYSTEMS
U.S. DEPARTMENT OF ENERGY

DISCLAIMER

This report was prepared as an account of work sponsored by an agency of the United States Government. Neither the United States Government nor any agency thereof, nor any of their employees, makes any warranty, express or implied, or assumes any legal liability or responsibility for the accuracy, completeness, or usefulness of any information, apparatus, product, or process disclosed, or represents that its use would not infringe privately owned rights. Reference herein to any specific commercial product, process, or service by trade name, trademark, manufacturer, or otherwise does not necessarily constitute or imply its endorsement, recommendation, or favoring by the United States Government or any agency thereof. The views and opinions of authors expressed herein do not necessarily state or reflect those of the United States Government or any agency thereof.

SOLAR AND THERMAL SYSTEMS DIVISION
DEPARTMENT OF APPLIED SCIENCE
BROOKHAVEN NATIONAL LABORATORY
ASSOCIATED UNIVERSITIES, INC.

Under Contract No. DE-AC02-76CH00016 with the
U.S. Department of Energy

DISTRIBUTION OF THIS DOCUMENT IS

ABSTRACT

This report describes the first phase of a project to design a water-to-air heat pump optimized for ground coupling applications. The project is being conducted jointly by Brookhaven National Laboratory (BNL), Oak Ridge National Laboratory (ORNL), and an industrial partner to be selected via a competitive procurement. In the completion of Phase I, three major tasks were completed. First, based on experimental work performed at BNL, water-refrigerant heat exchanger models were developed for incorporation into the ORNL heat pump optimization program. Next a procedure was developed to generate correlations between heat pump entering fluid temperature and load. The correlations, called "Source Temperature/Load Maps", will tell the optimization program how many hours/season the heat pump will operate with any pair of values for these quantities. This report discusses these first two tasks within Phase I.

ACKNOWLEDGMENTS

The authors thank Oak Ridge National Laboratory, particularly Phil Fairchild and Van Baxter, for assistance and support. One of us (M.C.) thanks Tom Irvine for assistance in heat exchanger model development.

CONTENTS

1. INTRODUCTION 1
   1.1 Project Overview 1
   1.2 Phase I Overview 3
      1.2.1 Task 1 3
      1.2.2 Task 2 3
      1.2.3 Task 3 4
   1.3 Format of This Report 4
   References 5
2. BACKGROUND 6
   References 8
3. TASK 1. WATER-REFRIGERANT HEAT EXCHANGER MODEL 9
   3.1 Introduction 9
   3.2 Role of the Water-Refrigerant Heat Exchanger Model 9
   3.3 How the Models Work 12
   3.4 Heat Exchangers Modeled 12
   3.5 Selection of Correlations 13
      3.5.1 Heat Transfer Correlations 13
      3.5.1.1 Evaporation 14
      3.5.1.2 Condensation 15
   3.6 Heat Exchanger Model Design 18
      3.6.1 Shell-and-Tube Model 18
      3.6.2 Tube-in-Tube Model 19
   3.7 Experimentation 22
      3.7.1 BNL Heat Pump Test Facility 22
      3.7.2 Test Procedure 25
      3.7.2.1 Evaporating and condensing mode tests 25
      3.7.2.2 Single phase tests 27
      3.7.3 Data Acquisition and Verification 27
   3.8 Model Validation 28
      3.8.1 Validation Approach 28
      3.8.2 Validation Results 30
   References 38
4. TASK 2. SOURCE TEMPERATURE/LOAD MAP DEVELOPMENT 39
   4.1 Overview and Methodology 39
      4.1.1 Role of the Source Temperature/Load Map 39
      4.1.2 Approach 39
      4.1.3 Task Methodology 41
   4.2 How GROCS-TRNSYS Works 46
      4.2.1 Description of GROCS-TRNSYS 46
      4.2.2 TRNSYS Description 46
      4.2.3 Design of GROCS 47
      4.2.4 Integration of GROCS with TRNSYS 48
      4.2.5 Isolated Pipe Model 49
   4.3 GROCS-TRNSYS Program Validation 52
      4.3.1 Validation Procedure 52
      4.3.2 Constant Heat Output Results 53
      4.3.2.1 Analytical calculations 54

CONTENTS (cont.)

4.3.2.2 GROCS-TRNSYS model..... 57
4.3.2.3 Comparison of GROCS-TRNSYS vs. analytical results..... 60
4.3.3 Behavior of GROCS-TRNSYS Under Intermittent Operation... 60
4.3.3.1 Where does the earth temperature vary?..... 60
4.3.3.2 The R-C model..... 63
4.3.3.3 Evaluation of the final GROCS-TRNSYS program under intermittent operation..... 68
4.4 Selection of Sample Test Conditions..... 73
4.4.1 Weather and Load Data..... 73
4.4.2 Heat Pump Performance Data..... 73
4.4.3 Ground Heat Exchanger Configuration and Sizing..... 74
4.5 Generation of Sample Source Temperature/Load Maps..... 74
References..... 80
5. CONCLUSION..... 81
5.1 Task 1. Water-Refrigerant Heat Exchanger Model Development..... 81
5.2 Task 2. Source Temperature/Load Map Development..... 81
APPENDIX A: CYLINDRICAL HEAT EXCHANGER SOLUTION..... 82
A.1 Steady Heat Output..... 82
A.2 Pulsed Heat Output..... 83
References..... 87
APPENDIX B: MATHEMATICAL DEVELOPMENT OF R-C HEAT FLOW MODEL..... 88

TABLES

3.1 Best-Fit Correlation Constants..... 30
3.2 Standard Deviations of Correlations..... 30
3.3 Heat Transfer Coefficients Obtained from Wilson Plots..... 36
4.1 Vertical Heat Exchanger Properties..... 54
4.2 GROCS-TRNSYS Models Block Radii..... 59
4.3 Temperature Ratios θ_I/θ_c..... 68
4.4 Comparison of Source Temperatures for Different COP's..... 74
4.5 Heat Pump Performance Values Used in GROCS-TRNSYS Runs..... 75
4.6 Heating Season Source Temperature Load Map (6 pipes)..... 77
4.7 Heating Season Source Temperature Load Map (7 pipes)..... 78
4.8 Heating Season Source Temperature Load Map (8 pipes)..... 79

FIGURES

3.1 Simplified flow diagram of ORNL heat pump model..... 10
3.2 Purpose of water-refrigerant heat exchanger model subroutine..... 11
3.3 Shell-and-tube heat exchanger model flow chart..... 20
3.4 Tube-in-tube heat exchanger model flow chart..... 21

FIGURES (cont.)

3.5 Heat pump simulator configured for evaporator tests..... 23
3.6 Subcomponent test stand..... 24
3.7 Data acquisition reduction/control system..... 26
3.8 Procedure for fitting evaporator model to experimental data..... 29
3.9 Comparison of model-predicted vs experimental inlet pressure for shell-and-tube heat exchanger..... 31
3.10 Comparison of model-predicted vs experimental inlet pressure for Turbotec heat exchanger..... 32
3.11 Comparison of model-predicted vs experimental inlet pressure for Noranda heat exchanger..... 33
3.12 Comparison of model-predicted vs experimental pressure drop for Turbotec heat exchanger..... 34
3.13 Comparison of model-predicted vs experimental pressure drop for Noranda heat exchanger..... 35
3.14 Sample Wilson plot: heat transfer (U) as a function of mass flow ($\dot{m}$)..... 37
4.1 Ground coupled heat pump optimization flow chart..... 40
4.2a Source temperature/load map development flow chart..... 42
4.2b Source temperature/load map development flow chart..... 43
4.2c Source temperature/load map development flow chart..... 44
4.3 Schematic of isolated buried pipe model..... 50
4.4 Pipe fluid temperature minus far field temperature (ΔT), steady heat output of 50 Btu/ft-hr: computed and exact solutions..... 56
4.5 Ground temperature minus far field temperature vs. radial distance for t = 10, 100, 1000 hrs, with a steady heat output of 50 Btu/ft-hr..... 58
4.6 Pipe fluid temperature minus far field temperature vs. time, steady heat output = 50 Btu/hr-ft; 12 block model and exact solution..... 61
4.7 Pipe fluid temperature minus far field temperature vs. time various GROCS element interaction assumptions, steady heat output of 50 Btu/hr-ft, 12 element model..... 62
4.8 Heat output rates for pulsed and steady operation with equal average heat outputs..... 64
4.9 Pipe temperature minus far field temperature vs. time; pulsed compared to steady heat removal for 50 Btu/hr-ft average heat ouput..... 65
4.10 Simplified ground coupling model..... 67
4.11 Comparison of exact solution to GROCS-TRNSYS computation (0.25 hour cycle for 20 and 50% on time)..... 70
4.12 Comparison of exact solution to GROCS-TRNSYS computation (0.5 hour cycle for 20 and 50% on time)..... 71
4.13 Comparison of exact solution to GROCS-TRNSYS computation (1.0 hour cycle for 20 and 50% on time)..... 72
4.14 Cross-section diagram of GROCS-TRNSYS vertical heat exchange model..... 76
A.1 Pulsed heat output can be represented as a sum of steady heat outputs..... 84

1. INTRODUCTION

This report describes the first phase of a project to design a water-to-air heat pump optimized for ground coupling applications. The project is being conducted jointly by Brookhaven National Laboratory (BNL), Oak Ridge National Laboratory (ORNL), and an industrial partner to be selected via a competitive procurement will also participate.

1.1 Project Overview

The goal of this project is to design an optimized ground coupled heat pump to provide space heating, cooling, and domestic hot water for given load, climate and soil conditions. The project is divided into two phases and seven tasks as follows.

Phase I. Analysis Tools Development

TASK 1. Develop water-refrigerant heat exchanger model and integrate into ORNL heat pump optimization program.

The ORNL heat pump optimization program has been selected for use in this project because it appears to be the most comprehensive nonproprietary program of this type. However, the program as written models air-to-air heat pumps only. This task's objective is to adapt the program to water-to-air heat pumps by writing water-refrigerant heat exchanger models, validating them, and incorporating them into the ORNL program.

TASK 2. Develop parametric correlations for ground coil outlet temperature as a function of flow rate, coil geometry, cycling history, location, soil type, and time of year.

In lieu of entering outdoor air temperature, the heat pump optimization model will require entering water temperature from the ground coil. Obtaining such temperatures from an hour-by-hour simulation program may be prohibitive in terms of computer time, since it would require the use of two large iterative computer programs operating simultaneously. It is therefore necessary to obtain, on the basis of existing data and experience, a parameterization of ground coil fluid temperature as a function of a small number of variables.

TASK 3. Select candidate subcomponents (compressors, heat exchangers, expansion devices) for possible use in the optimized heat pump.

It is anticipated the optimized heat pump will be constructed from off-the-shelf components, with no new compressor or heat exchanger development required. It is therefore necessary to know the capabilities and limitations of available hardware, to serve as input to the heat pump performance optimization of Task 4 and the cost/performance tradeoffs of Task 5. These in turn will lead to the final design effort of Task 7.

Phase II. Heat Pump Optimization

TASK 4. Perform heat pump performance optimization and sensitivity studies.

The program software as modified in the previous tasks will be used to explore options for improving ground-coupled heat pump seasonal performance. Both horizontal and vertical heat exchangers will be considered in at least three climates. Sensitivity studies of major component parameters will be performed to serve as input to the cost/performance tradeoffs of Task 5. The major responsibility for this Task will be carried by Oak Ridge National Laboratory. Brookhaven personnel will play a support role in interfacing this Task with preceding Tasks and will maintain a capability for point calibration runs of the ORNL heat pump optimization program.

TASK 5. Develop cost/performance tradeoffs.

The selection of a subcomponent having the optimal thermal performance may not represent the economic optimum if it costs significantly more than an alternative that performs slightly less well. This task will use the sensitivity studies of Task 4 together with cost data obtained as part of Task 3 to rank subcomponents in terms of relative economic advantage.

TASK 6. Validate performance predictions via laboratory testing of "breadboard" models correlated with computer modeling.

It is anticipated that the computer modeling effort will indicate design choices having the potential to improve performance significantly. These will be tested via "breadboard" model heat pumps on the BNL hardware simulator. An additional objective of this work will be to maximize the capability of the heat pump with respect to domestic hot water production. This task will seek to establish means for achieving this goal.

TASK 7. Select subcomponents and complete final design.

On the basis of the results of the preceding tasks, a design team comprising members from ORNL, BNL, and an industry subcontractor will perform the final design of the optimized, reversible, water-to-air heat pump for ground coupling applications. The cost/performance goal shall be compatibility with a maximum installed system cost of $7000 (including ground coil) for a 2-1/2 ton heat pump providing a heating seasonal performance factor of 3.0 in New York. The industry subcontractor shall possess significant experience both in ground coupled systems design and installation and in heat pump manufacture. The industry subcontractor shall be selected by BNL with approval by ORNL.

1.2 Phase I Overview

As is evident from the task descriptions above, Phase I encompasses three quite different tasks. What ties these tasks together is that each provides an essential element required for the heat pump optimization called for in Phase II.

The air-source heat pump optimization work carried out by Oak Ridge National Laboratory demonstrated the utility of the ORNL Heat Pump Model[1] in designing optimized air-source heat pumps. The goal of this project--design of an optimized water-to-air heat pump for ground coupling applications--required three major developments before the ORNL Heat Pump Model could be applied.

1.2.1 Task 1

First, because the ORNL Heat Pump Model was originally developed for air-source heat pumps, it was necessary to develop and incorporate a water-refrigerant heat exchanger model into the ORNL program in order to model water-source heat pumps. Based on experimental work performed at the BNL heat pump hardware simulator, shell-and-tube and coaxial tube-in-tube water-refrigerant heat exchanger models have been developed and validated. Work is now underway to incorporate these into the ORNL Heat Pump Model.

1.2.2 Task 2

For air-source heat pumps, ambient conditions, particularly air temperature, determine both the building space conditioning load and the heat pump entering air temperature. For ground coupled heat pumps, the load is still

determined by ambient conditions, but the heat pump source temperature now depends in a complicated way on the ground temperature, ground heat exchanger, system history, and other factors. Thus, to optimize ground coupled heat pumps, it is necessary to develop correlations between heat pump entering water temperature and load as a function of location, soil properties, and ground heat exchanger design.

Task 2 concerns the development of a procedure to generate these correlations. The correlations developed, called "Source Temperature/Load Maps," tell the optimization program how many hours/season the heat pump will operate with any given pair of values for load and source temperature, for any selected combination of climate, soil properties, and ground heat exchanger design. Sample source temperature/load maps are presented in this report. The maps used for heat pump optimization will be developed in cooperation with ORNL for three climates as part of Task 4.

1.2.3 Task 3

The last major input required to optimize water-source heat pumps is the selection of suitable heat pump subcomponents. The performance of these subcomponents is needed to perform the heat pump optimization studies called for in Task 4. The subcomponent costs and performance characteristics are required for the development of cost/performance tradeoffs in Task 5.

1.3 Format of this Report

In Section 2, the definition and history of ground coupling are briefly described. Section 3 presents the water-refrigerant heat exchanger experimental and model development results obtained in Task 1. Section 4 describes the procedure developed under Task 2 to generate the earth coil outlet temperature parametric correlations--the source temperature/load maps--required by the optimization program. Section 5 is a brief summary and conclusion.

Section 1. References

1. C.K. Rice, S.K. Fischer, W.L. Jackson, R.D. Ellison, Design Optimization and the Limits of Steady-State Heating Efficiency for Conventional Single-Speed Air-Source Heat Pumps, ORNL/CON-63, October 1981.

2. BACKGROUND

Ground coupling refers to the use of the ground as a source of heat to the evaporator of a heat pump used in building heating applications. In addition, the ground can be used as a heat sink for space cooling, and in certain applications it has been used as a storage element as well. Ground coupling stands in contrast to the more widely used heat pump technology which employs ambient air as a thermal source and sink.

A fair amount of research was done on ground-coupled heat pumps in the late 1940s and early 1950s[1-7]. Although this work indicated that ground-coupled heat pumps could operate satisfactorily, it is nevertheless evident that ground coupling did not enter the mainstream of American heating, ventilating and air-conditioning (HVAC) engineering practice. There are a number of reasons for this, including low energy prices, unavailability of suitable plastic pipe for use in ground-coupling heat exchangers, and perhaps most important, a conscious decision on the part of industry to emphasize air-source heat pumps. Nevertheless, virtually all of the modern approaches to ground coupling had been thought of in this earlier period. Some of these are:

1. A simple well from which water is pumped, heat is extracted from the water (or rejected to the water) and the water is recycled to the ground or discharged (open loop system).

2. A closed system in which a U-tube is sunk into a vertical well and a heat transfer fluid pumped through the tube to pick up heat from the earth.

3. A modified U-tube system in which the entire well casing is utilized as part of the enclosed system for heat-transfer fluid.

4. A horizontal grid of buried pipe through which a heat transfer fluid is circulated.

5. A horizontal grid of buried pipe which forms part of the refrigerant circuit of the heat pump itself (direct-expansion).

6. A large buried storage tank constructed from large-diameter drain culvert pipe.

7. A coil of pipe surrounding the footings of the house foundation.

8. A series of shallow vertical holes, 15 to 20 feet deep, in which heat exchange coils are inserted.

After a hiatus of about 20 years, interest in ground-coupled heat pumps was revived in the 1970s as a result of the large increases in energy prices. Several projects were sponsored by the U.S. Department of Energy (DOE). In Europe, particularly in Sweden, ground coupling was commercialized in residential applications using heating-only water-to-water heat pumps. In the United States, available water-to-air heat pumps with reversing valves were generally utilized to permit both heating and cooling via a forced-air distribution system. These heat pumps are generally intended for use with source temperatures higher than those commonly found in closed-loop ground-coupling applications. Manufacturers' data are generally given for source temperature ranges of 40 to 80°F, while the source water temperatures commonly obtained in closed-loop ground-coupled systems fall in the 20 to 50°F range during most of the heating seasons of the northern and central United States. Experimental system performance data showed efficiencies significantly lower than what would have been expected on the basis of a simple extrapolation of manufacturers' data into the lower temperatures. For example, a test house in New York achieved a seasonal performance factor or SPF* of 2.5[8], whereas a value in excess of 3.0 is believed possible. For comparison, air-to-air heat pumps currently on the market delivered SPF's well below 2.0 in similar climates, if the necessary electric resistance supplemental heat is taken into account. The ground coupled heat pump considered in this example required no electric resistance supplemental heat, a fact which would favorably affect electric utility load factors were such systems to become widespread.

In the light of experience such as described above, the need was seen for a water-to-air heat pump, compatible with the U.S. market, which would be specifically tailored to the ground coupling application. The seasonal performance factor for heating should be 3.0 or better in northern U.S. climates, and the cooling mode performance should exceed that of top-of-the-line conventional heat pumps. In addition, a capability of the heat pump to produce hot water on demand at all times of the year would be a desirable attribute of the optimized heat pump.

---

*SPF = heat delivered to the house divided by electrical energy required to operate the heat pump compressor, source water pump, and duct blower.

Section 2. References

1. G.S. Smith, Factors Useful in Ground Grid Design for Heat Pumps, Transactions of Am. Soc. of Heating and Ventilating Engineers (ASHVE), Vol. 57, 1951, p. 189.
2. E.N. Kemler, Methods of Earth Heat Recovery for the Heat Pump, Heating and Ventilating, Sept. 1947, pp. 69-72.
3. B.F. Rober, C.F. Booster, and F.W. Hutchinson, The Heat Pump - How to Analyze Earth as a Heat Source, Heating, Piping and Air Conditioning, March 1948, p. 83.
4. L.R. Ingersoll, F.T. Adler, H.J. Plass, and A.C. Ingersoll, Theory of Earth Heat Exchangers for the Heat Pump, Transactions of the Am. Soc. of Heating and Ventilating Engineers (ASHVE), Vol. 57, 1951, p. 167.
5. G.S. Smith, Intermittent Ground Grids for Heat Pumps, Transactions of Am. Soc. of Heating and Ventilating Engineers (ASHVE), Vol. 63, 1956, pp. 473-488.
6. M. Baker, Design and Performance of a Residential Earth Heat Pump, Transactions of Am. Soc. of Heating and Ventilating Engineers (ASHVE), Vol. 59, 1953, pp. 371-394.
7. D.M. Vestal, Jr., and B.J. Fluker, Earth as a Heat Source and Sink for Heat Pumps, Transactions of Am. Soc. of Heating and Ventilating Engineers (ASHVE), Vol. 63, 1957, pp. 41-68.
8. P.D. Metz, Ground Coupled Heat Pump System Experimental Results, Pres. at ASME 1983 Ann. Mtg., Washington, DC, June 1983; BNL 33540.

3. Task 1. Water-Refrigerant Heat Exchanger Model

3.1. Introduction

The goal of Task 1 is to develop experimentally validated water-refrigerant heat exchanger models for incorporation into the ORNL Heat Pump Model. These will replace the existing air-refrigerant heat exchanger models, permitting the optimization of water-source heat pumps.

Models have been developed for two types of water-refrigerant heat exchangers: shell-and-tube heat exchangers with a baffled shell side, and coaxial tube-in-tube heat exchangers. In contrast to the situation for air-refrigerant heat exchangers, each of the water-refrigerant heat exchangers has features which necessitate special consideration in modeling their performance. For example, most of the compact water-refrigerant heat exchangers used in water source heat pumps employ heat transfer augmentation via extended surfaces, turbulence promoters, surface roughness, or any combination of these--conditions for which there is little published data.

Therefore, in order to develop the desired water-refrigerant heat exchanger models, heat exchanger tests were conducted on the BNL heat pump hardware simulator to provide the data upon which the models are based. The models were then developed by empirically fitting published heat transfer and pressure drop correlations--the heart of the models--to this data.

This section first briefly describes the role of the heat exchanger models in the ORNL Heat Pump Model and how they work. Then, the heat exchangers modeled, the correlations used, and the heat exchanger models developed are described. Finally the experimental methods employed and the model validation results obtained are presented.

3.2 Role of the Water-Refrigerant Heat Exchanger Model

Figure 3.1 is a highly simplified flow diagram of the ORNL Heat Pump Model (see e.g. discussion in references 1 and 2). As indicated by the arrows in the figure, the outputs from one component, say the pressure, temperature and mass flow of refrigerant leaving the compressor, serve as inputs to the next component, in this case the condenser. In order to model heat pump performance, the program driver goes from one component model subroutine to the next, adjusting outputs and inputs until self-consistency is achieved.

The job of the water-refrigerant heat exchanger model, as illustrated in Figure 3.2, is to take given input conditions and to compute the resulting

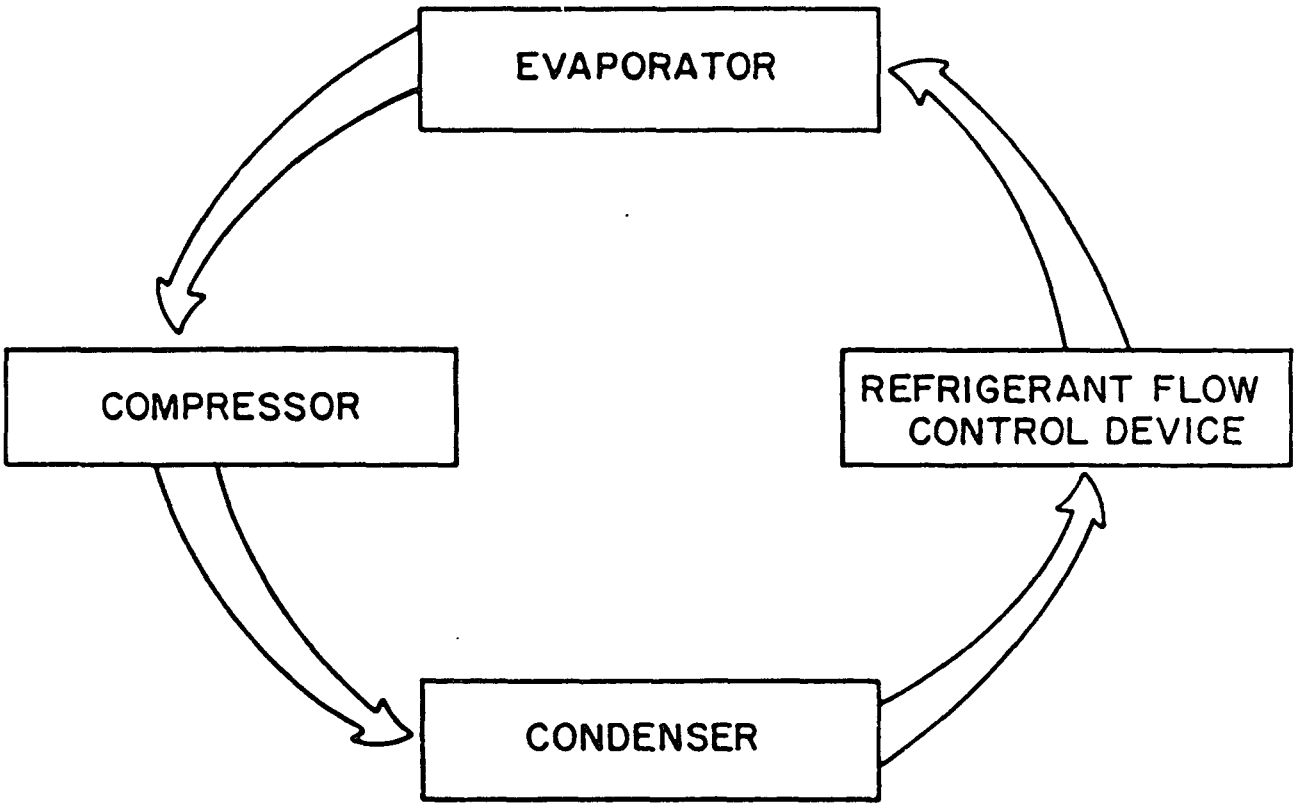

Figure 3.1 Simplified flow diagram of ORNL heat pump model.

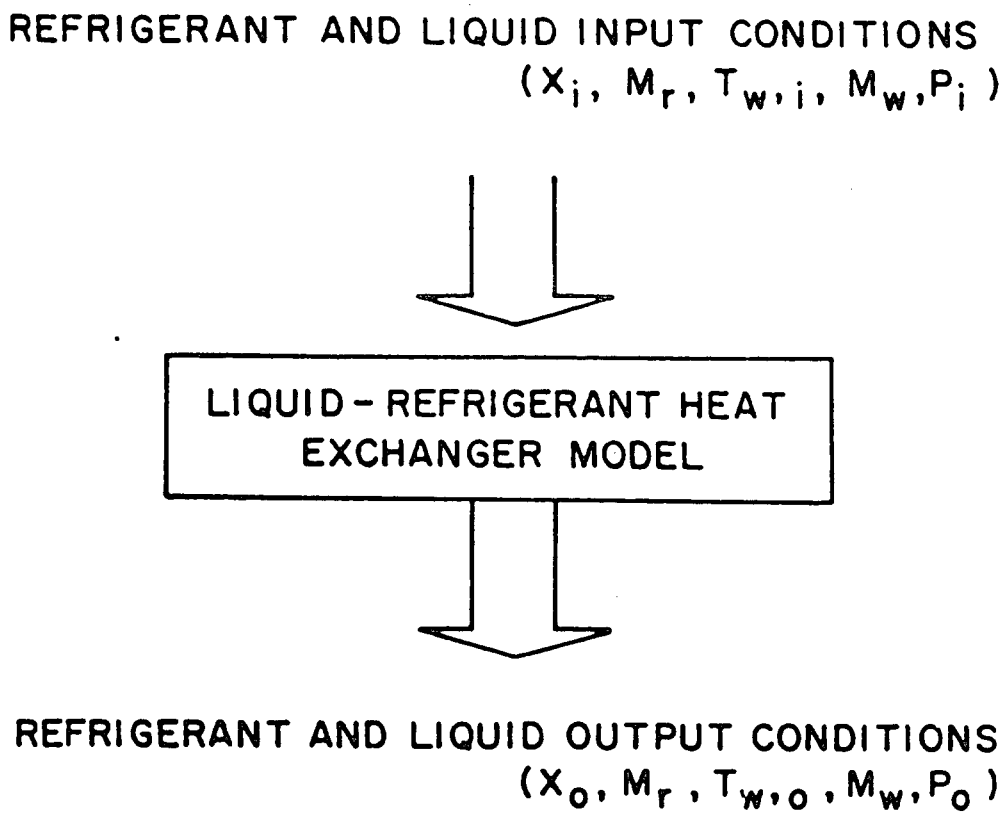

Figure 3.2 Purpose of water-refrigerant heat exchanger model subroutine.

output conditions. The conditions of interest are the refrigerant quality (x) (the ratio of vapor to total refrigerant mass), the refrigerant mass flow rate (M_r), the water temperature (T_w), the water mass flow rate (M_w), and the refrigerant pressure (P). The subscripts "i" and "o" in Figure 3.2 refer to inlet and outlet conditions.

3.3 How the Models Work

Of the input/output quantities indicated in Figure 3.2, the mass flow rates are conserved, leaving only the changes in refrigerant pressure, refrigerant enthalpy, and water temperature to be calculated by the model (refrigerant temperature has been supressed). The model computes the changes in these remaining variables via heat transfer and pressure drop correlations. The forms of these correlations were obtained from the literature, but it was necessary to fit free parameters in them to data obtained at BNL in order to model the heat exchangers of interest. Also, since the two phase heat transfer correlations apply to restricted ranges of refrigerant quality, the model must sometimes use several pairs of correlations to model one heat exchanger.

3.4 Heat Exchangers Modeled

Two shell-and-tube units have been modeled and tested. Each has a baffled shell side through which the water flows and refrigerant is conveyed on the tube side. Both heat exchangers are identical except for length.

Four coaxial tube-in-tube heat exchangers have been modeled and tested. Two were manufactured by Turbotec Products Incorporated, and two by Noranda Metals Industries Incorporated. The Turbotec units differ in length and diameter, while the Noranda units differ only in length.

The two coaxial types employ very different means of heat transfer augmentation. The Noranda heat exchanger has a roughened outer surface on the inner tube and low profile helical fins on the inside surface. The Turbotec units have helical convolutions on the inner tube which affect the flow of both the water in the tube and the refrigerant in the annulus. The Turbotec and Noranda heat exchangers were chosen because, in contrast with most other

coaxial heat exchangers in their price range, they exhibit excellent evaporating performance, and acceptably low pressure drop[3,4]. Unfortunately, the heat transfer augmentation which makes these units so desirable also makes them difficult to model, as discussed below.

3.5 Selection of Correlations

The air-refrigerant heat exchanger model subroutines used in the ORNL Heat Pump Model program guided the present effort. However, the nature of the water-refrigerant heat exchangers used, necessitated major changes in the calculation methods employed. The four main differences are:

1. augmented heat transfer surfaces
2. counter and cocurrent flow rather than cross flow
3. high refrigerant-side pressure drops
4. refrigerant heat transfer coefficient comparable to water-side heat transfer coefficient

Because appropriate correlations were not available--even from the manufacturers involved--correlations for the local heat transfer coefficients for these new surfaces had to be developed.

A literature search was conducted to identify relevant correlations and experimental data. The information available on two phase and single phase heat transfer and pressure drop for the augmented tubes was scarce, and judged insufficient to develop the required models.[5] Because of the complexity of diabatic water-gas flow systems and the variety of heat transfer augmentation methods available, few researchers have attempted to develop correlations for the numerous channel geometries encountered. Nevertheless, it was found that a number of experimenters had successfully adapted existing smooth tube correlations to fit their augmented surface experimental data over broad ranges of experimental conditions.[6-9] This approach was adopted for this project. Section 3.5 presents the correlations used, while section 3.6 describes their integration into the heat exchanger models developed.

3.5.1 Heat Transfer Correlations

The heat transfer correlations in the published literature have many forms. Some are based upon analytically derived formulas, while others are almost entirely empirical. Our approach has been to use, where possible, heat transfer correlations with an analytical foundation which have also been used successfully to model real heat exchangers. Free parameters were retained to

fit the effects of heat transfer augmentation. The correlations used are now discussed separately for evaporation and condensation.

3.5.1.1 Evaporation. As in the existing air refrigerant heat exchanger subroutine in the ORNL Heat Pump Model, the evaporation process is divided into three regions on the basis of the local vapor quality for all heat exchangers modeled. A different heat transfer correlation is used within each region because the mechanisms of heat transfer are quite different. The first two regions are regarded as two phase flow with wet and dry walls respectively. The transition is considered to occur at a vapor quality of 0.65. The third region is simply single phase vapor flow. This characterization follows that of many authors in the field of heat transfer.[10-12]

Most of the relevant heat transfer correlations for two phase flow relate the evaporating heat transfer coefficient to fluid properties (which in turn are related to pressure and temperature), vapor quality, and local heat flux. The single phase correlations are simpler, more accurate, and more widely applicable. For saturation conditions, which are assumed to exist in the two phase regions of the evaporator, the temperature and the pressure are coupled and do not vary independently. Thus, there are four independent variables on which the two phase evaporating heat transfer coefficient depends: pressure (or temperature), vapor quality, mass flux, and heat flux.

Heat flux is not considered in many correlations used for heat exchangers of the type being considered here for the following reason. In the first flow region the heat flux is a relatively sensitive variable only in heat exchangers where bubble nucleation has a significant effect on heat transfer. In the heat exchangers modeled here, bubble nucleation is considered to be suppressed due to the efficiency of convection and evaporation. This limits the achievable wall superheats, and thus prevents nucleation from occuring, resulting in forced convection evaporation as opposed to boiling.

In the first region, the forms of the correlations available vary. The correlation selected for all heat exchangers modeled--and the correlation used in the air-refrigerant model--is

$$h_{TP} = h_L \, a\left[\frac{1}{X_{tt}}\right]^b \tag{3.1}$$

where h_{TP} is the two phase heat transfer coefficient, h_L is the heat transfer coefficient if all of the mass were flowing as water, and a and b

are constants. In some correlations a multiplier or an additional term is included which is a function of one or more other variables including heat flux and vapor quality.[13] In Eq. (3.1) X_{tt}, the Lockhart-Martinelli parameter, is given by

$$X_{tt} = \left[\frac{1-x}{x}\right]^{0.9} \left[\frac{\rho_v}{\rho_l}\right]^{0.5} \left[\frac{\mu_l}{\mu_v}\right] \tag{3.2}$$

where ρ is density, μ is viscosity, x is the local vapor quality, and the subscripts v and l refer to vapor and water phases respectively.

For the second flow region, a number of correlations are available, but they are more limited than those applicable to the first flow region. Thus, for the dry out region (as in the existing air-refrigerant evaporator subroutine), the heat transfer coefficient is given by a quadratic interpolation between the heat transfer coefficient at transition (x=0.65) and the single phase vapor heat transfer coefficient (x=1.0). The heat transfer coefficient in the single phase region is well-known and discussed below.

3.5.1.2 Condensation. The condensing process is divided into four regions:

1. Superheated vapor
2. Incipient condensation region with superheated bulk fluid temperatures prevailing
3. Condensation with saturated bulk fluid temperatures prevailing
4. Subcooled water

The first and second regions are treated as single phase vapor flow and the average heat transfer coefficient calculated for the third region adjusted to account for the condensation that occurs in the second region. Many of the heat transfer correlations applicable to the third region employ the Lockhart Martinelli parameter. The one used in the existing air-refrigerant heat exchanger model is a complicated function with two step function terms which depend on quality and Reynolds number as well as fluid properties. There are a number of others that have been fitted to a wide variety of data, and which can be adjusted to fit the data from our coaxial heat exchanger tests. The correlation chosen, which has shown very general applicability, is that of Shah[14].

$$h_{TP} = h_L \left[(1-x)^{0.8} + \frac{3.8x^{0.76}(1-x)^{0.04}}{P_r^{0.38}}\right] \tag{3.3}$$

where h_L is the heat transfer coefficient for water only, P_r is the reduced pressure, and x is the vapor quality.

The correlations applicable to the subcooled region are, of course, those for single phase flow. There are a number of correlations available for single phase flow in pipes. The two that have been used are the Dittus-Boelter relation and the closely-related Sieder-Tate relation, which accounts for nonisothermal fluid conditions typical of diabatic flow. The Dittus Boelter relation is used here:

$$h = \frac{k}{D} \left(\frac{GD}{\mu}\right)^{.8} \left(\frac{C\mu}{k}\right)^{.4} \tag{3.4}$$

where k is the fluid conductivity, D is the equivalent diameter, μ is the fluid viscosity, C the fluid specific heat, and G the mass flux. The Sieder-Tate relation is the Dittus Boelter relation multiplied by the ratio of the viscosities of the fluid at the wall temperatures to that at the bulk fluid temperature to the power of 0.1.

3.5.2 Pressure Drop Correlation

The most widely used correlation for pressure drop aplicable to single phase turbulent flow is the Darcy-Weisbach relation:

$$\frac{\Delta P}{\Delta z} = \frac{2fG^2}{\rho D} \tag{3.5}$$

where f is the friction factor which depends on Reynolds number and wall roughness, G is the mass flux, ρ is the fluid density, and D is the equivalent diameter. The pressure drop correlations for single phase systems with augmented surfaces generally follow the same basic scheme for flow in round pipes. Data has been fairly well correlated to functions of the same form as Eq. (3.5) with empirical friction factors.[15] This is the approach used here.

In the case of two phase flow with phase change there are two significant components to the pressure drop--the accelerational and frictional components. The accelerational term is easy to compute when the fluid can be considered homogeneous at the beginning and end of the region under consideration. It is simply the theoretical pressure required to resist the acceleration of the fluid due to phase change. The expression is:

$$\Delta P_a = \frac{G^2}{g}(v_o - v_i)$$

where g is the gravitational constant, and v_o and v_i are the specific volumes leaving and entering the section of interest.

Two types of correlations have been used to describe frictional pressure drop in two phase flow. The less sophisticated models assume the two phase flow to be homogeneous. That is, no difference between the velocities of the two phases is assumed to exist. Such relationships are generally less global in their applicability but much simpler to use. The more sophisticated relationships regard the phases of the flow as separated, with some specialized for application only where specific flow patterns exist (eg. slug flow, annular flow, etc.).

For the homogeneous model the following relation has been recommended.[16]

$$\frac{dP}{dz} = \frac{2cFG^2}{\rho_\ell D}\left[1+x\left(\frac{\rho_\ell-\rho_v}{\rho_v}\right)\right]\left[1+x\left(\frac{\mu_\ell-\mu_v}{\mu_v}\right)\right]^{-0.25} \tag{3.7}$$

where F is the single phase friction factor assuming all the fluid flows as water and c is a constant to be determined.

The correlation (3.7) is used for tube-in-tube heat exchangers where the high refrigerant mass flux permits the use of a homogeneous model. For the shell-and-tube heat exchanger where refrigerant velocity is much lower, the separated flow model Friedel correlation is used[17]:

$$\frac{dp}{dz} = \left(\frac{dp}{dz}\right)_{LO} \phi_{LO}^2 \tag{3.8}$$

where

$$\phi_{LO}^2 = E + \frac{3.24\ FH}{Fr^{0.045} We^{0.035}}$$

$$E = (1-x)^2 + x^2 \frac{\rho_L f_G}{\rho_G f_L}$$

$$F = x^{0.78} (1-x)^{0.24}$$

$$H = \left(\frac{\rho_L}{\rho_G}\right)^{0.91} \left(\frac{\mu_G}{\mu_L}\right)^{0.19} \left(1 - \frac{\mu_G}{\mu_L}\right)^{0.7}$$

$$Fr = \frac{G^2}{gD\rho_H^2} \qquad \text{(Froude Number)}$$

$$We = \frac{G^2 D}{\rho_H \sigma} \qquad \text{(Weber Number)}$$

In Eq. (3.8) $(dp/dz)_{LO}$ is the single phase pressure drop assuming all of the mass flows as water, x is the vapor quality, f_G and f_L are the vapor and water friction factors, and σ is surface tension.

3.6 Heat Exchanger Model Design

Two separate models have been developed, one for each of the two basic heat exchanger types: the shell-and-tube type with one tube pass and an arbitrary number of shell passess, and the tube-in-tube type which can be used with tubes of various surface geometries. The tube-in-tube model is used for both the Turbotec and Noranda type surfaces, although the correlations used to calculate heat transfer and pressure drop are different. It is envisioned that the user of the final water/air heat pump model will input a choice of which surface geometry he wishes to model which will cause the model to choose different heat transfer and pressure drop correlations.

3.6.1 Shell-and-Tube Model

The shell-and-tube exchanger is regarded as a number of serially connected cross flow heat exchangers. The number of such cross flow exchangers is the number of inter-baffle spaces in the entire heat exchanger. Given the

heat transfer correlations discussed in section 3.5, the model calculates an average heat transfer coefficient by integrating with respect to quality assuming the ΔT between the water and refrigerant varies linearly with length. An effectiveness for each heat exchanger subsection is then computed. The fraction of the heat exchanger required is calculated from this effectiveness for cross flow as in the ORNL Model. This method is employed separately within each section of the exchanger. The shell side heat transfer coefficient is calculated for cross flow of a fluid over a tube bank and the coefficient degraded to account for the leading rows of tubes. A second degradation factor, found experimentally, accounts for the axial direction component of the flow due to leakage between the tubes and baffles.

Figure 3.3 is a flow chart for the shell-and-tube heat exchanger model. For each inter-baffle space (IBS) an average two-phase heat transfer coefficient is calculated based on the inlet quality for the IBS and an outlet quality guess. The number of transfer units (Ntu) and the effectiveness are then calculated and used to calculate outlet quality. If the outlet quality does not agree with the guess, an improved guess is calculated and iterated. The water temperature leaving the IBS becomes the water temperature entering the next IBS where the procedure is repeated. When the outlet quality reaches 0.65, the heat transfer coefficient is calculated via the dryout region correlation as indicated in section 3.5. When the vapor quality reaches 1.0, the single phase correlation Eq. (3.4) is used. In the single phase region the Ntu and effectiveness are calculated using the relationships for a cross-flow exchanger (refrigerant unmixed and the water mixed).

The accelerational component of the pressure drop correlation is given by the homogeneous fluid expression Eq. (3.6). The frictional component is given by the separated flow model correlation Eq. (3.8).

3.6.2 Tube-in-Tube Model

Figure 3.4 is a flow chart for the tube-in-tube heat exchanger model. The tube-in-tube heat exchanger is divided into a number of segments of equal increment of refrigerant quality. Heat transfer coefficients are calculated for the inlet and outlet qualities of each segment. The refrigerant-fluid temperature difference is assumed to vary linearly with vapor quality in each. Then, the physical length of each segment is determined. The pressure drop is then found using the correlations in section 3.5.

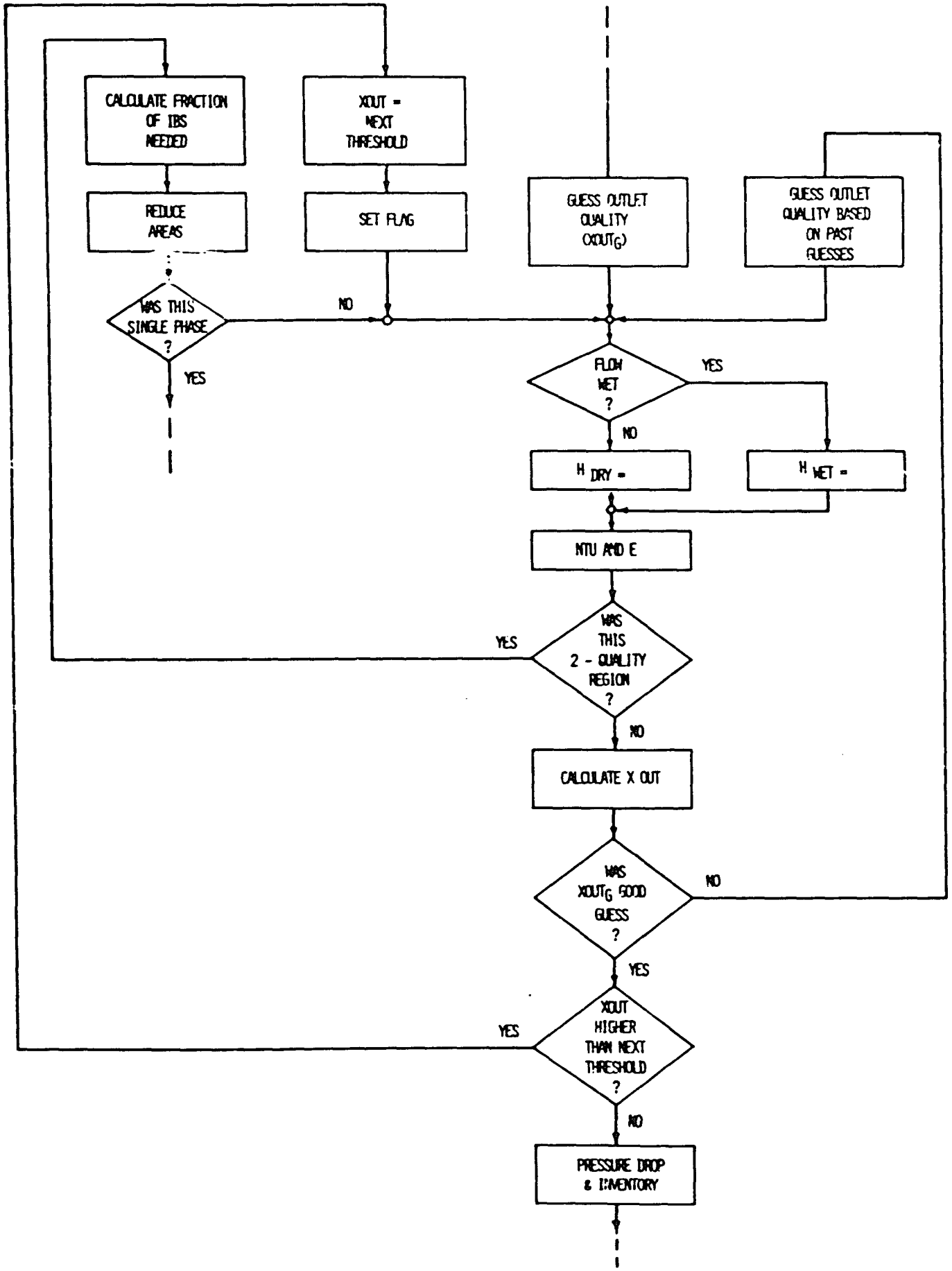

Figure 3.3 Shell-and-tube heat exchanger model flow chart.

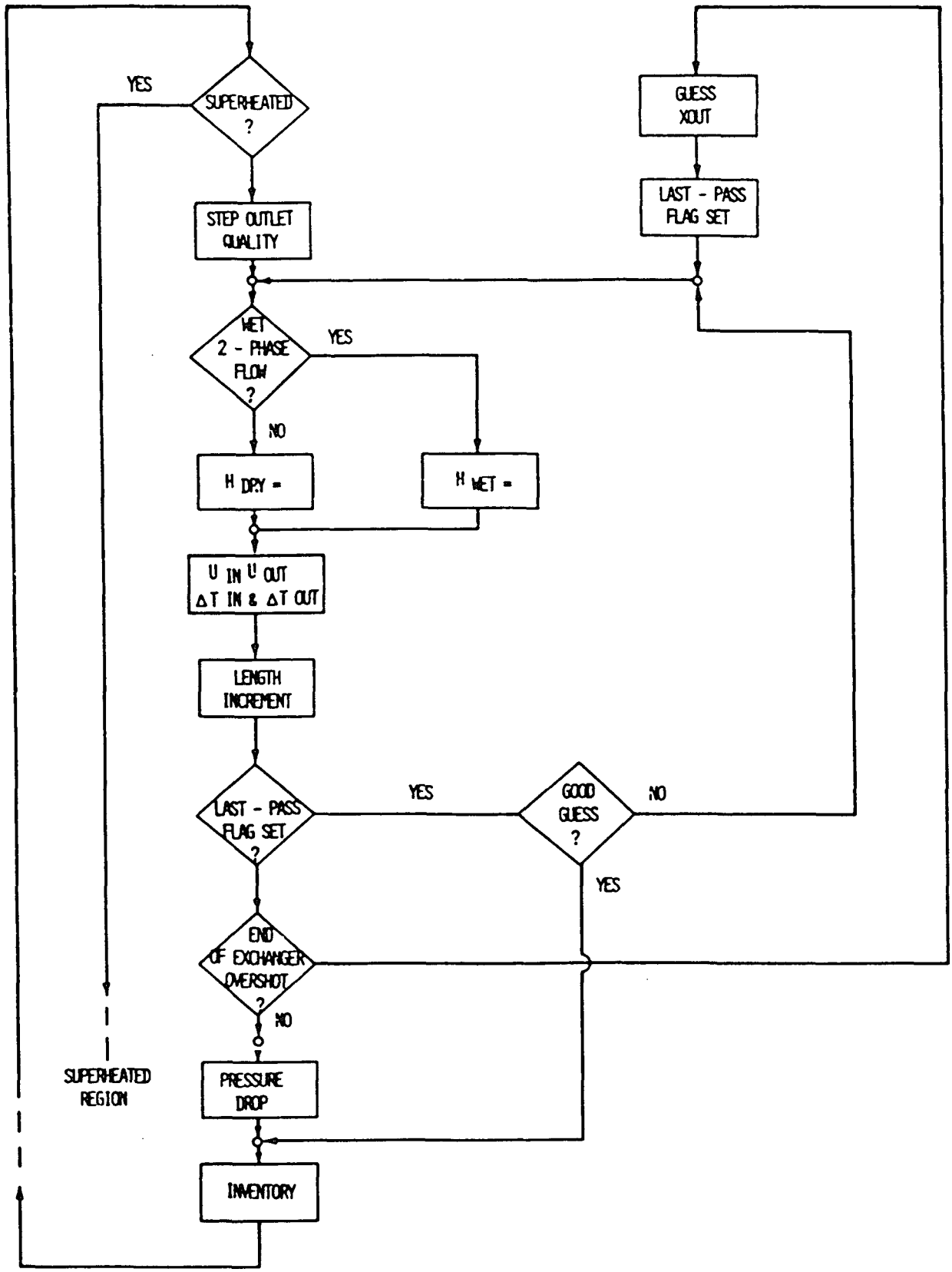

Figure 3.4 Tube-in-tube heat exchanger model flow chart.

3.7 Experimentation

The purpose of the experimental portion of Task 1 is to provide the data needed to detemine the empirical parameters in the correlations given in section 3.5, and to verify that the resultant heat exchanger models work.

3.7.1 BNL Heat Pump Test Facility

Heat exchanger tests were performed on the units cited in section 3.4 using the BNL heat pump test facility called the Heat Pump Simulator. Figure 3.5 is a schematic of the simulator as configured for these tests.

For component tests a heat source and a heat sink subsystem, called the Liquid Source and Liquid Load Subsystems (LSS and LLS) respectively, are used to supply water at controlled temperatures and flowrates to a water-to-water breadboard heat pump called the Subcomponent Test Stand (STS). The STS, shown in Figure 3.6, is equipped to measure and control all conditions pertaining to water/refrigerant heat exchangers. Data acquisition and reduction and automatic control of equipment are performed by a microcomputer based subsystem called DAR/CS.

The LSS consists simply of a tank, a pump, and two means of measuring water flow. The heat required to maintain temperatures in the LSS is supplied by electric resistance heaters which are controlled directly by the DAR/CS. The LLS consists of three fluid circuits which are coupled via heat exchangers. The primary circuit circulates fluid, usually water, through the condenser of the heat pump and is cooled via a heat exchanger by the secondary circuit. The flow through the secondary temperature controlling circuit is governed by a control valve which is in turn controlled by DAR/CS. The LLS like the LSS has two different flow measuring devices.

The STS was built to test heat pump components with a wide range of capacities. Its construction allows components to be interchanged quickly and easily. For these heat exchanger tests, a three phase compressor connected to a variable frequency drive was used. This system allowed compressor speed to be varied continuously over the range of 50 to 120 percent of the nominal speed. Other features of the STS are:

- an auxiliary tandem evaporator which allows the test evaporator outlet vapor quality to be varied at will,
- a subcooler supplied by an independent coolant circuit,

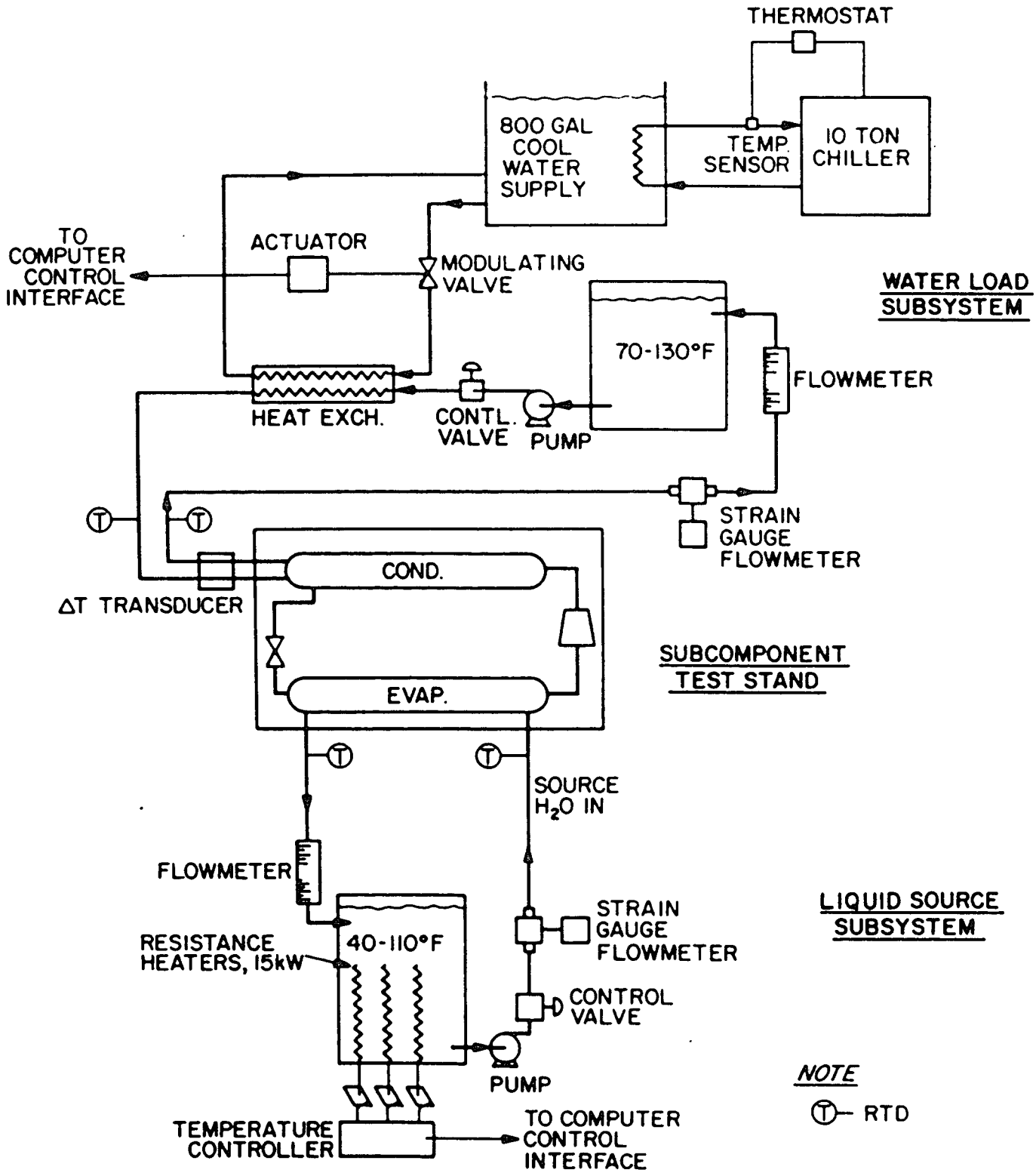

Figure 3.5 Heat pump simulator configured for evaporator tests.

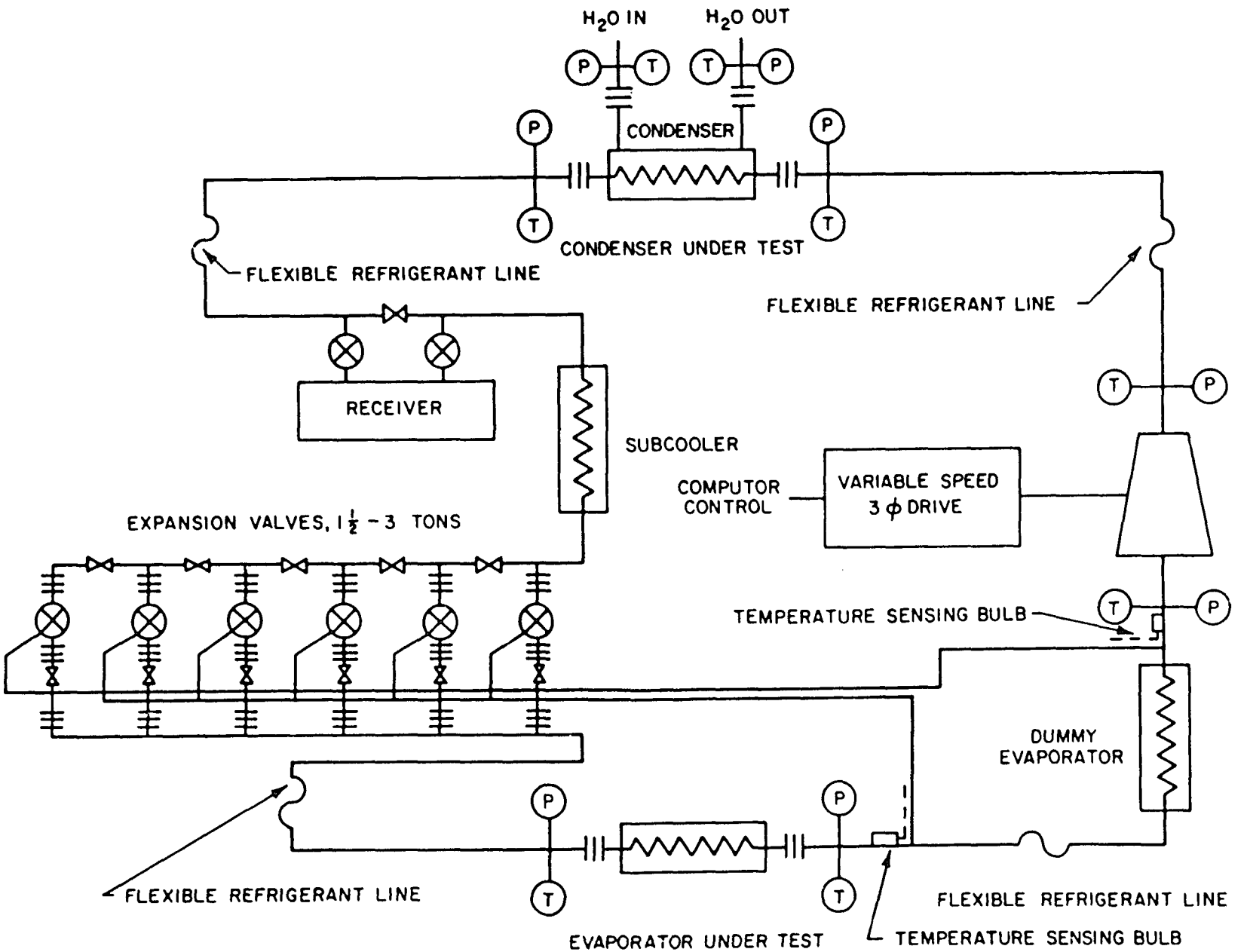

Figure 3.6 Subcomponent test stand.

- refrigerant receiver and accumulator,

- fully immersed platinum resistance thermometers for refrigerant and water temperature measurement,

- pressure transducers to measure absolute and differential pressure in refrigerant and water lines,

- many flexible refrigerant lines with quick connectors for fast interchange of components,

- DAR/CS controlled expansion valve and a bank of externally balanced thermostatic expansion valves.

In all tests the refrigerant R-22 was used. The evaporator heatant was 45% ethylene glycol in water. The condenser coolant was water.

The elements composing the DAR/CS are shown in Figure 3.7. In the DAR/CS all sensors are read by a programmable datalogger which is controlled by a microcomputer. The microcomputer performs all data reduction and control computations based on input from the datalogger. The microcomputer outputs reduced data on a line printer, and stores raw data on a hard disk. Control signals are generated by the computer via d/a components and the resulting voltage signals translated to those needed by the final controllers by BNL-built transducers.

3.7.2 Test Procedure

Each heat exchanger was tested as both an evaporator and as a condenser on the simulator's STS. In addition, each was tested in a single phase mode in order to investigate the single phase heat transfer on the coolant or heatant side of each exchanger.

3.7.2.1 Evaporating and condensing mode tests. The heat exchangers were tested in pairs, one operating as the evaporator and one as the condenser of the STS. After each test run the heat exchangers switched roles so that each unit was tested as both a condenser and an evaporator. The flow configuration was counterflow for the condenser and cocurrent flow for the evaporator.

The evaporator superheat was maintained at about 10°F for most test. For some of the tests the outlet quality was maintained between 0.35 and 0.6. Hunting of the expansion valve was prevented by using the smallest valve capable of passing the flow at all respective conditions. The STS subcooler was bypassed during all tests so that any subcooling occurred in the condenser under test. The system was insensitive to charge because of the use of the water line receiver.

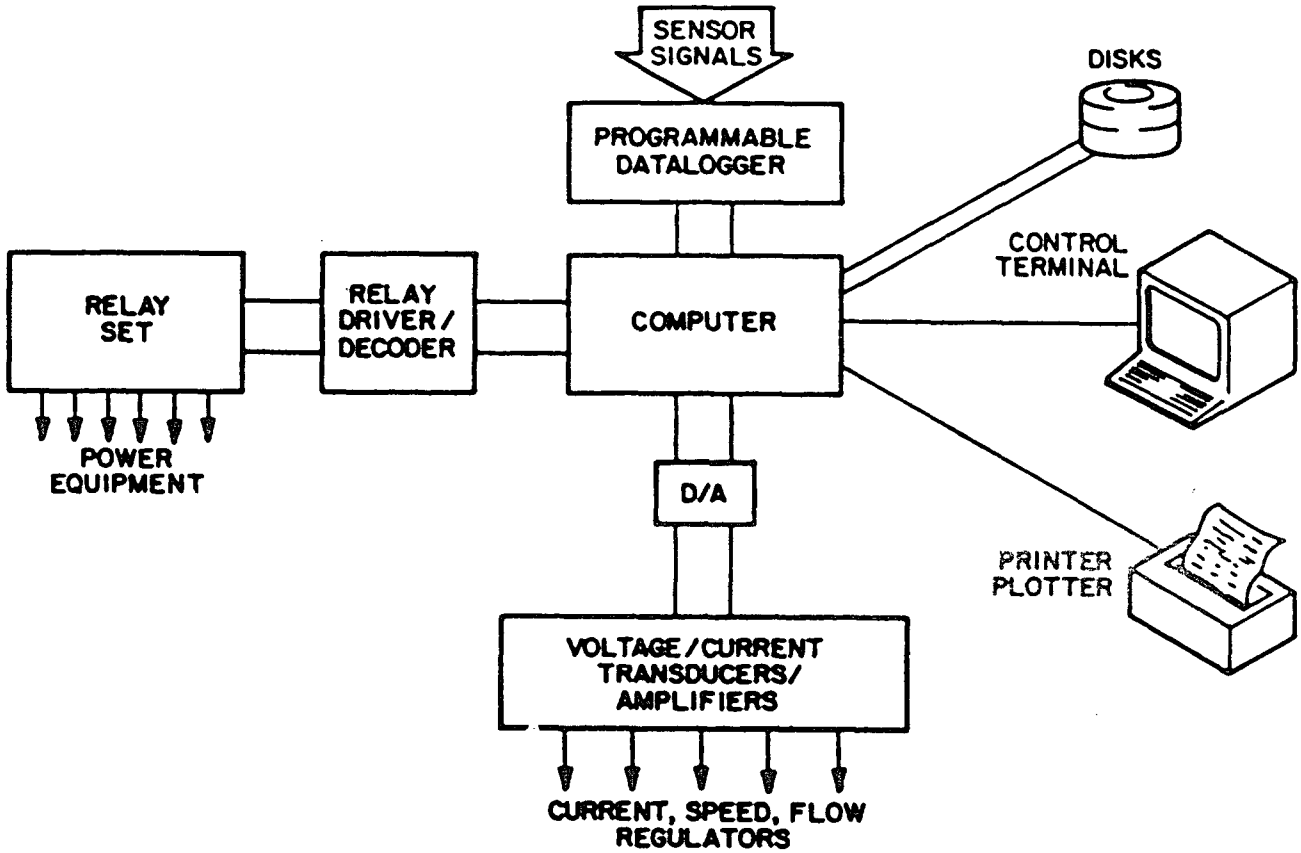

Figure 3.7 Data acquisition reduction/control system.

For each of three compressor speeds the condenser and evaporator entering water temperatures were varied so that the refrigerant mass flow would vary independent of the condenser and evaporator pressure. The computer control system allowed the temperatures of both heatant and coolant to drift at a rate less than 1°F/6 min. Steady state points were established by the DAR/CS at approximately 4 points during each temperature sweep to compare with the quasi steady state data.

During all evaporator and condenser tests the following parameters were measured.

- refrigerant pressure and temperature at inlet and outlet of condenser, test evaporator, and auxiliary evaporator,
- compressor power consumption,
- heatant and coolant mass flowrate,
- heatant and coolant temperature and pressure at inlet and outlet of test exchangers and temperature at inlet of auxiliary evaporator.

3.7.2.2 Single phase tests. In order to obtain overall heat exchanger experimental U-values, the primary circuit of the LLS was connected to what is normally the refrigerant side of the heat exchanger. The LSS circuit which contained the antifreeze was connected as for the refrigerant tests. The antifreeze flowrate was held constant while the water (LLS) flowrate was stepped from at least 4000 lb/hr to less than 1200 lb/hr in at least four water flow increments. This was done for three antifreeze flow increments. The parameters measured during these tests were the inlet and outlet fluid temperatures and flowrates. These tests were conducted after the condensing and evaporating mode tests had been performed because of the resulting contamination of the refrigerant side of the heat exchangers.

3.7.3 Data Acquisition and Verification

The measurements made during operation of the simulator provided several independent heat balances. These were used to verify the accuracy of all measurements made. Mass flow was given by the heat exchanger load divided by the enthalpy change of the refrigerant in the heat exchanger. The inlet enthalpy of the evaporator was taken to be that at the condenser outlet which was calculated from the measured values of pressure and temperature. The enthalpies at the evaporator outlet and the condenser inlet were calculated from the measured temperature and pressure.

Other parameters needed for the analysis are the vapor qualities at the inlet and outlet of the evaporator. The inlet quality is the difference between the saturated water enthalpy at the inlet pressure and the evaporator inlet enthalpy, as assumed above, divided by the latent heat of vaporization at the inlet pressure. The outlet quality is the enthalpy change in the evaporator divided by the latent heat of fusion at the evaporator outlet pressure. The enthalpy change is the ratio of cooling load to calculated refrigerant mass flow.

The mass flowrate of ethylene glycol solution was measured by a calibrated impact type strain gauge flowmeter. This unit was originally calibrated for use with water and the measured values corrected for the aqueous ethylene glycol. Part way through the test program it was recalibrated for use with 20% aqueous ethylene glycol. This calibration was double checked via energy balances and direct measurement of integrated fluid volume.

3.8 Model Validation

3.8.1 Validation Approach

Provisional subroutines were written for each heat exchanger model in a form expected to be suitable for use in the final model. Four different subroutines have been developed, one for each type of heat exchanger in each mode of operation. The models have been validated by adjusting the empirical constants in the correlations to obtain the best least squares fit to the experimental data.

The fitting procedure is illustrated for the case of the evaporator subroutine in Figure 3.8. A Fortran function subroutine was written to perform the least squares fit by minimizing the "error"

$$\sum_j \left\{ \left[\frac{\Delta P_e - \Delta P_c}{\Delta P_e} \right]^2 + \left[\frac{P_{i,e} - P_{i,c}}{P_{i,e}} \right] \right\}^2$$

where ΔP and P_i are (for evaporation) the evaporator pressure drop and inlet pressure, and e and c refer to experimentally measured and calculated values respectively. The index j designates the particular experimental point to which the experimental and calculated values correspond. In operation, the inputs to the error subroutine are the values of each of the empirical correlation constants; the output is the error defined above. A library function minimizing routine makes many calls to the error subroutine and finds the combination of values for which the errror is smallest.

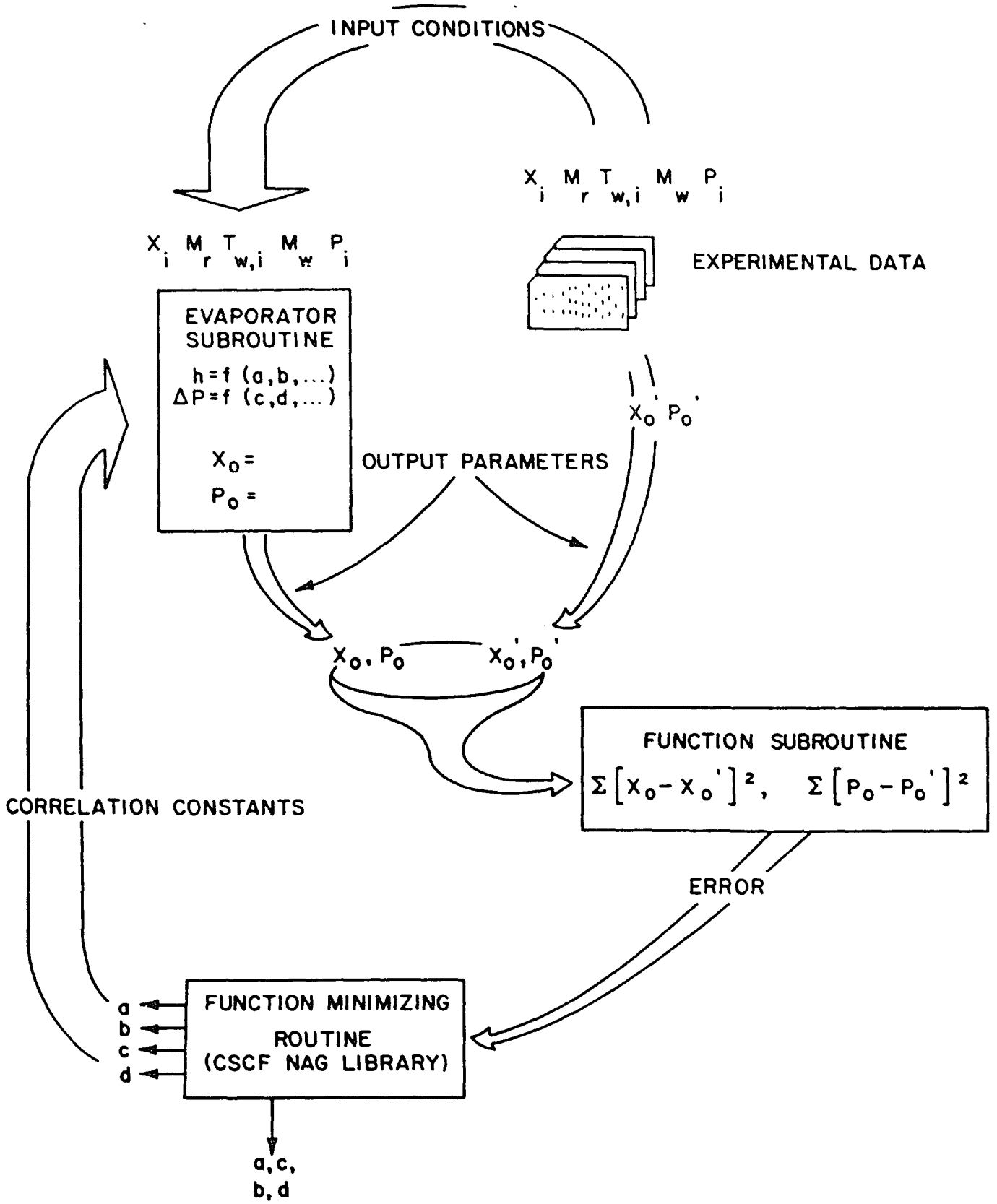

Figure 3.8 Procedure for fitting evaporator model to experimental data.

3.8.2 Validation Results

Table 3.1 gives the values of the free constants in equations (3.1) and (3.7) which gave the best agreement with the experimental data for each type of heat exchanger. In the case of the shell-and-tube evaporator the unmodified Friedel correlation gave acceptable results.

Table 3.1.
Best-Fit Correlation Constants

Heat Exchanger Type	Constants		
	a	b	c
shell-and-tube	1.20	0.500	*
Turbotec	4.56	0.613	43.3
Noranda	3.97	0.741	6.81

*Use Friedel correlation with no changes.

It was found that Turbotec coils of different diameters could be modeled successfully using the same correlation constants. The equivalent diameter and flow area required for the heat transfer correlations (3.1) and (3.4) were calculated using an inner tube diameter equal to 0.86 times the actual maximum external diameter, as determined by the fitting procedure. Average tube dimensions were used to correlate the Noranda data.

The heat exchanger subroutine was made to predict the refrigerant inlet pressure given the measured inlet and outlet vapor qualities, refrigerant and antifreeze mass flowrates and inlet antifreeze temperature for all of the heat exchanger tests conditions. Figures 3.9, 3.10, and 3.11 are plots of the predicted inlet pressures versus the measured inlet pressures for the shell-and-tube, Turbotec and Noranda heat exchangers. The straight lines define the ±10% boundaries. Figures 3.12 and 3.13 are plots of the predicted versus measured refrigerant pressure drops for the Turbotec and Noranda units. The standard deviations of the agreement between the predicted and measured quantities are given in Table 3.2.

Table 3.2
Standard Deviations of Correlations

Heat Exchanger Type	Pressure Drop	Inlet Pressure
shell-and-tube	*	1.60
Turbotec	2.58	3.11
Noranda	1.07	1.91

*very small

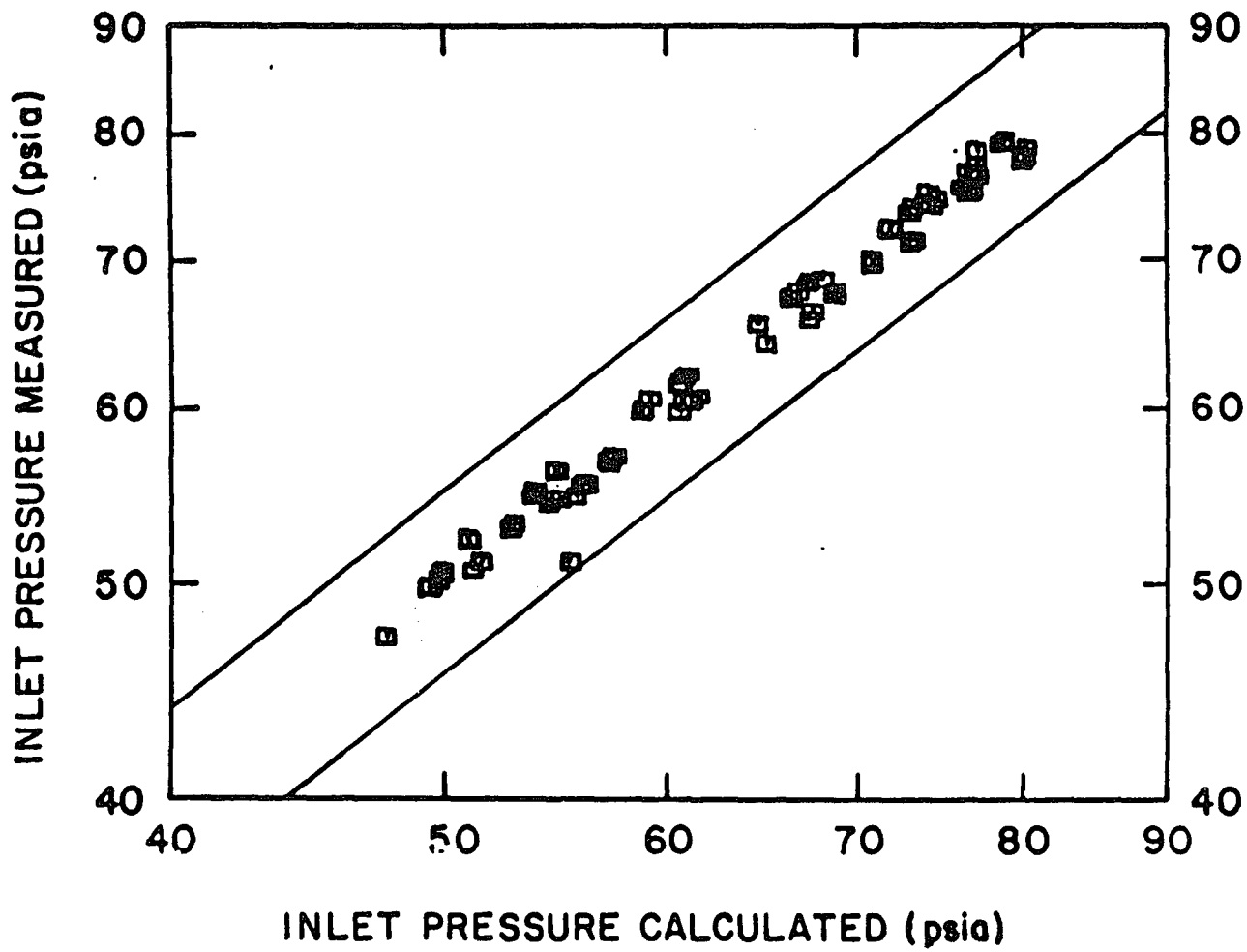

Figure 3.9. Comparison of model-predicted vs experimental inlet pressure for shell-and-tube heat exchanger.

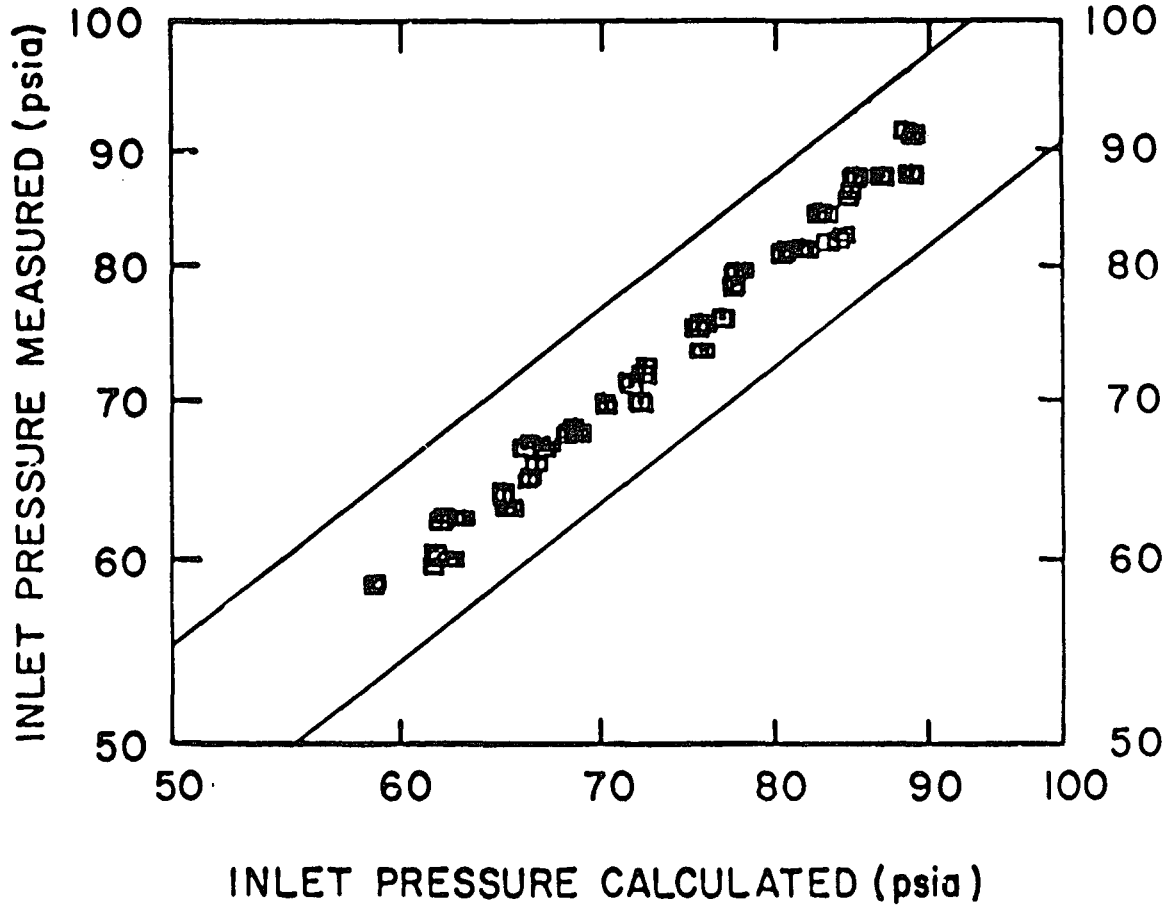

Figure 3.10. Comparison of model-predicted vs experimental inlet pressure for Turbotec heat exchanger.

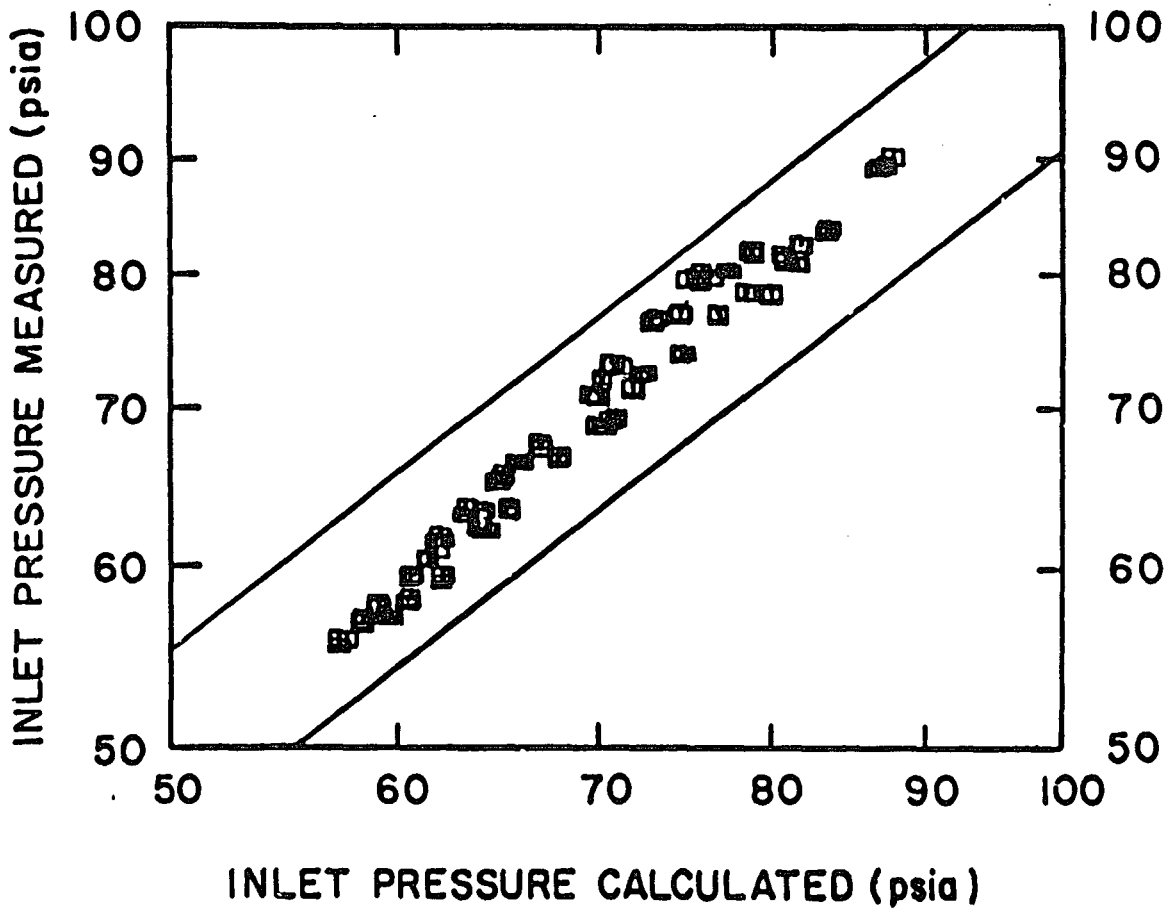

Figure 3.11. Comparison of model-predicted vs experimental inlet pressure for Noranda heat exchanger.

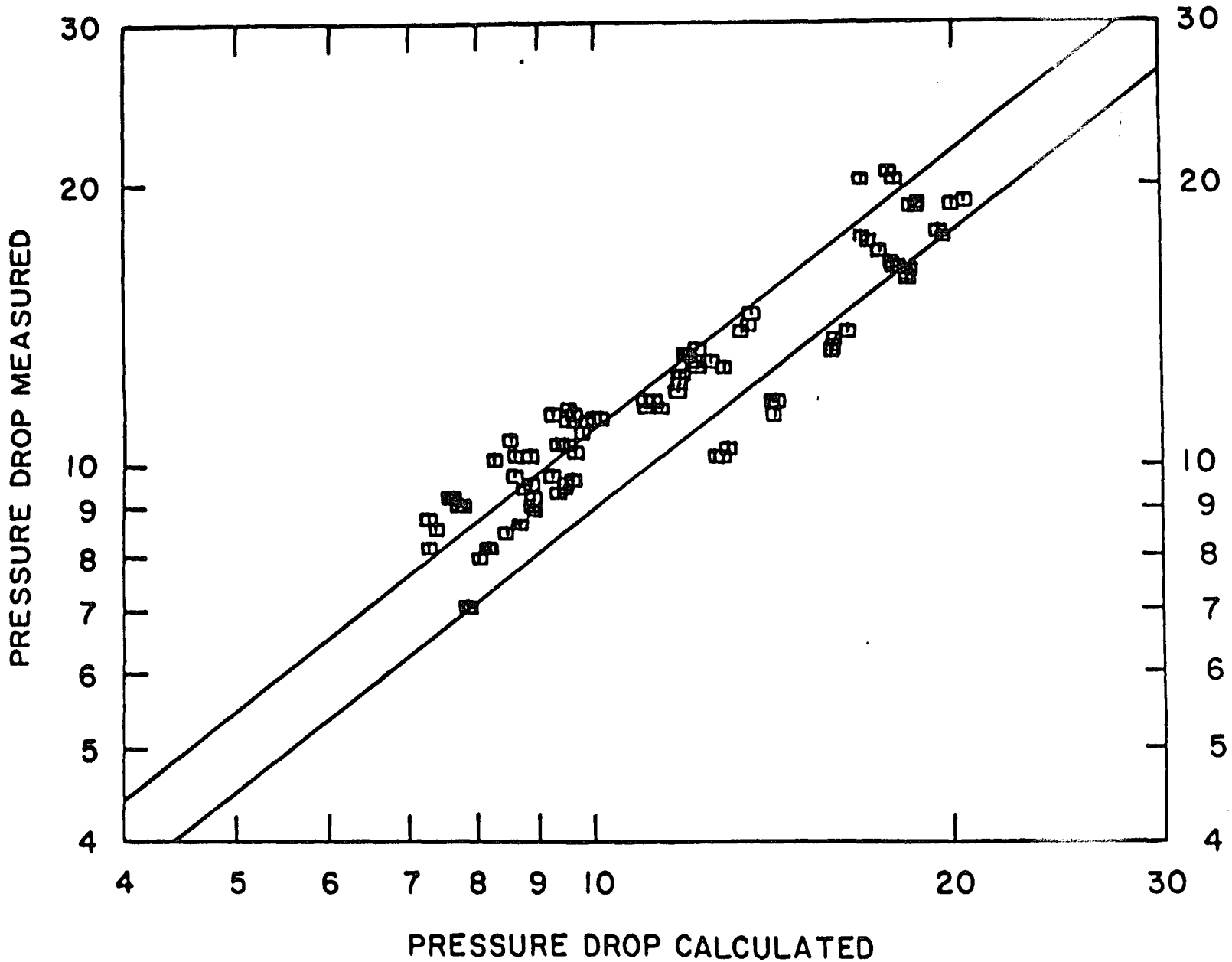

Figure 3.12. Comparison of model-predicted vs experimental pressure drop for Turbotec heat exchanger.

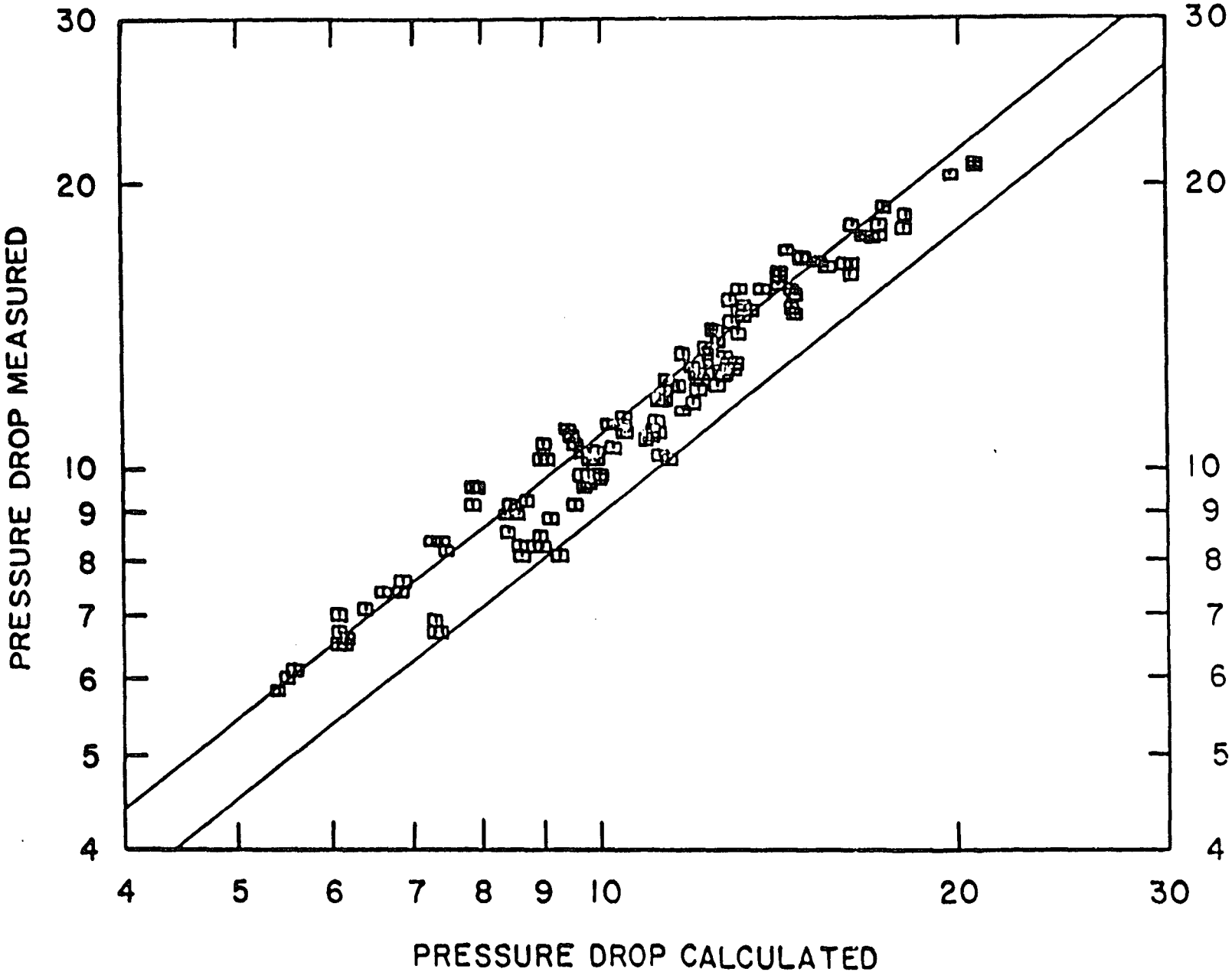

Figure 3.13. Comparison of model-predicted vs experimental pressure drop for Noranda heat exchanger.

After the heat exchanger tests were completed one problem appeared. The flexible refrigerant tubing which was used in some parts of the subcomponent test stand had apparently begun to shed large pieces of material. These were found in the filters when the STS was checked out after the tests. It is not known if some pieces of material were lodged in any of the heat exchangers during the tests. It is expected that the pressure drop data would be very difficult to correlate if shards of material were accumulating in the exchangers during tests. As a check, it was confirmed that our pressure drop data were in reasonable agreement with Turbotec's.

The antifreeze side heat transfer coefficient for the six heat exchangers are shown in Table 3.3. For the Turbotec units the maximum external diameter

Table 3.3
Heat Transfer Coefficient Obtained from Wilson Plots
($Btu/hr\text{-}ft^2\text{-}^oF$)

Fluid flow (lbs/hr)	5124	3985	2846
Heat exchanger:			
Turbotec 30		1809.0	
Turbotec 36		1274.0	
Noranda 16		1502.0	
Noranda 20		1409.0	
Shell-and-tube 1.1	292.0	392.0	461.0
Shell-and-tube 1.5	241.0	343.0	398.0

was used; for the Noranda heat exchangers, the average diameter was used. In the final model heat transfer enhancement factors are used with the standard correlations to predict the single phase heat transfer coefficients. In the case of the coaxial heat exchangers the enhancement factor is simply the ratio of the measured heat transfer coefficient to that calculated for an equivalent smooth tube under the same conditions using the Dittus-Boelter relation. The equivalent smooth tube dimensions for the Noranda type heat exchanger were the unfinished tube dimensions. For the Turbotec heat exchangers it was the maximum internal diamter. For the shell-and-tube exchanger a degradation factor equal to the ratio of the measured heat transfer coefficient to that calculated using Eq. (3.4) is used. A sample Wilson plot for Turbotec unit BTSSC-30 is presented in Figure 3.14 for average antifreeze temperature of 62.5°F and antifreeze flowrate of 3985 lb/hr.

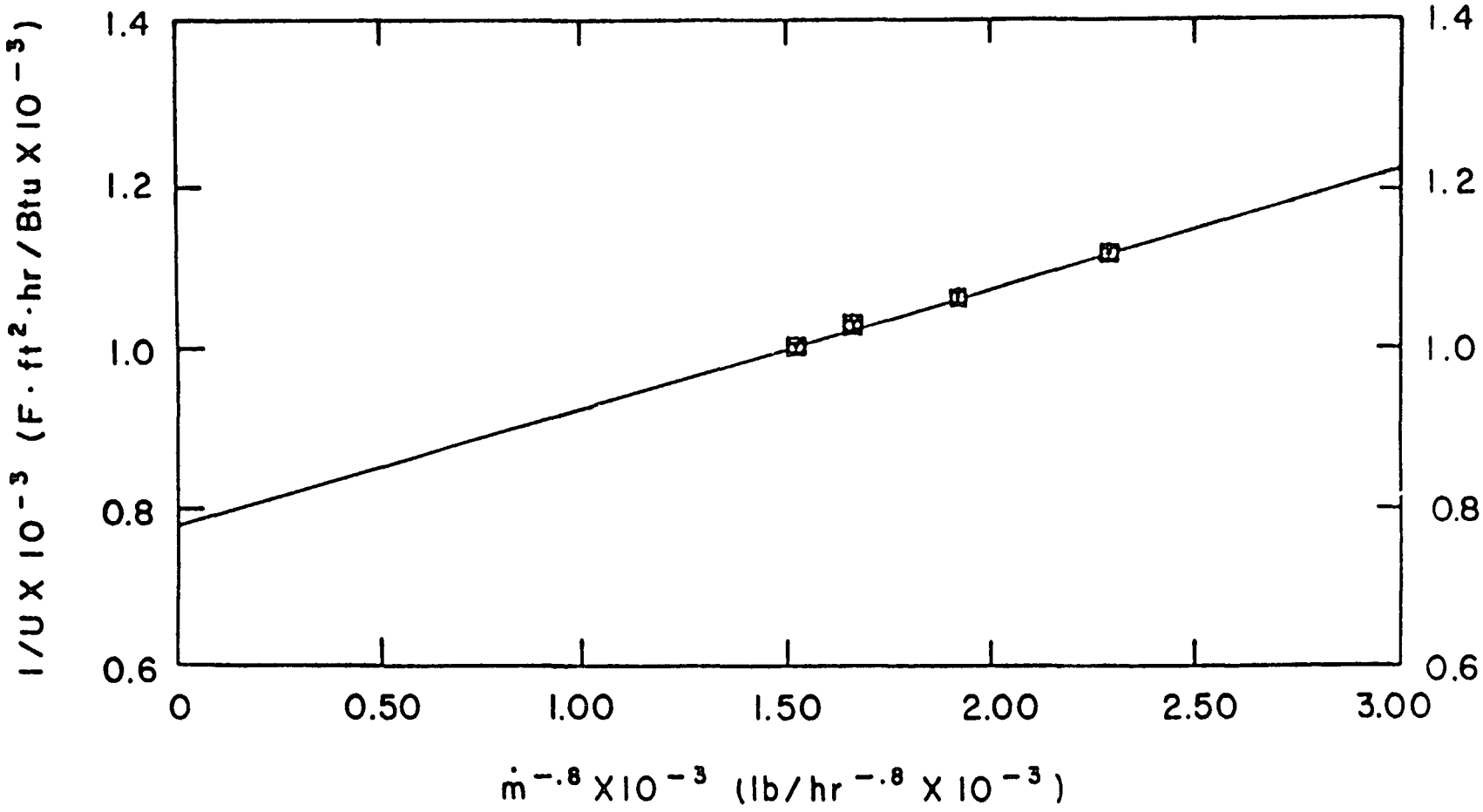
1.4
1.2
1.0
0.8
0.6
0
0.50
1.00
1.50
2.00
2.50
3.00
$1/U \times 10^{-3}$ $(F \cdot ft^2 \cdot hr / Btu \times 10^{-3})$
$\dot{m}^{-.8} \times 10^{-3}$ $(lb/hr^{-.8} \times 10^{-3})$

Section 3. References

1. C.K. Rice, S.K. Fischer, W.L. Jackson, R.D. Ellison, Design Optimization and the Limits of Steady-State Heating Efficiency for Conventional Single-Speed Air-Source Heat Pumps, ORNL/CON-63, October 1981.
2. R.D. Ellison and F.A. Creswick, A Computer Simulation of Steady-State Performance of Air-To-Air Heat Pumps, ORNL/CON-16, March 1978.
3. Personal conversations with Ajit Kumar of Turbotec, and M. Hughes of Friedrich Corporation.
4. M.A. Catan, Solar assisted heat pumps: impact of evaporator characteristics on performance, BNL 51638, March 1982.
5. J.G. Lavin and H. Young, Heat transfer to evaporating refrigerants in two phase flow, AIChE J., 1, November 1965.
6. G.R. Kubanek and D.L. Miletti, Evaporative heat transfer and pressure drop performance of internally finned tubes with Refrigerant-22, ASME J. of Heat Transfer, 101, August 1979.
7. C. Boling, W. Donovan and A. Decker, Heat transfer of evaporating freon with inner-fin tubing, Refrigerant Eng., December 1953.
8. W.L. Bryan and L.G. Seigel, Heat transfer coefficients in horizontal tube evaporators, Refrigerant Eng., May 1955.
9. T. Blatt and R.R. Adt, Jr., The effects of twisted tape swirl generators on the heat transfer rate and pressure drop of boiling Freon II and water, ASME, Paper No. 63-WA-42 (1963).
10. G.F. Hewitt, Burnout, Handbook of Multiphase Systems, ed. G. Hetsroni, pp. 66, 69-70.
11. S.K. Fischer and C.K. Rice, A steady state computer design model for air-to-air heat pumps, Oak Ridge Nat'l. Lab. report, ORNL CON-80.
12. G. Wallis, One Dimensional Two Phase Flow, pp. 366-68, 376-77.
13. Handbook of Multiphase Systems, Ed. G. Hetsroni, p. 6-63.
14. M.M. Shah, A general correlation for heat transfer during film condensation inside pipes, Int. J. Heat Transfer, 22, p. 547-56.
15. A. Bergles, Heat transfer characteristics of Turbotec tubing, ISU-ERI-Ames-81018.
16. Handbook of Multiphase Systems, Ed. G. Hestroni, p. 2-56.
17. Ibid., p. 2-60.

4. Task 2. Source Temperature/Load Map Development

4.1. Overview and Methodology

The goal of this task is to develop a procedure to generate source temperature/load maps, i.e. maps of water source heat pump entering fluid temperature versus load versus hours/season for ground coupled heat pump systems. These maps will provide the water-source heat pump optimization program being developed with the necessary correlations between heat pump entering fluid temperatures and load.

This section describes the role of the source temperature/load maps in the overall heat pump optimization project, and the methodology followed in developing the procedure to generate them. The procedure and its validation are described in detail, followed by examples of sample source temperature/load maps generated to verify that the procedure works.

4.1.1. Role of the Source Temperature/Load Map. The role of the source temperature/load map in the overall heat pump optimization program is illustrated by the flow chart shown in Figure 4.1. These maps (4)* will provide the heat pump operating conditions needed by the ground coupled heat pump optimization routine (5) now under development. This routine is based on the existing ORNL air-source heat pump optimization routine (3), modified to optimize water-source heat pumps. As discussed in detail in section 3, work has been conducted at BNL to develop the water-refrigerant heat exchanger performance model (2) required for this modification.

The ground coupled heat pump optimization routine (5)--given the source temperature/load map (4) based on the load, heat pump performance, and local climate and soil conditions selected--will generate the optimized ground coupled heat pump design (6), and provide a performance map (7) for this heat pump. This heat pump performance map (7) will be compared (8) to the map used to generate the original source temperature/load map (4), and if necessary a new map will be developed (1) and the process repeated. After one or more iterations the optimized ground coupled heat pump (9) will result.

4.1.2. Approach. The approach adopted for source temperature/load map development is transient computer simulation of ground coupled heat pump systems using a modified version of the GROCS-TRNSYS[1] program already developed

*The numbers is parentheses refer to the block numbers in Figure 4.1.

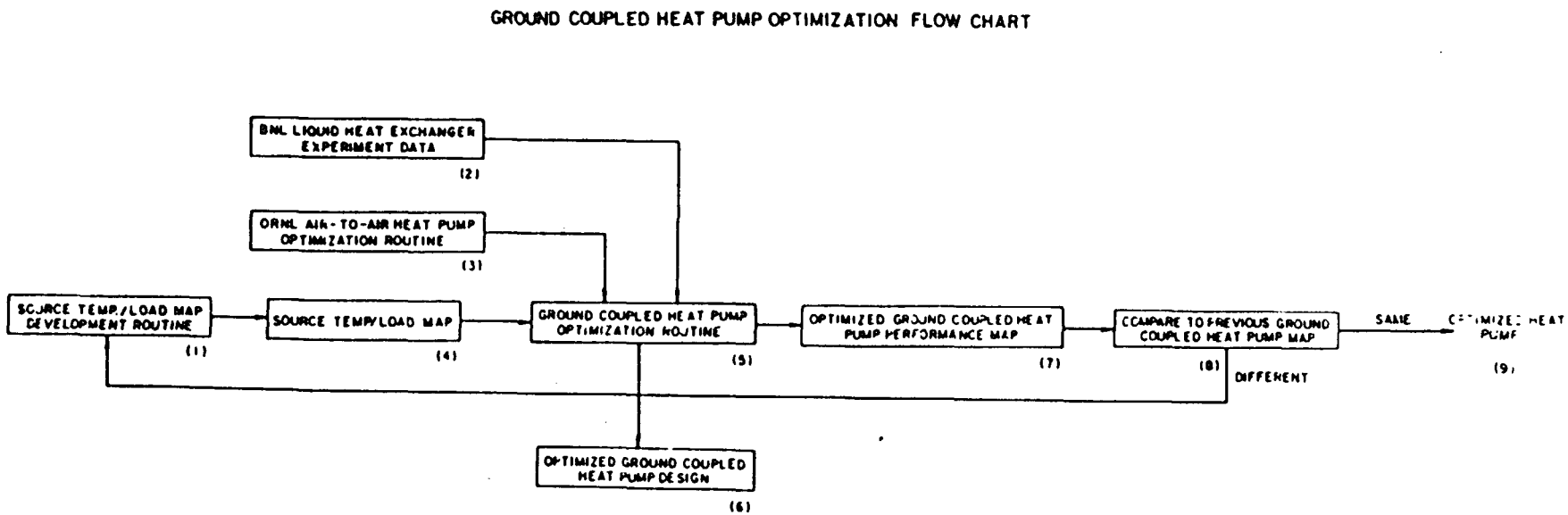

Figure 4.1. Ground coupled heat pump optimization flow chart.

at BNL. This program is based on the widely used University of Wisconsin solar system transient simulation program TRNSYS[2], using special "TYPE" subroutines to incorporate the BNL program GROCS[3] (GROund Coupled Systems) developed to model underground heat flow. This approach was selected because considerable experience exists with it, real short-term weather variations can be dealt with, and the validity of GROCS-TRNSYS has been tested, both experimentally and analytically, and been found to be satisfactory in closely related situations[3-5].

4.1.3. Task Methodology. The methodology followed in developing the procedure to generate source temperature load maps is presented as a flow chart in Figure 4.2. As the flow chart indicates, the task is divided into three subtasks:

1. GROCS-TRNSYS Program Development and Validation
2. Selection of Sample Test Conditions
3. Source Temperature/Load Map Generation

GROCS-TRNSYS uses a finite element approach to model underground heat flow. The number of elements has been restricted to minimize the time required for ground coupling device physical model design, and to minimize the computer time and memory required. The existing GROCS-TRNSYS program has provision for modeling buried tanks or serpentine earth coils. When small pipes are modeled--as for earth coils--a near-pipe steady-state approximation[1,5] has been used. This helps to minimize the number of finite elements required, and permits the use of a reasonably long (#1 hr) iteration timestep.

For this project, it was necessary to add two new capabilities to the program. The first was the provision to model isolated pipes--as for vertical heat exchangers. This was straightforward. The more difficult problem was to compute accurately heat pump entering fluid temperature taking into account system on/off cycling (which yields significantly different earth coil temperatures than continuous operation), without the use of very small elements or timesteps.

A ground coupling device (1.1)* was selected for program development and validation. Two physical models (1.3) were written to simulate this device, one containing 52 elements and one, similar to the models expected to be used

*The numbers in parentheses refer to the block numbers in Figure 4.2.

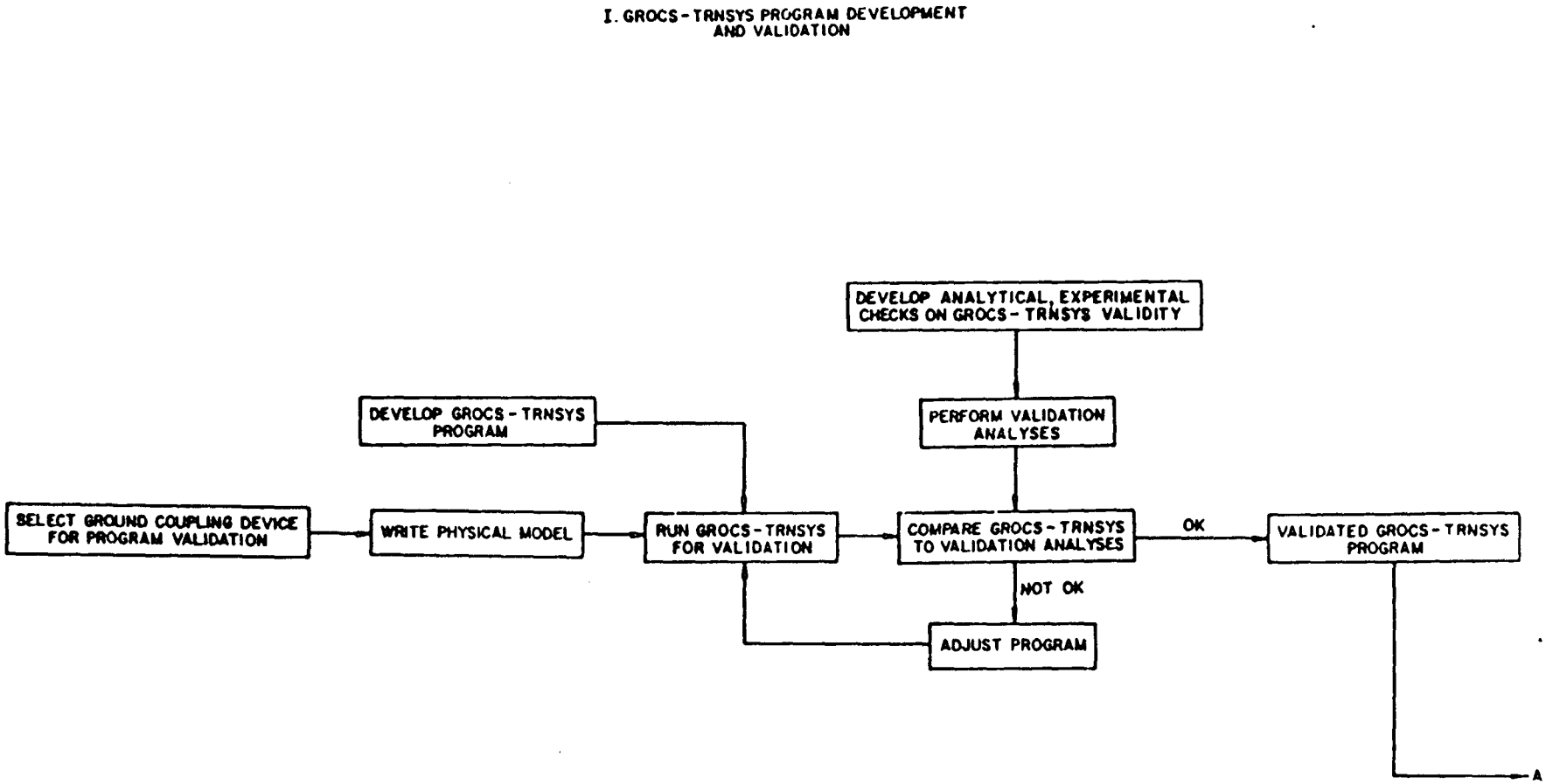

Figure 4.2.a. Source temperature/load map development flow chart.

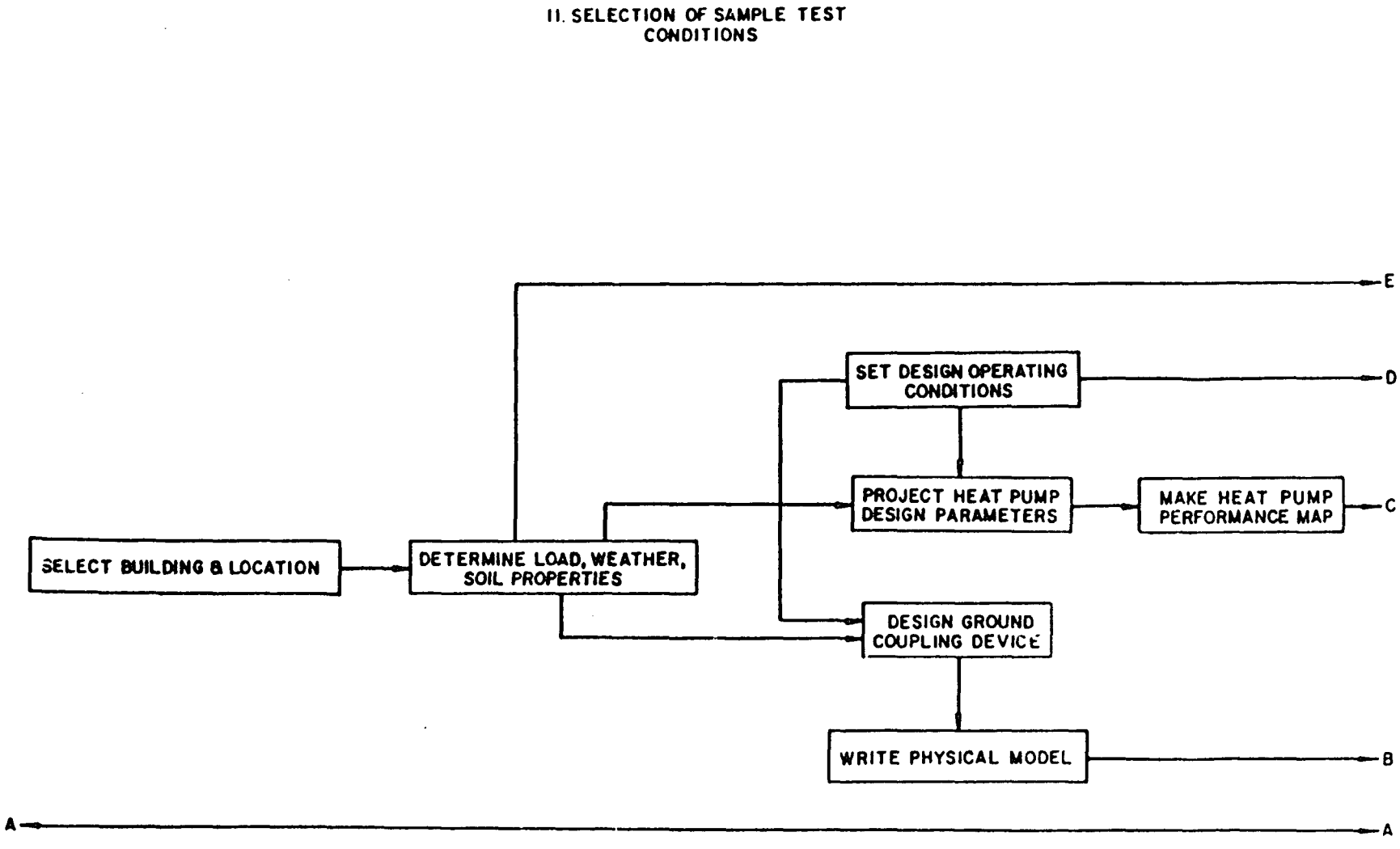

Figure 4.2.b. Source temperature/load map development flow chart.

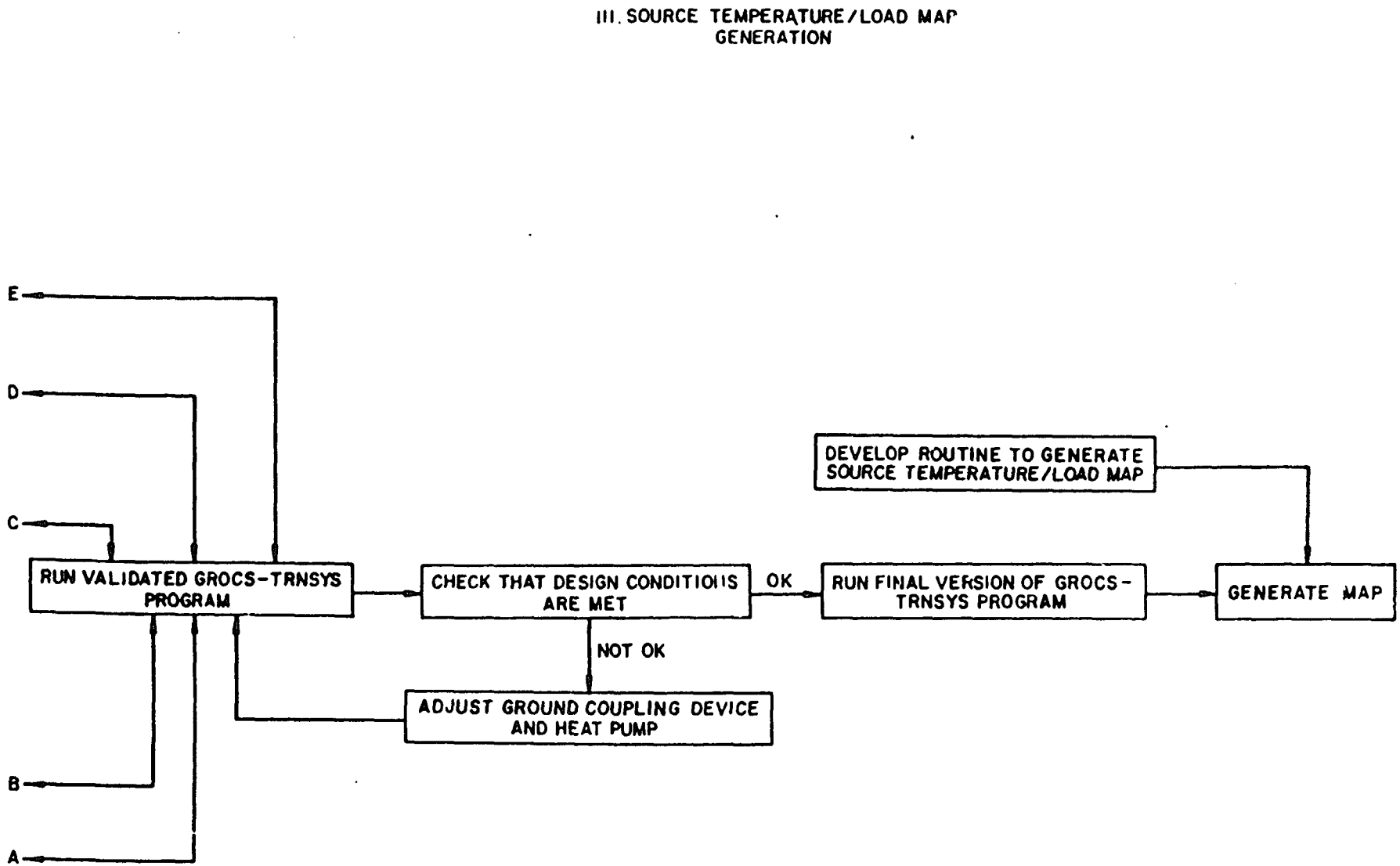

Figure 4.2.c. Source temperature/load map development flow chart.

in practice, containing only 12 elements. The modified GROCS-TRNSYS program (1.2) was run (1.4) with these ground coupling device models, using constant far-field temperatures and estimated soil thermal properties. Heat pump and heat exchanger fluid temperatures were determined for a variety of steady and pulsed heat inputs. Only radial heat flow was permitted.

Analytical checks were developed (1.5) and performed exactly (1.6). The GROCS-TRNSYS results obtained using the 12 element model with reasonable time-steps (15 minutes) were compared (1.7) to the analytical checks and to the results obtained using the 52 element model with very short timesteps. GROCS-TRNSYS development and validation are discussed in detail in section 4.3.

The next step in source temperature/load map development was the selection of sample test conditions for which to generate a map. A building and location (2.1) were selected. Weather tapes and typical soil properties were chosen (2.2). Using the performance of existing heat pumps as a guide, a somewhat improved heat pump performance map (2.7) was developed. The ground coupling device (2.5) used was similar to the pipe modeled for GROCS-TRNSYS validation. The physical model (2.6) used (shown in Figure 4.14) was somewhat more realistic, permitting axial heat flow.

To generate sample source temperature/load maps, the validated GROCS-TRNSYS program was run (3.1) with the sample test conditions selected. The results were inspected for errors and self-consistency (3.2). Sample source temperature/load maps were generated (3.6) by a small program developed (3.4) which extracts the required information from the GROCS-TRNSYS outputs and presents it in the form desired.

4.2. How GROCS-TRNSYS Works

4.2.1. Description of GROCS-TRNSYS. GROCS-TRNSYS[1] is an amalgamation of two programs, GROCS and TRNSYS, in order to make possible hour-by-hour simulations of ground-coupled heat pump systems. GROCS (GRound Coupled Systems)[3] was developed at Brookhaven National Laboratory to model in-ground heat flow. TRNSYS[2] was developed at the University of Wisconsin to simulate solar systems. It can, however, be used to simulate nonsolar heating and cooling systems on an hour-by-hour basis where this is desirable.

4.2.2. TRNSYS Description. TRNSYS is a large program able to perform a complex simulation task. Readers who are unfamiliar with TRNSYS and interested in the details of the program's structure and function are urged to consult the appropriate literature[2]. For our purposes, a quote from ref. 2 may suffice.

"A system is defined to be a set of components, interconnected in such a fashion so as to accomplish a specified task. For example, a typical solar water-heating system may consist of a solar collector, an energy storage unit, an auxiliary energy heater, a pump, and several temperature sensing controllers. One obvious characteristic of a system is its modularity. Because the system consists of components, it is possible to simulate the performance of the system by collectively simulating the performance of the interconnected components.

"The performance of a system component will normally depend upon characteristic fixed parameters, the performance (or outputs) of other components, and time-dependent forcing functions. For a solar water-heating system knowledge of the weather (i.e., solar radiation, ambient temperature, etc.) and the hot water demand as a function of time are necessary in order to determine the transient system performance. It is important to realize that time dependent forcing functions can be thought of as outputs of specialized system components and they can thus be treated in the same manner as any other component.

"The modular simulation technique greatly reduces the complexity of system simulation because it essentially reduces a large problem into a number of smaller problems, each of which can be more easily solved independently. In addition, many components are common to different systems and provided that the performance of these components is described in a general form, they

can then be used in many different systems with little or no modification. This feature makes modular simulation most attractive.

"With a program such as TRNSYS which has the capability of interconnecting system components in any desired manner, solving differential equations, and facilitiating information output, the entire problem of system simulation reduces to a problem of identifying all of the components and formulating a general mathematical description of each. In some cases, the description of a component may be complex."

4.2.3. Design of GROCS. The realm of interesting underground heat flow problems that can be solved without a large digital computer is limited. Thus, the need was seen to do underground heat flow modeling on such a computer. The usual method of numerically solving differential equations such as the heat flow equations on a computer is to convert the differential equations to finite difference equations which are solved on a "mesh" of equally spaced points. The mesh spacing sets a scale which determines the accuracy of the solution. It is not possible for the solution to have meaning over distances smaller than the mesh spacing. In 3-dimensional systems, the number of mesh points grows as the cube of a system dimension so that mesh-based 3-dimensional programs usually require large amounts of computer time. This approach was seen as undesirable, especially because of our intention to integrate GROCS with TRNSYS, the University of Wisconsin solar system simulation program, which is already quite large.

Therefore, instead of mesh points, GROCS solves the heat flow finite difference equations over a system of finite elements or "blocks" of earth. Each block is a volume of earth whose size and shape are determined by a hand-drawn model.

A block-type model has two advantages:

1. Useful problems can be solved with a short, simple, and economical computer program.

2. New ground-coupling configurations can be studied by creating new hand-drawn models, a process which takes a few hours.

GROCS uses two different kinds of blocks, called "rigged blocks" and "free blocks." The rigged blocks surround the free blocks and provide the necessary spatial boundary conditions. The temperatures of the rigged blocks are determined at each timestep by a function subprogram called TFARSIN, which computes the temperature of undisturbed ground at any depth and any time of the year, given the mean annual ground temperature, the temperature amplitude at the surface, the phase shift of the minimum temperature, and the ground thermal diffusivity.

The free block temperatures are initially determined by specifying them as data input or, if a default value is specified (which is a timesaver), by TFARSIN as described above. At all future timesteps, however, the free blocks have their temperatures determined by their thermal interaction with each other and with the rigged blocks, and by heat inputs placed in them to simulate the effect of a ground coupling device and load.

A number of physical parameters of the model must be specified for input to GROCS. These include the numbers of free and rigged blocks, the initial temperature or the default temperature, the volume and volume heat capacity ($C\rho$) for each free block, the depth of each block, all nonzero heat transfer areas, and center-to-center distances of adjoining blocks.

4.2.4. Integration of GROCS with TRNSYS. In order to merge GROCS successfully into TRNSYS it was necessary to make provision for the simulation processes going on in each program to proceed without interfering with the other, and yet to allow appropriate thermal interactions to occur between them. To make this possible, subroutines were written in the same format as other component TYPE subroutines in TRNSYS, which model solar components and building loads and in some cases perform various algebraic manipulations necessary to a simulation. These subroutines, of which TYPE 40 is used for the buried pipe, in turn communicate with GROCS. During each simulation timestep, the TYPE subroutines are called in turn by a central "command" subroutine in TRNSYS called EXEC. As each TYPE subroutine is called, its inputs are adjusted to reflect the outputs of previously called subroutines, and after it finishes processing, its outputs in turn affect the inputs of subroutines to be called later. After (usually) several passes through the set of subroutines which constitute the system to be simulated, the inputs and

outputs of all the subroutines converge to a set of mutually consistent values.

4.2.5. Isolated Pipe Model. The simulation of an isolated buried pipe presents problems not encountered with a buried tank. Most of these problems are related to the fact that the typical pipe diameter is small enough to require very small block sizes, and therefore timesteps much shorter than the 15-min typical for TRNSYS runs. Thus, straightforward modeling of the pipe along the same lines as the tank would require inordinate amounts of computer time. For this reason it was necessary to employ a model which was not based upon calculating a derivative of the pipe water temperature, as would be done with a tank, but rather upon the calculation of an output temperature on the basis of an input temperature. This approach permitted a validation procedure to be carried out which, among other things, allowed for reasonable block sizes and timesteps.

The determination of the fluid outlet temperature proceeds along lines described below and illustrated in Figure 4.3. The fluid in the pipe is considered to be surrounded by a resistive medium which consists of the pipe wall and of the earth in the first GROCS block surrounding the pipe, out to the mean radius of the annular block. (There is some ambiguity over whether this mean should be the arithmetic mean, geometric mean, log mean, or a weighted mean based on soil volume at each radius; this is taken up below.)

An energy balance is set up at each point along the pipe, represented here by the differential length between x and x + dx. The heat flow rate from the side between x and x + dx is given by

$$\dot{Q}_{SIDE} = \frac{T_b - T(x)}{R} \tag{4.1}$$

where T_b is the boundary temperature (temperature of the first GROCS block), T(x) is the pipe fluid temperature, and R is the thermal resistance between the pipe wall and the boundary (mean radius of the first GROCS block) for the length of pipe between x and x + dx.

If we define R_o as the resistance of a unit length of cylinder, then

$$R = \frac{R_o}{dx} \tag{4.2a}$$

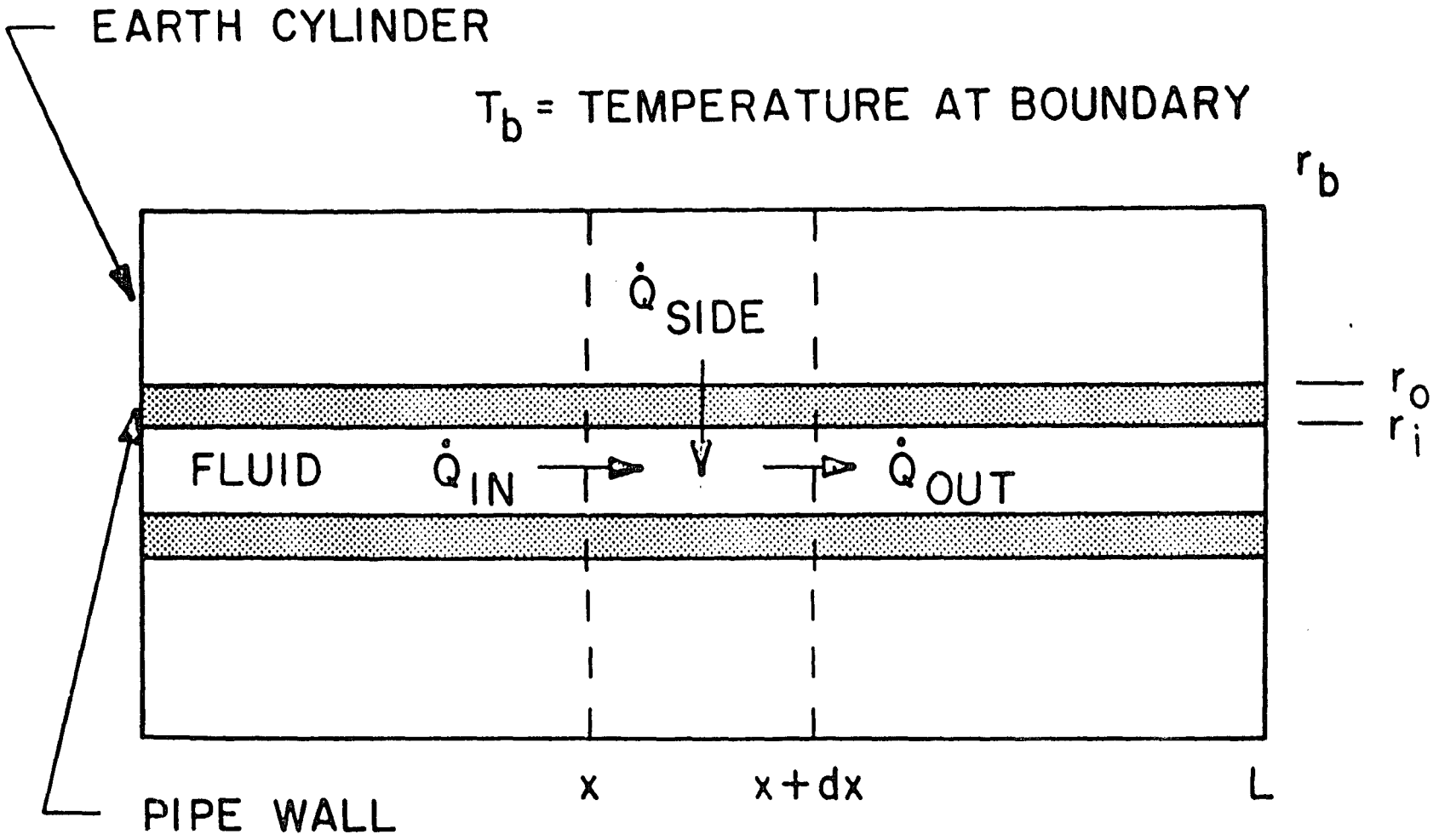

Figure 4.3. Schematic of isolated buried pipe model.

and

$$R_o = \frac{\ln r_b/r_o}{2\pi\ k_e} + \frac{\ln r_o/r_i}{2\pi\ k_p} \tag{4.2b}$$

where k_e and k_p are the thermal conductivities of the earth and the pipe, respectively, and r_b, r_o, and r_i are the radii of the boundary, outer pipe wall surface, and inner pipe wall surface, respectively.

To complete the energy balance, the heat flowing into and out from the differential region with the pipe fluid are given by

$$\dot{Q}_{IN} = \dot{m}\ Cp\ T(x) \tag{4.3a}$$

$$\dot{Q}_{OUT} = \dot{m}\ Cp\ T(x + dx) \tag{4.3b}$$

where $\dot{m}$ and Cp are the mass flow rate and the specific heat of the liquid in the pipe.

Assuming quasi-steady-state conditions, we set

$$\dot{Q}_{OUT} - \dot{Q}_{IN} = \dot{Q}_{SIDE} \tag{4.4a}$$

or

$$\dot{m}\ Cp\ [T(x + dx) - (T(x)] = \frac{[T_b - T(x)]dx}{R_o} \tag{4.4b}$$

This equation has the solution

$$T(x) = T_o e^{-\mu x} + T_b\ (1-e^{-\mu x}) \tag{4.5}$$

where $\mu = 1/(R_o\ \dot{m}\ Cp)$ and T_o is the initial fluid temperature.
The outlet temperature for a pipe of length L is then

$$T_1 = T(L) = T_o e^{-\mu L} + T_b\ (1-e^{-\mu L}) \tag{4.6}$$

and the overall rate of heat flow into the pipe is

$$\dot{Q}_{TOTAL} = \dot{m}\ Cp\ (T_1 - T_o)$$

$$= \dot{m}\ Cp\ (T_b - T_o)\ (1 - e^{-\mu L}) \quad . \tag{4.7}$$

If a succession of blocks is used along the length of the pipe, the inlet temperature for each succeeding block is set equal to the outlet temperature of the preceding block.

4.3 GROCS-TRNSYS Program Validation

4.3.1 Validation procedure. The validation of the GROCS-TRNSYS program had to proceed in several steps, in each of which a modification was made that was necessary or highly desirable in the final program, either because of accuracy of the results or because of the need to limit the amount of computer time used by the program. These steps are briefly described in sequence below. Later sections describe them in more detail and document the results. All validation runs used a 100 ft vertical heat exchanger with a constant-temperature boundary condition 40 ft away in the radial direction and no heat transfer to regions above or below. This was chosen to be simple enough to enable the use of an exact analytical calculation for comparison, yet permitting sufficient flexibility to allow the essential features of the final model to be tested.

1. The first step was a comparison of GROCS-TRNSYS results with those obtained from an analytical calculation for a constant rate of heat uptake* by the central pipe. A large number of narrow (0.05 ft) blocks was used with short (0.025 hr) timesteps. The purpose of this comparison was to ensure that no gross errors had been made in tying GROCS to TRNSYS or in setting up the heat exchanger subroutine that serves as an intermediary between GROCS and TRNSYS. The stand-alone version of GROCS, it should be remembered, has been extensively validated as part of previous work[3-5]. Comparisons were made of pipe temperature vs. time and of ground temperature vs. distance from the pipe for specific times of 10, 100, and 1000 hours. Close agreement between the model and the analytical calculation was obtained.

2. At this point we have a validated model for steady heat output. However, it has only been validated for block sizes too small and timesteps too short for general application with reasonable amounts of computer time. We therefore pursued comparisons of models using fewer, larger blocks (0.5 ft minimum thickness) and longer timesteps (0.25 hr) compatible with reasonable processing time.

---

*All computer runs simulated building heating, i.e., heat withdrawal from the ground. Analytical calculations used heat addition to the ground as is customary for these. Thus, in Section 4, "heat withdrawal" and "heat output" are used interchangeably. Algebraic signs are correct in all comparisons.

3. The third step was to compare the behavior of the model under pulsed withdrawal of heat with that for steady-state withdrawal. The pulsed withdrawal was intended to mimic the behavior of the system under cycling operation. It was found that, outside the pipe wall, the system behavior for the two cases was very similar for on/off cycles of #1 hr or less. This is fortunate, since the heat pump subroutine of TRNSYS accounts for part-load operation by extracting heat from the source water at a reduced rate over the entire timestep. It must do this since TRNSYS is not capable of splitting up timesteps. Thus, the only area where a cycling correction factor was found to be necessry was the pipe itself, including the pipe wall (thermal resistance) and the water in the pipe (thermal capacitance).

4. The fourth step was to incorporate a correction factor for resistance/capacitance effects in the pipe itself. For the case where there is no thermal capacitance in the pipe, the temperature difference across the pipe wall under cycling is 1/f times the temperature difference if the same total amount of heat is extracted (more slowly) at a steady rate, where f is the fraction of the time that heat is being extracted. This is true because the same amount of heat is being extracted over only a fraction of the time. For very large thermal capacitance (turning the pipe, essentially, into a tank), the temperature difference across the wall is unaffected by cycling because of the thermal inertia of the water. In this step a simple theory was developed to handle intermediate cases. It was incorporated into the model by increasing the pipe wall thermal resistance by an appropriate factor between 1 and 1/f and then applying steady state heat flow within the timestep.

5. Finally, an exact analytical solution was derived for pulsed heat uptake from a pipe including pipe wall resistance and fluid heat capacity. These results were used to verify the accuracy of the final GROCS-TRNSYS model.

4.3.2 Constant Heat Output Results.

As stated above, all validation runs used a 100 ft vertical heat exchanger with a constant-temperature boundary condition 40 ft away in the radial direction and no heat transfer to regions above or below. The physical properties and dimensions of this heat exchanger are given in Table 4.1, along with the variable names used for these quantities.

Table 4.1
Vertical Heat Exchanger Properties

Property	Variable Name	Value
Pipe length	L	100 ft
Pipe outer diameter	r_o	1.824 in.
Pipe inner diameter	r_i	1.608 in.
Pipe thermal conductivity	k_p	0.27 Btu/ft-hr-°F
Earth thermal conductivity	k_e	1.00 Btu/ft-hr-°F
Earth volume heat capacity	$C\rho$	30.0 Btu/ft^3-°F
Earth thermal diffusivity	$\alpha(=k_e/C\rho)$	0.0333 ft^2/hr
Constant heat output rate	Q	50.0 Btu/ft-hr
Fluid heat capacity	-	1.00 Btu/lb-°F

4.3.2.1 Analytical calculations.

The pipe fluid temperature. Because only radial heat flow has been allowed, the heat exchanger may be treated as an infinitely long cylindrical pipe in the analytical calculations. It is assumed that the pipe is imbedded in an infinite medium of uniform thermal properties. It will be verified afterwards that the use of constant temperature boundary conditions 40 ft from the pipe in the computer calculations produces negligible errors. Both the film resistance on the inside of the pipe wall and any contact resistance on the outside of the pipe are neglected. These resistances could be factored into the pipe wall resistance if necessary.

The fluid inside the pipe is assumed to be perfectly mixed so that is may be treated as a perfect conductor. This assumption is slightly different from the computer treatment described in Section 4.2.5 where the fluid temperature changes as it travels through the pipe, due to heat transfer with the ground. The radial gradient will be seen to be much larger, though, so the error introduced is small.

The pipe wall is treated as a pure resistance with no heat capacity in both calculations. For the pipe sizes and wall thicknesses considered, the resulting error is small. If desired, the heat capacity of the pipe could be added to that of the fluid.

With these approximations, the analytical problem to be solved is that of the temperature T(t) of a cylinder of radius r_o of a perfect conductor, surrounded by an infinite medium of uniform thermal properties. For time t>0, the perfect conductor is heated at a constant rate of Q/(unit length - unit time). A surface resistance of R_p/unit length is assumed. All initial temperatures are zero. This problem is one variation of the "buried electric cable" problem which has been solved exactly.[6] The temperature inside the perfect conductor--our fluid--at time t is given by

$$T(t) = \frac{Q}{k_e} G(h, \alpha_1, \infty, \tau) \tag{4.8}$$

where k_e is the earth thermal conductivity and $G(h, \alpha_1, \infty, \tau)$ is defined in Appendix A.

The function G has not been tabulated, an impediment to performing calculations. However, as shown in Appendix A, for the heat exchanger properties selected, over the range of times of interest (t>10 hrs), a much simpler expression for the fluid temperature,

$$T(t) = \frac{Q}{4\pi k_e} \left\{2h + \ln\left(\frac{4\tau}{c}\right)\right\} \tag{4.9}$$

is accurate to within 1%. In Eq. (4.9) $h = 2\pi R_p k_e$, $\tau = \alpha t/r_o^2$, where α is the earth thermal diffusivity, and $c \equiv e^{\gamma} = 1.7811$, where $\gamma = 0.5772...$ (Euler's constant). In Figure 4.4, the pipe fluid temperature, as given by Eq. (4.9) is compared to the GROCS-TRNSYS results described below.

<u>The ground temperature outside the pipe</u>. The pipe fluid temperature Eq. (4.9) can be rewritten as:

$$T(t) = QR_p + \frac{Q}{4\pi k_e} \left\{\ln\left(\frac{4\alpha t}{r_o^2}\right) - \gamma\right\} \tag{4.10}$$

The first term in Eq. (4.10) is the temperature rise across the thermal resistance R_p. It can be shown (see e.g. reference 7) that the second term in Eq. (4.10) is the large time ($\tau \gg 1$) approximation for the temperature a distance r_o from a continuous line source emitting heat at a rate Q/(unit length - unit time) in a medium with the thermal properties given above.

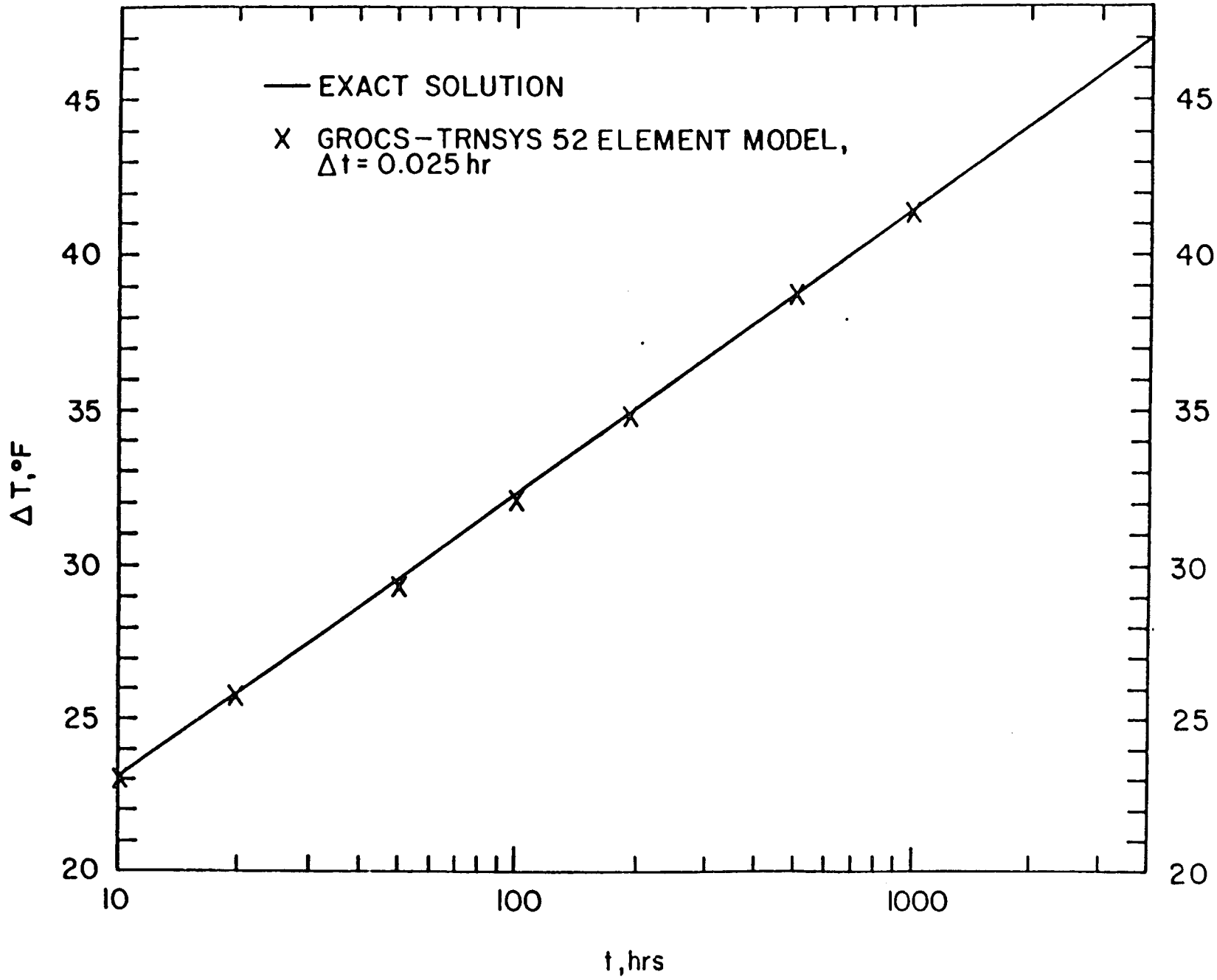

Figure 4.4 Pipe fluid temperature minus far field temperature (ΔT), steady heat output of 50 Btu/ft-hr: computed and exact solutions.

The temperature just outside the pipe is given by Eq. (4.10) without the thermal resistance term QR_p. Thus, for t > 10 hours, the line source solution correctly (to ≈1%) gives the ground temperature just outside the pipe. This suggests that the exact line source solution should work well elsewhere in the ground, for t > 10 hours, even at a distance r far from the pipe where $\alpha t/r^2$ may not be large. Thus, the temperature in the ground at distance r from the center of the pipe at time t (t > 10 hours) is given by:[7]

$$T(r, t) = \frac{Q}{4\pi k_e} \left\{-Ei\left(\frac{-r^2}{4\alpha t}\right)\right\} \tag{4.11}$$

where $-Ei(-x) \equiv \int_x^\infty \frac{e^{-u}}{u} du$

Ei(-x), called the exponential integral function, has been tabulated (see e.g. reference 8), and for small x gives:

$$Ei(-x) = \gamma + \ln x.$$

Figure 4.5 compares Eq. (4.11) with the equivalent GROCS-TRNSYS results for t = 10, 100, and 1000 hours, for 0.076 ft < r < 40 ft.

4.3.2.2 GROCS-TRNSYS Model.

A 100 foot long, 1.824 inch O.D. plastic pipe was selected for all validation runs. Initially, to identify any gross errors in the program, 52 blocks were used spanning a radius of forty feet. Each block was a cylindrical shell with thickness ranging from 0.05 feet near the pipe to 4 feet far from the pipe. Table 4.2 shows the grid layout for this model along with the layout for a simpler 12 block model discussed below. It was necessary to compute by hand the thermal resistances due to the pipe wall and 1/2 the thickness of the first block. These were input into the model using Eq. (4.2b).

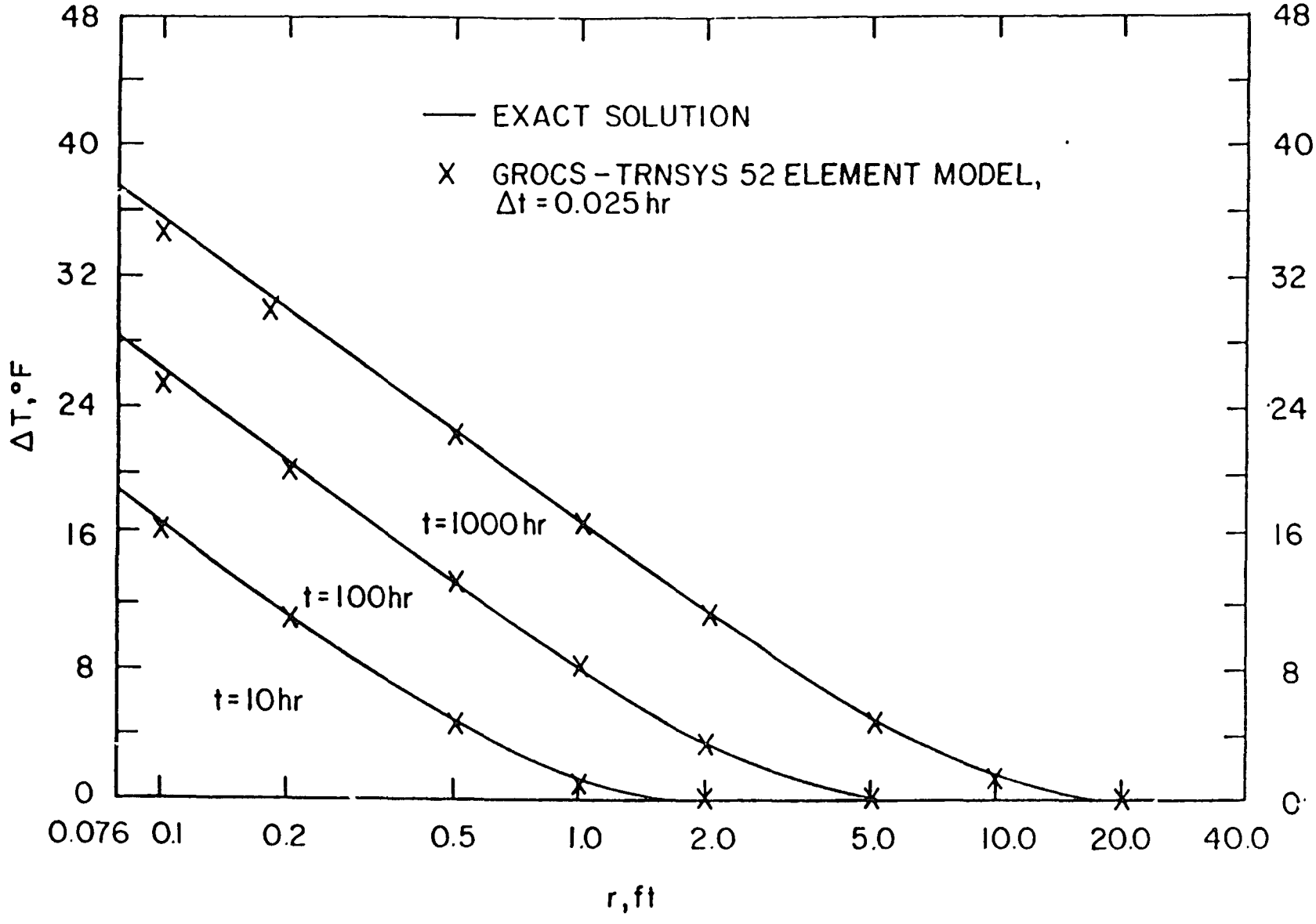

Figure 4.5 Ground temperature minus far field temperature vs. radial distance for t = 10, 100, 1000 hrs, with a steady heat output of 50 Btu/ft-hr.

Table 4.2
GROCS-TRNSYS Models Block Radii

Block Number Pipe O.D.	Outer Radius (ft)	Block Number Pipe O.D.	Outer Radius (ft)	Block Number Pipe O.D.	Outer Radius (ft)
52 Block Model					
1	0.13	19	1.1	37	5.0
2	0.18	20	1.2	38	6.0
3	0.23	21	1.3	39	7.0
4	0.28	22	1.4	40	8.0
5	0.33	23	1.5	41	9.0
6	0.38	24	1.6	42	10.0
7	0.43	25	1.7	43	12.0
8	0.48	26	1.8	44	14.0
9	0.53	27	1.9	45	16.0
10	0.58	28	2.0	46	18.0
11	0.63	29	2.2	47	20.0
12	0.68	30	2.4	48	24.0
13	0.73	31	2.6	49	28.0
14	0.78	32	2.8	50	32.0
15	0.83	33	3.0	51	36.0
16	0.88	34	3.5	52	40.0
17	0.93	35	4.0		
18	1.0	36	4.5		
12 Block Model					
1	0.5	5	3.0	9	10.0
2	1.0	6	4.0	10	15.0
3	1.5	7	5.0	11	25.0
4	2.0	8	7.0	12	40.0

The final program version does this computation internally. The heat extraction rate, $\dot{Q}$, was held constant at 5000 Btu/hr (50 Btu/ft-hr) and the fluid flow rate, $\dot{m}$, was 5000 lbs/hr. This gave a water temperature drop of $\dot{Q}/(\dot{m}Cp) = 1^{o}F$.

The iteration time step was selected by the convergence criterion for the finite difference form of the unsteady heat conduction equation[9] as:

$$\Delta t < \frac{(\Delta x)^2}{2\alpha} \tag{4.12}$$

where Δx is the width of the smallest block. For the test case with $\Delta x = 0.05$ feet, $\alpha = 1/30$ ft^2/hr, $\Delta t < 0.035$ hr. In the following runs, Δt was taken as 0.025 hours.

4.3.2.3 Comparison of GROCS-TRNSYS vs. analytical results.

Figure 4.4 compares the average fluid temperature as computed by GROCS-TRNSYS using the 52-element model to the exact solution as a function of time. Figure 4.5 compares the soil temperatures as a function of radius for times of 10, 100 and 1000 hours. The agreement is seen to be very close.

Unfortunately, the grid size and time steps associated with the 52-block model are too small for reasonable computation times during a full heating season simulation. For this reason a second, coarser model was formulated which uses 12 blocks with radii ranging from 0.50 feet close to the pipe to 40 feet far away as shown in Table 4.2. The time step can now be made much larger, according to Eq. (4.2). Figure 4.6 compares the 12 block computations to the exact solution for time steps of 0.025 hour and 1 hour. Again, the agreement is very close.

During the development of the 12 block model we questioned the method of computing the heat transfer area and block center to center distances required by GROCS-TRNSYS. GROCS calculates the block temperature change by considering the heat flow across an area between the centers of two adjacent blocks. This area is assumed to be constant between centers. For small cylindrical blocks this is a good assumption, but at small radii for large blocks, the area varies significantly. Consequently, several methods of computing an average area and block center location were considered. The first method uses the actual block interface area and locates the centers at the arithmetic mean radius of the block. A second method uses the log mean area $[A = 2\pi L(R_o-R_i)/\ln(R_o/R_i)]$ and locates the block center at the log mean radius $[\bar{r} = (R_o-R_i)/\ln(R_o/R_i)]$. Finally, since the first block experiences the most relative variation in radius, various methods of independently computing the first block center were tried, including arithmetic mean, log mean and centroid. Figure 4.7 shows the results of the computations and clearly indicates that arithmetic mean areas and centers on all blocks compare best with the exact solution.

4.3.3 Behavior of GROCS-TRNSYS Under Intermittent Operation.

4.3.3.1 Where does the earth temperature vary?

At heating loads less than the heat pump capacity, the heat pump will cycle on and off. This results in a pulsed heat withdrawal from the ground,

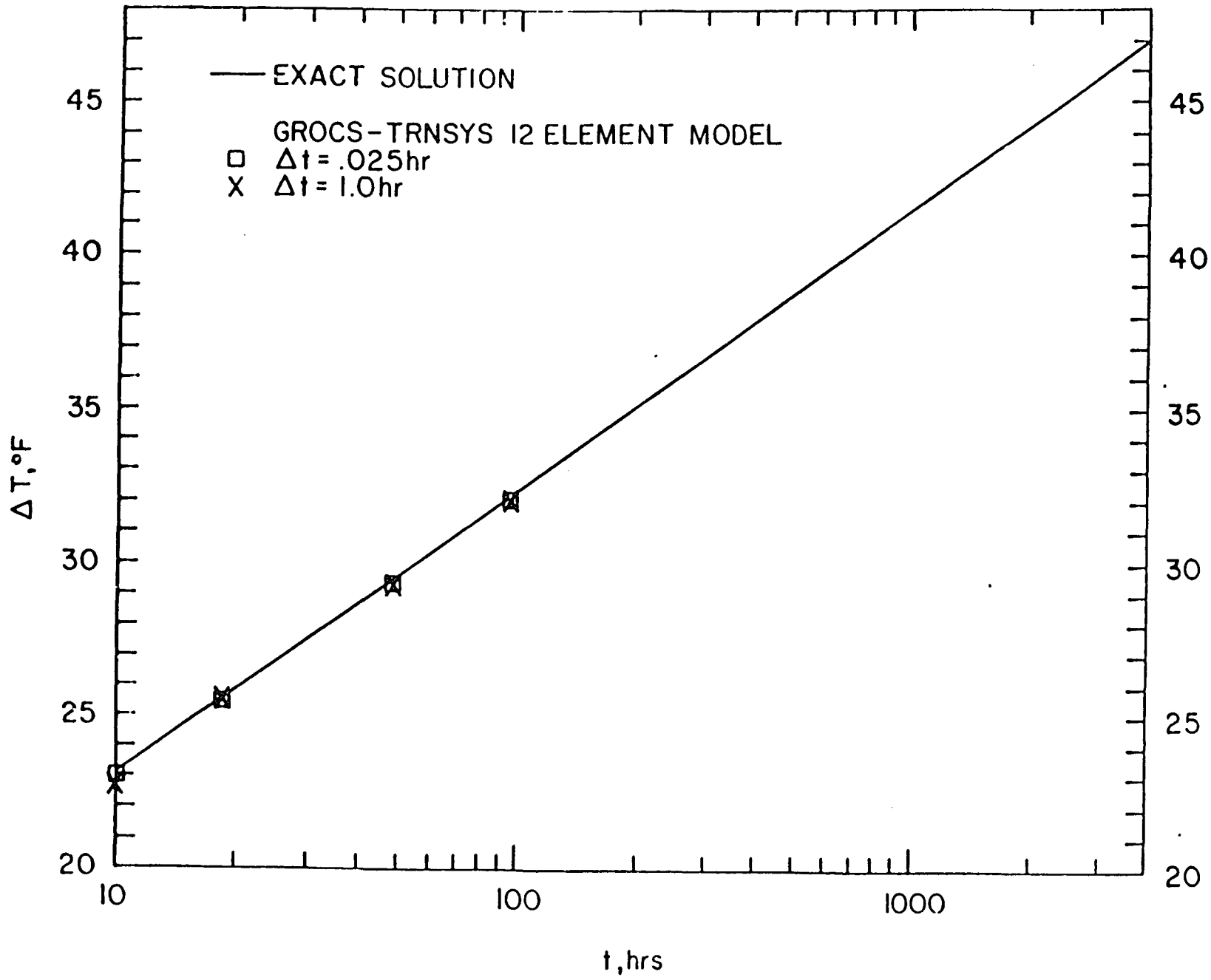

Figure 4.6 Pipe fluid temperature minus far field temperature vs. time, steady heat output = 50 Btu/hr-ft; 12 block model and exact solution.

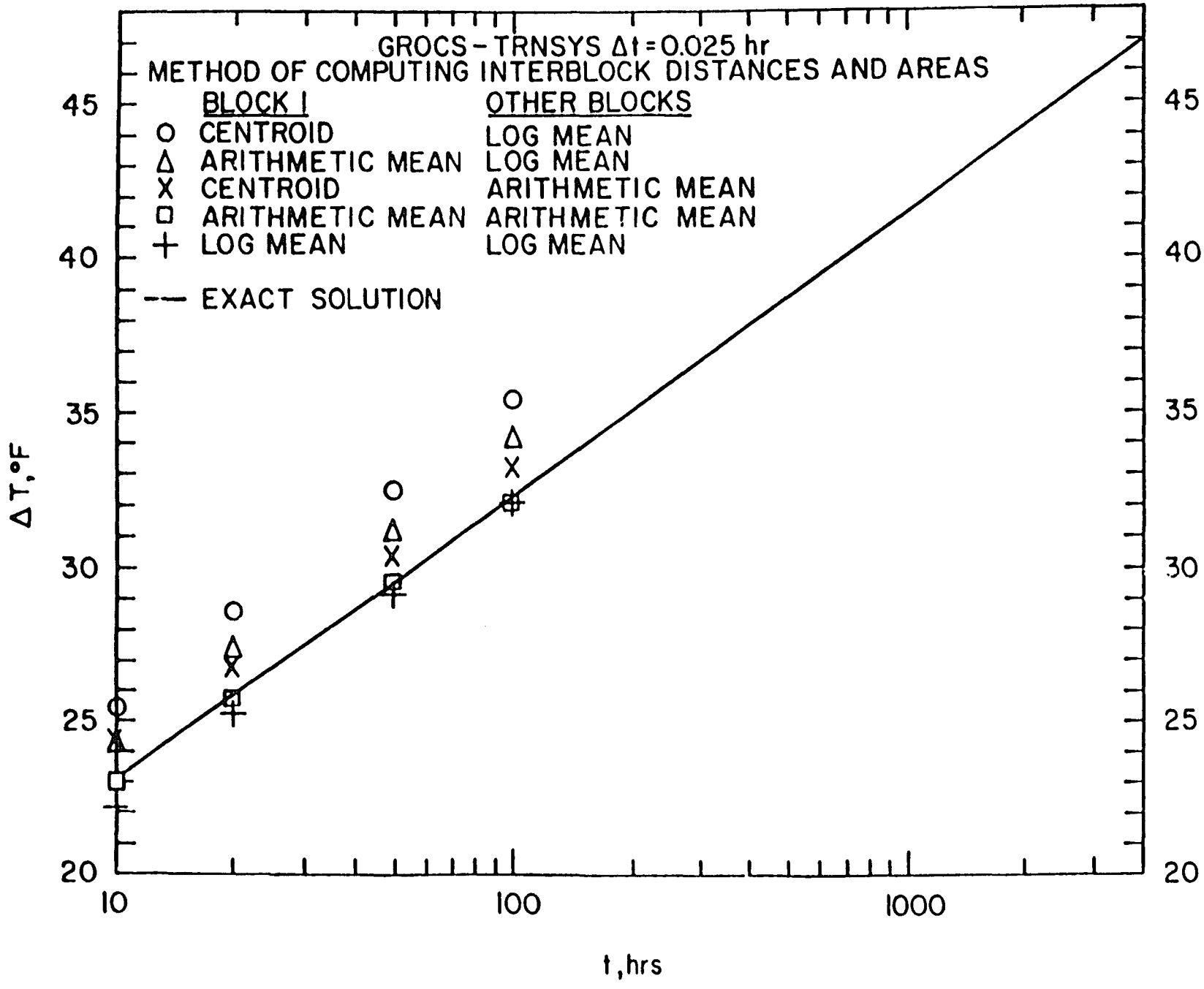

Figure 4.7 Pipe fluid temperature minus far field temperature vs. time for various GROCS element interaction assumptions, steady heat output of 50 Btu/hr-ft, 12 element model.

which gives a different fluid temperature than a steady heat withdrawal of the same average rate. We want to account for cycling (i.e. determine the correct average fluid temperature during the on-cycle), but still use large blocks and time steps. Consequently, we will withdraw heat steadily in GROCS and apply a correction factor for cycling. The derivation and justification of that factor are the subjects of this section.

First we examine the difference in earth temperature for cycling versus steady heat removal with the same total heat removed. That is, we compare the ground temperatures obtained for steady heat output of $\dot{Q}_o t_1/t_2$ to those obtained via pulsed output at the rate $\dot{Q}_o$. Here t_1 is the pulse width, and t_2 is the total cycle time, as illustrated in Figure 4.8. Computations were made of the earth temperature surrounding the pipe for pulse widths of 20%, 50%, and 80% and cycle times of 0.25, 0.5, and 1 hours. Results for the 0.5 hour run with these pulse widths are compared to the steady removal exact solution in Figure 4.9. It can be seen that the differences due to cycling are confined to a region near the pipe wall.

Figure 4.9—which it is emphasized shows the end of cycle (worst case) temperatures for the pulsed heat inputs—suggests that almost all the difference in fluid temperature between the pulsed and steady heat output cases is due to the resistance in the pipe wall and soil very near the pipe, plus the effects due to the heat capacity of the fluid in the pipe (and the pipe wall and soil near the pipe). In Section 4.3.3.2, the method developed for GROCS-TRNSYS to deal with these effects is presented.

4.3.3.2 The R-C model.

The model as constructed so far does not account for the capacitance of the pipe fluid, nor does it allow for the effects of cycling operation. It was seen in Section 4.3.3.1 above that the effects of cycling are largely confined to the pipe itself and the earth nearby, the ground outside the pipe behaving nearly the same under both steady-state and cycling operation. Also, the effects of the fluid in the pipe itself have not yet been accounted for. It was therefore decided to apply a simple resistance-capacitance model to model the behavior of the pipe under cycling conditions.

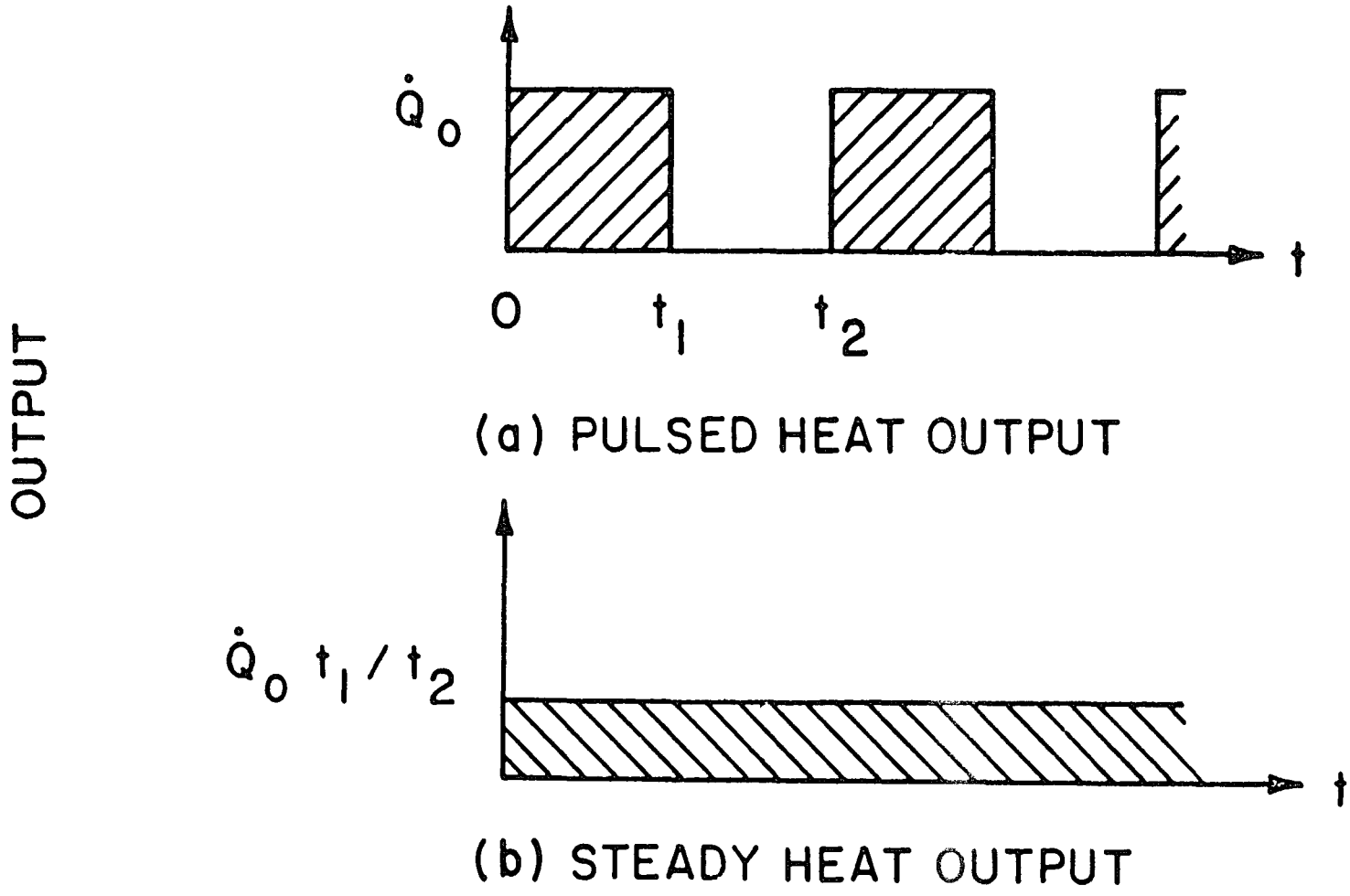

Figure 4.8 Heat output rates for pulsed and steady operation with equa average heat outputs.

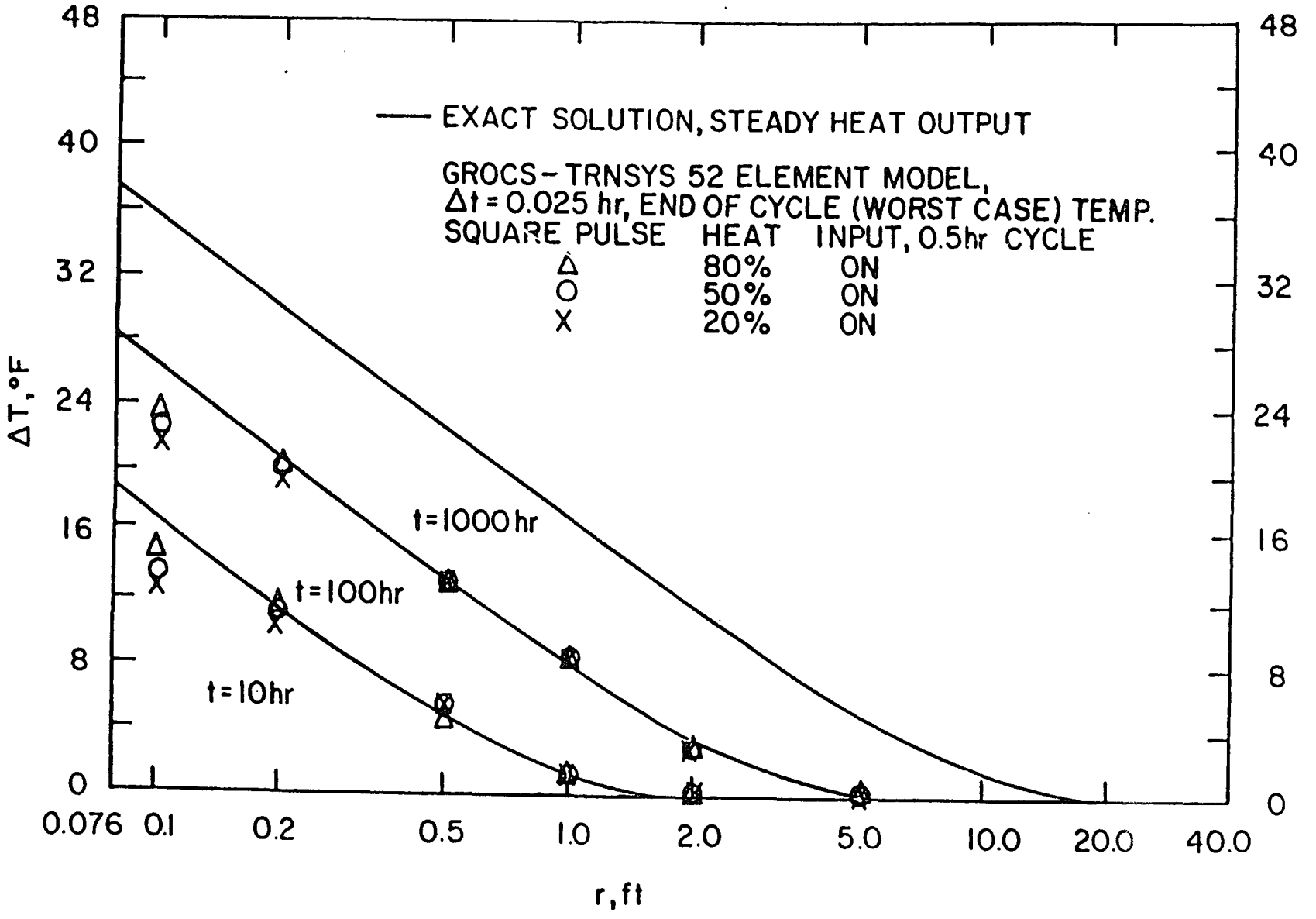

Figure 4.9 Pipe temperature minus far field temperature vs. time; pulsed compared to steady heat removal for 50 Btu/hr-ft average heat ouput.

The pipe is modeled as a simple parallel RC network, as shown in Figure 4.10, grounded on one side, that is connected to the temperature of the surrounding earth, i.e., the midpoint of GROCS block 1, and on the other side connected to the heat pump. The heat pump is assumed to cycle on and off in a repeating step function as in Figure 4.8a. During its on-cycle it extracts heat at a constant rate $\dot{Q}_o$. This assumption ignores the variation in heat pump capacity over the cycle due to changes in source water temperature during the cycle. If we let θ equal the difference between the pipe fluid temperature and the surrounding earth temperature (or equivalently the pipe fluid temperature itself on a scale where the surrounding earth temperature is zero), the governing differential equation for the R-C network shown in Figure 4.10 is:

$$Q = -C\dot{\theta} - 1/R\theta \tag{4.13}$$

The solution of this equation, derived in Appendix B, leads to the time-average source temperature during heat extraction

$$\theta_I = 1/t_1 \int_o^{t_1} \theta dt$$

$$= -\dot{Q}_o R + \frac{\dot{Q}_o R^2 C(1-e^{-(t_2-t_1)/RC})(1-e^{-t_1/RC})}{t_1(1-e^{-t_2/RC})}$$

Note that if the same amount of heat were to be removed continuously over the entire cycle $0 < t < t_2$, the ground could behave as a pure resistance and the source temperature would be

$$\theta_c = -\dot{Q}_o R t_1/t_2 \tag{4.15}$$

What is of interest is the ratio between the temperature differences for the cycling and steady state cases. If a dimensionless on-time $w = t_1/RC$ and a dimensionless off-time $\emptyset = (t_2-t_1)/RC$, then

$$\theta_I/\theta_c = \frac{1 - \dfrac{(1-e^{-w})\ (1-e^{-\emptyset})}{w[1-e^{-(w+\emptyset)}]}}{[w/(w+\emptyset)]} .$$

Table 4.3 shows some values of θ_I/θ_c for representative values of w and f. Note that all values fall between 1 and 1/f.

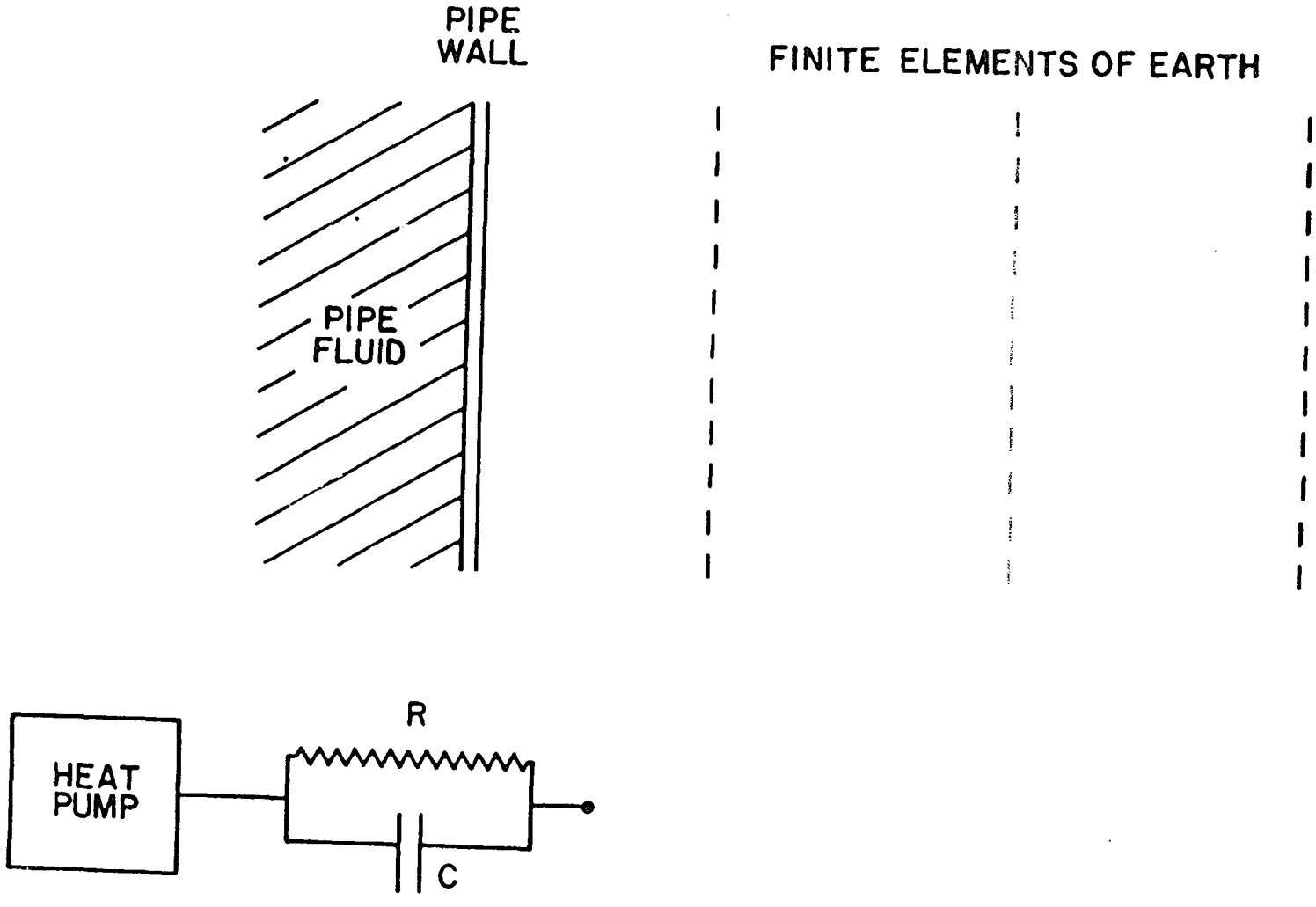

Figure 4.10 Simplified ground coupling model.

Table 4.3
Temperature Ratios θ_I/θ_c

ρ	Dimensionless On-Time $w = t_1/RC$						
	0	0.5	1.0	2.0	3.0	5.0	10.0
Duty Cycle $f = t_1/t_2$							
0.1	1.00	2.17	3.68	5.68	6.83	8.01	9.00
0.2	1.00	1.30	1.88	2.84	3.42	4.01	4.50
0.3	1.00	1.11	1.36	1.90	2.28	2.67	3.00
0.4	1.00	1.05	1.16	1.47	1.72	2.00	2.25
0.5	1.00	1.02	1.08	1.24	1.40	1.61	1.80
0.6	1.00	1.01	1.03	1.12	1.21	1.35	1.50
0.7	1.00	1.00	1.01	1.05	1.10	1.18	1.29
0.8	1.00	1.00	1.01	1.02	1.04	1.07	1.14
0.9	1.00	1.00	1.00	1.00	1.01	1.02	1.04
1.0	1.00	1.00	1.00	1.00	1.00	1.00	1.00

This result is incorporated into the GROCS-TRNSYS model by increasing the resistance of the pipe wall and 1/2 of the first block of earth by the ratio θ_I/θ_c, and then using the steady-state calculation to determine θ_c. This ratio must be recomputed at each timestep to reflect changing demands on the heat pump over time.

4.3.3.3 Evaluation of the final GROCS-TRNSYS program under intermittent operation.

To test the accuracy of the GROCS-TRNSYS approximations developed to model pulsed heat removal, an analytical solution was derived to calculate the pipe fluid temperature, given the pulsed heat input shown in Figure 4.8a. Both fluid heat capacity and pipe thermal resistance were incorporated. All physical assumptions were identical to those for the steady heat input case discussed in section 4.3.2. Exact results were obtained from the transient heat conduction equation in the form of an integral which was then evaluated numerically. Thus, this analytical solution, presented in Appendix A, provides an exact test of the GROCS-TRNSYS model results for pulsed heat withdrawal.

Figures 4.11, 4.12 and 4.13 compare the final GROCS-TRNSYS program results using the 12 block model described in Table 4.2 to the exact solution

derived in Appendix A for the pulsed heat output depicted in Figure 4.8a. Results are shown for three different fractional on-times. The average heat output rate is 5000 Btu/hr (50 Btu/ft-hr) in all cases. Agreement between the exact solutions and the GROCS-TRNSYS results are seen to be excellent.

It is interesting to note that, especially for short cycle times, the fluid temperature is close to the equivalent steady heat output result. This suggests that heat capacity effects play an important role in buffering the fluid temperature, at least for the diameter pipe and range of cycle times investigated here.

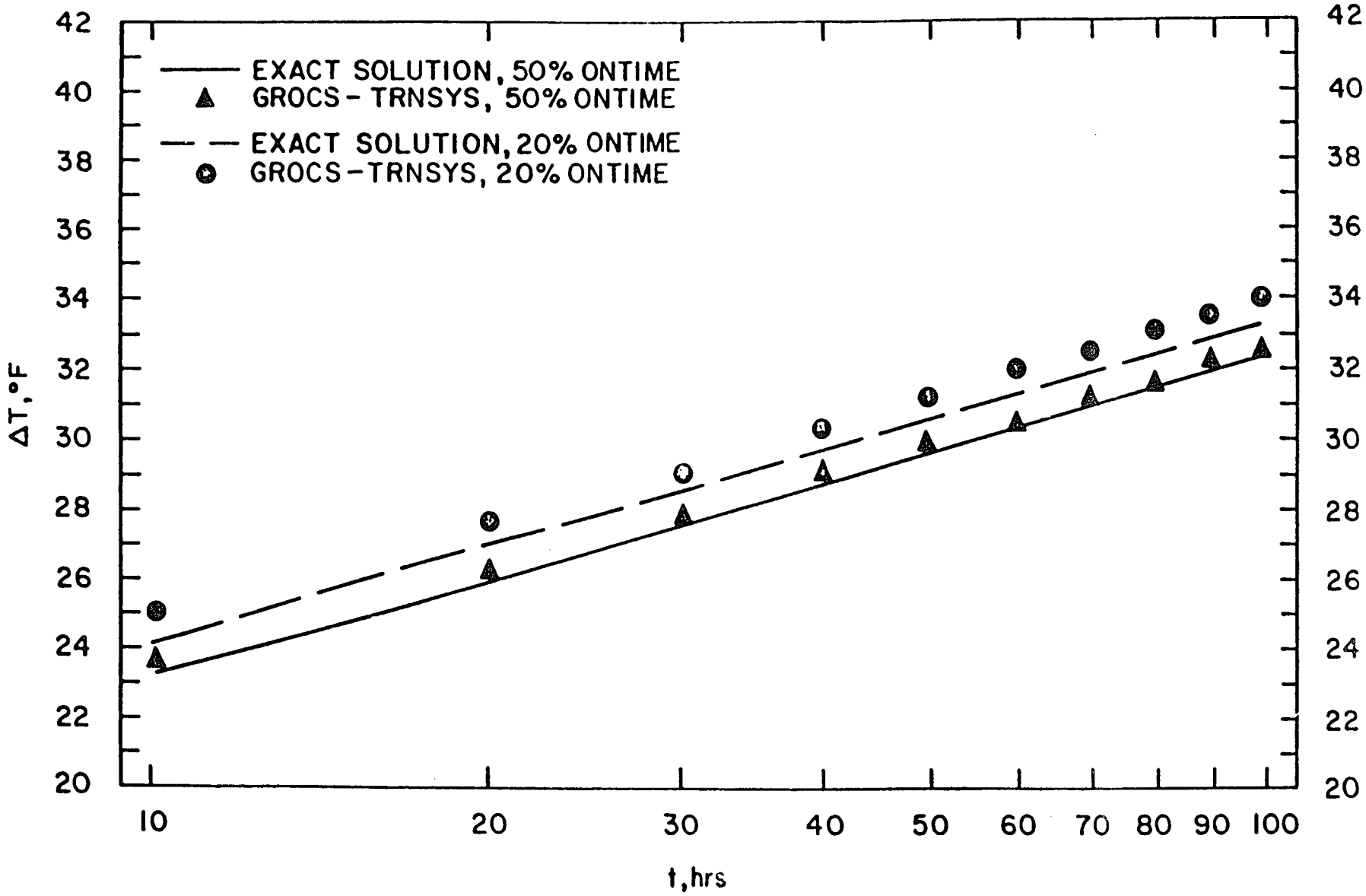

Figure 4.11 Comparison of exact solution to GROCS-TRNSYS computation (0.25 hour cycle for 20 and 50% on time).

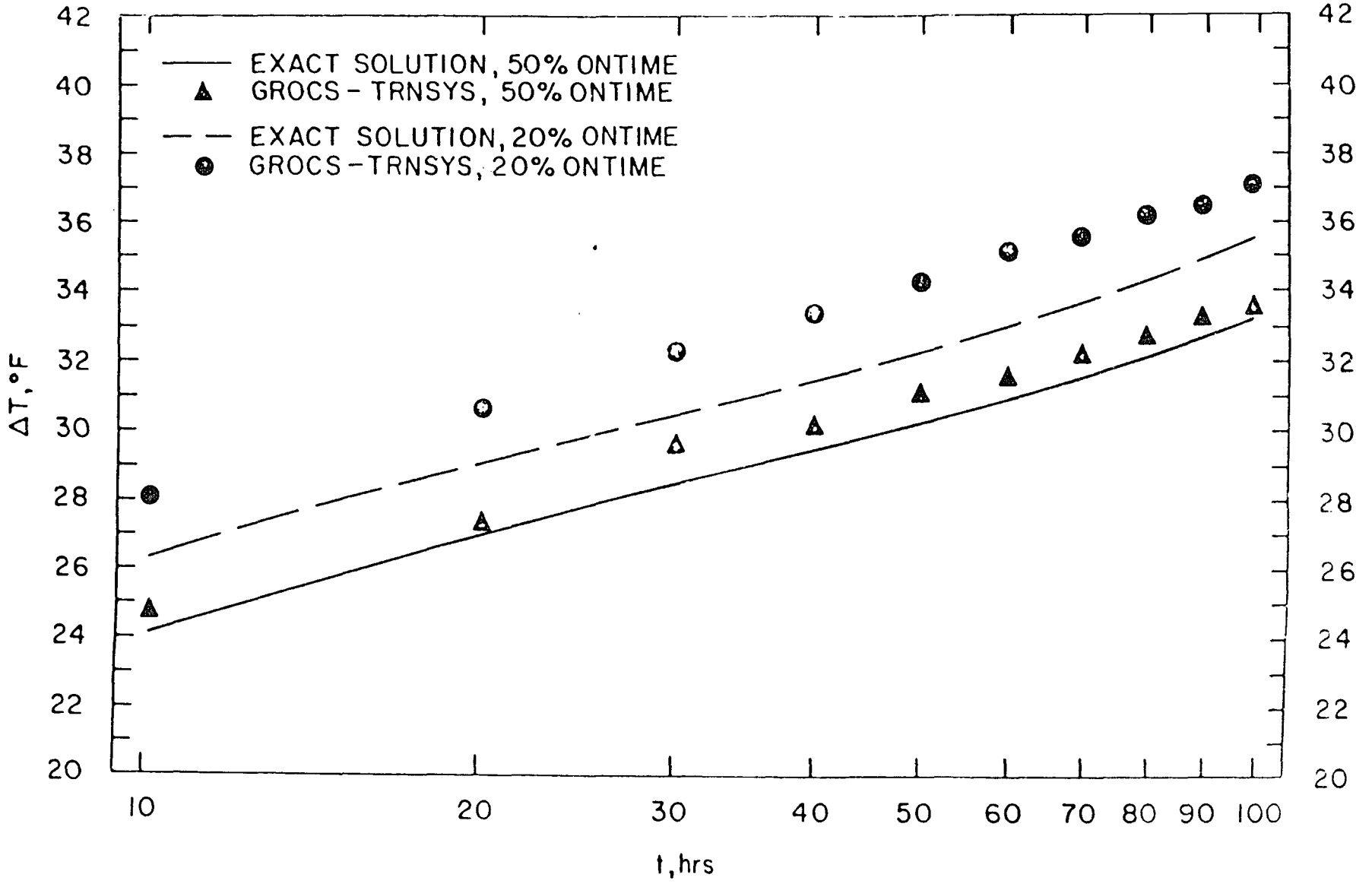

Figure 4.12 Comparison of exact solution to GROCS-TRNSYS computation (0.5 hour cycle for 20 and 50% on time).

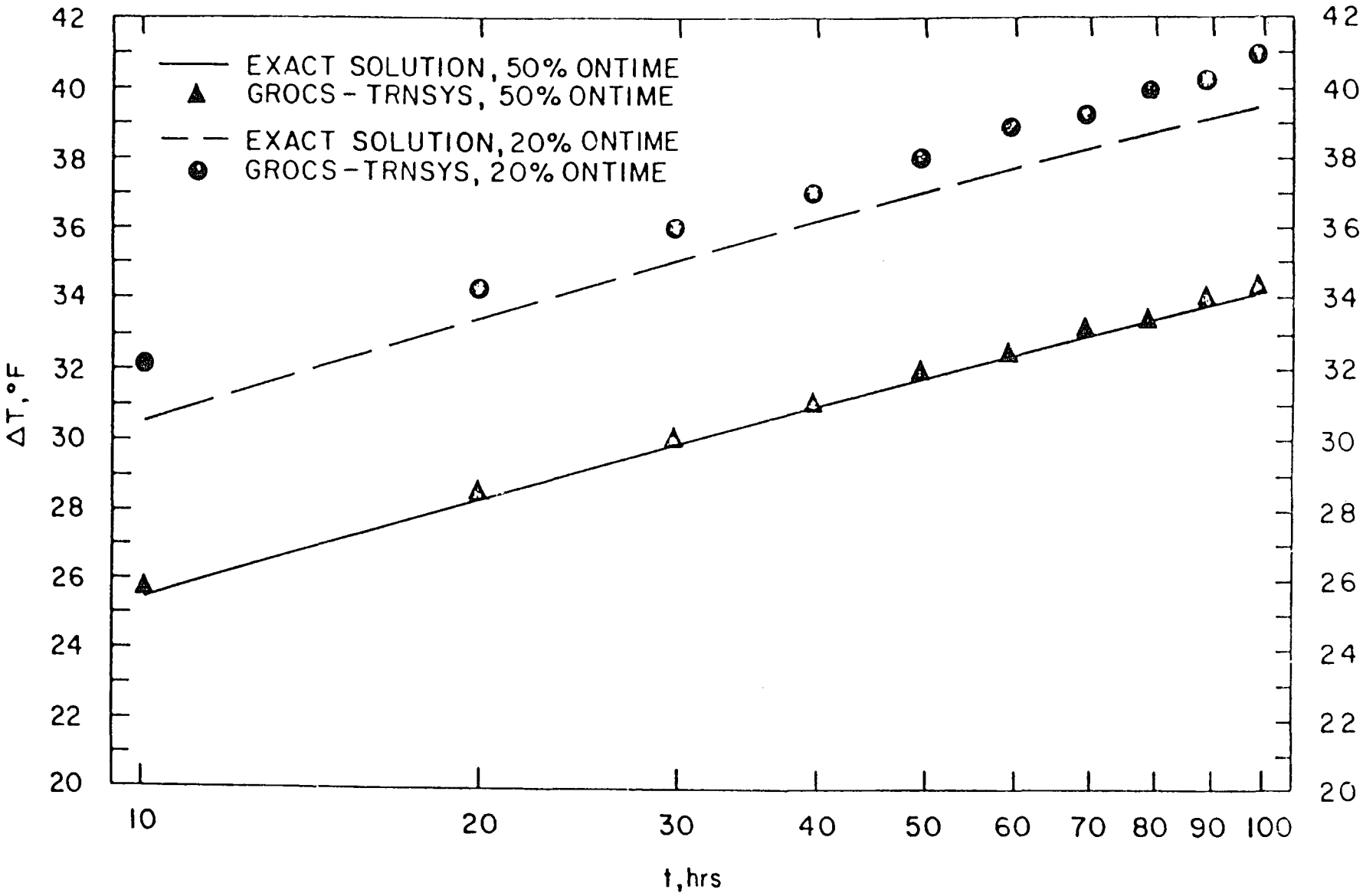

Figure 4.13 Comparison of exact solution to GROCS-TRNSYS computation (1.0 hour cycle for 20 and 50% on time).

4.4 Selection of Sample Test Conditions

4.4.1 Weather and Load Data.

An initial set of runs was performed for a house in Washington, D.C. The weather and load data for this house were taken from a tape prepared by Science Applications Inc.[10]. The house is a two-story wood-frame colonial with basement, having a 1733 ft^2 living area and 1744 ft^2 outside wall area, of which 301 ft^2 is double-glazed window. Roof insulation is 9 in. batt, wall insulation is 6 in. batt, and floor insulation is 3-1/2 in. batt. The design heating load is 31,260 Btu/hr; the design cooling load is 21,500 Btu/hr. The annual space heating load is 43.13 million Btu. The annual cooling load is 26.10 million Btu.

The weather data were taken from the Typical Meteorological Year (TMY) tapes prepared by Sandia National Laboratory[11]. These data were generated from #20 years of data by selecting the "most typical" January, Febraury, etc., and then merging these typical months (which come from different years) into a typical year for each location. Some efforts to smooth the boundaries between the months, to avoid unreasonably abrupt changes in meteorological conditions, were made.

4.4.2 Heat Pump Performance Data

Heat pump capacity and COP. In order to perform the simulation runs necessary to obtain source-temperature/load maps, it was necessary to specify the performance of the heat pump used in the system. This comes about because a more efficient heat pump will draw more heat from the ground and use less electricity to meet a given load than will a less efficient heat pump. Since the end result of this research effort is to be a heat pump with improved, but at present unknown, performance characteristics, there is a degree of circularity in the procedure. Fortunately, the influence of heat pump performance on the source temperatures is not expected to be too great within the range of COP's we can resonably expect. For example, consider a 400 ft vertical pipe field with an overall average heat extraction coefficient of 2.0 Btu/^{o}F-hr-linear ft. Assume a load of 30,000 Btu/hr, to be met alternatively at COP's of 3.0 and 3.5. As shown in Table 4.4, the change in source temperatures is less than 2°F.It is unlikely that a change as small as this will change the optimum heat pump design significantly.

Table 4.4
Comparison of Source Temperatures for Different COP's

COP	3.0	3.5
Load (Btu/hr)	30,000	30,000
Heat from ground (Btu/hr)	20,000	21,429
Source temperature, °F below far-field	25	26.79

In order to derive reasonable heat pump performance curves, data for two water source heat pumps used in system tests at BNL were used. These heat pumps are the Command Aire Model 210 and the Mammoth Model 027. In addition, data for a two-speed prototype constructed by Lennox Industries for solar applications were included. Water flow rates were 6 gpm for the Mammoth and Command-Aire units and 10 gpm for the Lennox unit.

For heating, the benchmark capacity curve was taken to follow the Mammoth and Command Aire units. The COP curve was taken to fall above those of the Mammoth, Command Aire, and Lennox high speed units but with the same slope. For cooling, benchmark COP and capacity curves were chosen to represent a rough average of the available data.

Heating capacity was pegged at 30,000 Btu/hr at 30°F EWT. The ratio of heating capacity at 45°F EWT and cooling capacity at 70°F EWT ranged from 0.77 to 0.84. A median value of 0.82 was selected, which then permitted cooling capacities to be calculated. The resulting set of performance data as used in GROCS-TRNSYS is shown in Table 4.5.

4.4.3 Ground Heat Exchanger Configuration and Sizing

For the sample runs, a vertical pipe 1.824 inches O.D. and 60 feet long was used as the basic ground heat exchanger. Figure 4.14 shows the GROCS-TRNSYS block layout for this system. The program allows the basic heat exchanger to be run in parallel by specifying the number of pipes on input. For these runs 6, 7, and 8 pipes were used.

4.5 Generation of Sample Source Temperature/Load Maps

The source temperature load map is a matrix representing the number of clock hours that the temperatures and loads fell into discrete bins. Table 4.6 shows a sample heating season run with 6 60-foot pipes. Temperature bins of 5°F and load bins of 2000 Btu/hr were used. Clock hours were generated with the histogram feature of TRNSYS by computing temperature histograms for

Table 4.5
Heat Pump Performance Values Used in GROCS-TRNSYS Runs
All Energy Quantities in Btu/hr

		Heating, Hot Water		
EWT (°F)	COP	Capacity	Compressor work	Heat absorbed
20	3.0	25160	8390	16770
25	3.1	27580	8900	18680
30	3.2	30000	9380	20620
35	3.3	32420	9820	22600
40	3.4	34840	10250	24590
45	3.5	37270	10650	26620
50	3.6	39690	11020	28670
55	3.7	42110	11380	30730
60	3.8	44540	11720	32820

		Cooling		
EWT (°F)	COP	Heat rejected	Compressor work	Capacity
40	5.668	42770	6410	36360
60	4.602	39550	7060	32490
80	3.536	36710	8090	28620
100	2.470	34770	10020	24750
120	1.404	35750	14870	20880

each load bin. Data was then written onto a file and read by a second program which printed the source temperature load maps. It is likely that heat pump running hours rather than clock hours are desired for input to the ORNL heat pump optimization program. If so, the conversion can easily be done with the following conversion, applied to each matrix element:

$$T_{HP} = \frac{LOAD}{CAPACITY} \cdot T_{CLOCK}$$

here T_{HP} is the number of heat pump running hours, T_{CLOCK} is the number of clock hours, LOAD is the midpoint of the load range in Btu/hr for the given matrix element, and CAPACITY is the heat pump capacity at an entering water temperature equal to the midpoint of the range for the given matric element. If there is a part-load correction to the capacity, this can be applied at this point in a straightforward manner.

The source temperature load map for 7 parallel pipes is shown in Table 4.7 and for 8 parallel pipes in Table 4.8. As expected, the source temperature for a given load is higher with more pipes, since the heat is withdrawn over a larger area. It should be noted that these maps are presented to illustrate the procedure in computing them and not as a final ground heat exchanger design. The appropriate design will be addressed in the second phase of the project.

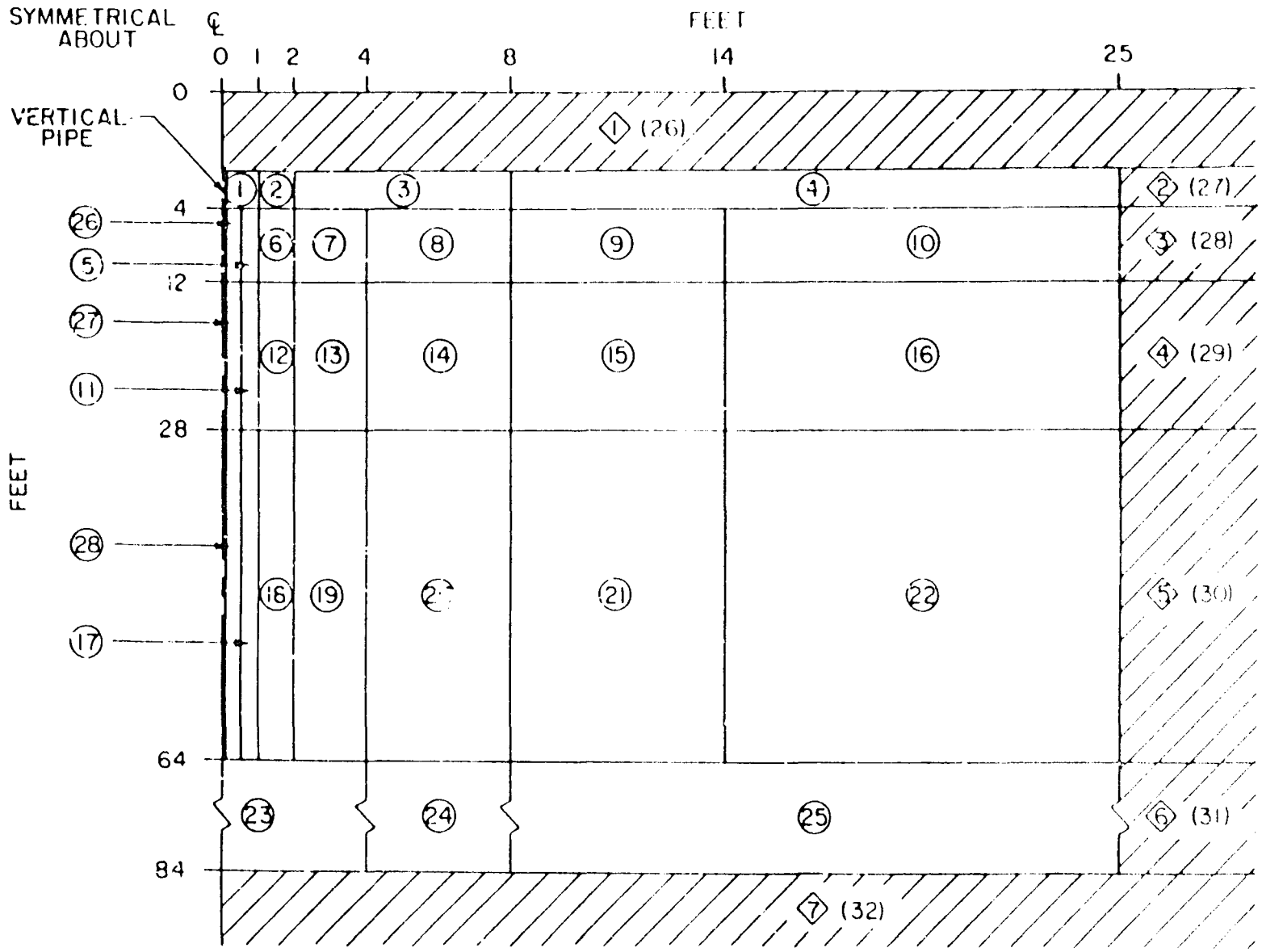

Figure 4.14. Cross-section diagram of GROCS-TRNSYS vertical heat exchanger model.

Table 4.6
Heating Season Source Temperature Load Map
(6 PIPES; $C\rho$ = 30 Btu/ft^3-^{o}F; k_e = 1 BTU/FT-HR-^{o}F)

	TEMPERATURES									
	<20	20-25	25-30	30-35	35-40	40-45	45-50	50-55	55-60	>60
LOAD	CLOCK HOURS/SEASON									
2000.0	0.0	0.0	0.0	0.0	1.0	23.0	54.0	61.0	8.0	7.0
4000.0	0.0	0.0	0.0	6.0	96.0	268.0	345.0	307.0	18.0	104.0
6000.0	0.0	0.0	0.0	16.0	83.0	190.0	170.0	90.0	6.0	21.0
8000.0	0.0	0.0	0.0	47.0	86.0	104.0	43.0	0.0	0.0	0.0
10000.0	0.0	0.0	4.0	129.0	140.0	87.0	31.0	0.0	0.0	0.0
12000.0	0.0	0.0	22.0	202.0	196.0	51.0	19.0	0.0	0.0	0.0
14000.0	0.0	0.0	60.0	252.0	154.0	31.0	3.0	0.0	0.0	0.0
16000.0	0.0	0.0	158.0	263.0	87.0	13.0	1.0	0.0	0.0	0.0
18000.0	0.0	7.0	232.0	176.0	43.0	2.0	0.0	0.0	0.0	0.0
20000.0	0.0	27.0	215.0	96.0	19.0	0.0	0.0	0.0	0.0	0.0
22000.0	0.0	67.0	118.0	24.0	1.0	0.0	0.0	0.0	0.0	0.0
24000.0	0.0	74.0	31.0	2.0	0.0	0.0	0.0	0.0	0.0	0.0
26000.0	0.0	63.0	4.0	0.0	0.0	0.0	0.0	0.0	0.0	0.0
28000.0	0.0	39.0	0.0	0.0	0.0	0.0	0.0	0.0	0.0	0.0
30000.0	0.0	10.0	0.0	0.0	0.0	0.0	0.0	0.0	0.0	0.0
32000.0	0.0	13.0	0.0	0.0	0.0	0.0	0.0	0.0	0.0	0.0
34000.0	0.0	0.0	0.0	0.0	0.0	0.0	0.0	0.0	0.0	0.0
36000.0	0.0	0.0	0.0	0.0	0.0	0.0	0.0	0.0	0.0	0.0
38000.0	0.0	0.0	0.0	0.0	0.0	0.0	0.0	0.0	0.0	0.0
40000.0	0.0	0.0	0.0	0.0	0.0	0.0	0.0	0.0	0.0	0.0

Table 4.7
Heating Season Source Temperature Load Map
(7 PIPES; $C\rho$ = 30 Btu/ft^3-^{o}F; k_e = 1 BTU/FT-HR-^{o}F)

	TEMPERATURES									
	<20	20-25	25-30	30-35	35-40	40-45	45-50	50-55	55-60	>60
LOAD	CLOCK HOURS/SEASON									
2000.0	0.0	0.0	0.0	0.0	0.0	12.0	55.0	66.0	13.0	7.0
4000.0	0.0	0.0	0.0	0.0	35.0	201.0	419.0	361.0	28.0	99.0
6000.0	0.0	0.0	0.0	1.0	44.0	156.0	204.0	143.0	11.0	18.0
8000.0	0.0	0.0	0.0	4.0	85.0	95.0	85.0	11.0	0.0	0.0
10000.0	0.0	0.0	0.0	19.0	172.0	147.0	51.0	1.0	0.0	0.0
12000.0	0.0	0.0	0.0	68.0	245.0	148.0	30.0	0.0	0.0	0.0
14000.0	0.0	0.0	0.0	158.0	202.0	128.0	12.0	0.0	0.0	0.0
16000.0	0.0	0.0	4.0	254.0	195.0	63.0	7.0	0.0	0.0	0.0
18000.0	0.0	0.0	30.0	315.0	101.0	14.0	0.0	0.0	0.0	0.0
20000.0	0.0	0.0	67.0	227.0	59.0	3.0	0.0	0.0	0.0	0.0
22000.0	0.0	0.0	95.0	98.0	17.0	1.0	0.0	0.0	0.0	0.0
24000.0	0.0	0.0	82.0	24.0	2.0	0.0	0.0	0.0	0.0	0.0
26000.0	0.0	0.0	67.0	0.0	0.0	0.0	0.0	0.0	0.0	0.0
28000.0	0.0	1.0	38.0	0.0	0.0	0.0	0.0	0.0	0.0	0.0
30000.0	0.0	0.0	9.0	4.0	0.0	0.0	0.0	0.0	0.0	0.0
32000.0	0.0	6.0	7.0	0.0	0.0	0.0	0.0	0.0	0.0	0.0
34000.0	0.0	0.0	0.0	0.0	0.0	0.0	0.0	0.0	0.0	0.0
36000.0	0.0	0.0	0.0	0.0	0.0	0.0	0.0	0.0	0.0	0.0
38000.0	0.0	0.0	0.0	0.0	0.0	0.0	0.0	0.0	0.0	0.0
40000.0	0.0	0.0	0.0	0.0	0.0	0.0	0.0	0.0	0.0	0.0

Table 4.8
Heating Season Source Temperature Load Map
(8 PIPES; $C\rho$ = 30 Btu/ft^3-^{o}F; k_e = 1 BTU/FT-HR-^{o}F)

	TEMPERATURES									
	<20	20-25	25-30	30-35	35-40	40-45	45-50	50-55	55-60	>60
LOAD	CLOCK HOURS/SEASON									
2000.0	0.0	0.0	0.0	0.0	0.0	5.0	50.0	68.0	23.0	6.0
4000.0	0.0	0.0	0.0	0.0	6.0	148.0	428.0	420.0	47.0	94.0
6000.0	0.0	0.0	0.0	0.0	15.0	126.0	239.0	167.0	12.0	17.0
8000.0	0.0	0.0	0.0	0.0	45.0	109.0	94.0	22.0	0.0	0.0
10000.0	0.0	0.0	0.0	0.0	127.0	172.0	79.0	12.0	0.0	0.0
12000.0	0.0	0.0	0.0	2.0	206.0	224.0	59.0	0.0	0.0	0.0
14000.0	0.0	0.0	0.0	12.0	283.0	180.0	25.0	0.0	0.0	0.0
16000.0	0.0	0.0	0.0	42.0	365.0	101.0	14.0	0.0	0.0	0.0
18000.0	0.0	0.0	0.0	138.0	264.0	57.0	1.0	0.0	0.0	0.0
20000.0	0.0	0.0	0.0	153.0	174.0	29.0	0.0	0.0	0.0	0.0
22000.0	0.0	0.0	0.0	153.0	54.0	3.0	0.0	0.0	0.0	0.0
24000.0	0.0	0.0	1.0	102.0	4.0	0.0	0.0	0.0	0.0	0.0
26000.0	0.0	0.0	14.0	54.0	0.0	0.0	0.0	0.0	0.0	0.0
28000.0	0.0	0.0	12.0	26.0	0.0	0.0	0.0	0.0	0.0	0.0
30000.0	0.0	0.0	6.0	4.0	0.0	0.0	0.0	0.0	0.0	0.0
32000.0	0.0	0.0	13.0	0.0	0.0	0.0	0.0	0.0	0.0	0.0
34000.0	0.0	0.0	0.0	0.0	0.0	0.0	0.0	0.0	0.0	0.0
36000.0	0.0	0.0	0.0	0.0	0.0	0.0	0.0	0.0	0.0	0.0
38000.0	0.0	0.0	0.0	0.0	0.0	0.0	0.0	0.0	0.0	0.0
40000.0	0.0	0.0	0.0	0.0	0.0	0.0	0.0	0.0	0.0	0.0

Section 4. References

1. Andrews, J.W., A TRNSYS-compatible model of ground-coupled storage, BNL 51061, Sept. 1979.
2. Klein, S.A., et al., TRNSYS, a transient simulation program, Univ. of Wisconsin-Madison, Report 38-10, 1979.
3. Metz, P.D., A simple computer program to model three-dimensional underground heat flow with realistic boundary conditions, ASME J. Solar Energy Eng., 105, 42-49, 1983.
4. Metz, P.D., The use of ground-coupled tanks in solar-assisted heat-pump systems, ASME J. Solar Energy Eng., 104, 366-372 (1982).
5. Metz, P.D., The use of serpentine earth coil in ground coupled heat pump systems, to be presented at the ASME 5th Ann. Solar Energy Div. Tech. Conf., April 18-21, 1983, Orlando, FL.
6. H.S. Carlslaw and J.C. Jaeger, Conduction of Heat in Solids, 2nd ed., p. 344-345, Oxford at the Clarendon Press, 1959.
7. H.S. Carlslaw and J.C. Jaeger, op. cit, p. 261-262.
8. M. Abramowitz and I.A. Stegun, Handbook of Mathematical Functions, Dover Publications, Inc., NY, 1970. [Note that these authors call -Ei(-x) as defined here, $E_1(x)$].
9. J. P. Holman, Heat Transfer, McGraw Hill, New York (1968).
10. P.J. Hughes and J.H. Morehouse, "A TRNSYS - Compatible Standardized Load Model for Residential System Studies - Final Report," SERI/TR-98150-3, June 1980.
11. J.J. Hall, et al., "Generation of Typical Meteorological Years for 26 SOLMET Stations," Sandia Laboratories Report No. SAND-78-1601 (1978).

5. CONCLUSION

5.1 Task 1. Water-Refrigerant Heat Exchanger Model Development

Experimentally validated models have been developed for both shell-and-tube and tube-in-tube water-refrigerant heat exchangers. Work continues to integrate these models into the ORNL Heat Pump Model. The BNL Heat Pump Simulator has proven to be a valuable and flexible experimental tool in this work. A powerful approach for modeling water-refrigerant heat exchangers has been developed.

5.2 Task 2. Source Temperature/Load Map Development

The goal of this task has been achieved. Sample source temperature load maps have been generated. In addition, a greatly improved GROCS-TRNSYS program, capable of simulating ground coupled heat pump systems under realistic cycling conditions, has been developed.

An isolated pipe model, suitable for either vertical or horizontal pipe ground heat exchangers, has been developed. This model can be used as is in a modular form (developed but not discussed here) to simulate shallow horizontal earth coils. For either vertical tube-in-tube or U-tube heat exchangers, additional correction factors will have to be developed.

APPENDIX A

CYLINDRICAL HEAT EXCHANGER SOLUTION

A.1 Steady Heat Output

The problem to be solved is that of the temperature T(t) of a cylinder of radius r_o of a perfect conductor with finite heat capacity, surrounded by an infinite medium of uniform thermal properties. For time t>0, the perfect conductor is heated at a constant rate of Q/(unit length - unit time). A surface resistance of R_p/unit length is assumed. All initial temperatures are zero. This problem is one variation of the "buried electric cable" problem which has been solved exactly.[1] The temperature inside the perfect conductor--our fluid--at time t is given by

$$T(t) = \frac{Q}{k_e} G(h, \alpha_1, \infty, \tau) \tag{A.1}$$

where k_e is the earth thermal conductivity, $h = 2\pi R_p k_e$, $\alpha_1 = 2\pi r_o^2 \rho C/S_1$, r_o = pipe radius, S_1 = fluid thermal capacity/unit length, ρ = ground density, C = ground heat capacity, $\tau = \alpha t/r_o^2$, and $\alpha = k_e/C\rho$.
G is given by[1]:

$$G(h, \alpha_1, \infty, \tau) = \frac{2\alpha_1^2}{\pi^3} \int_0^\infty \frac{\left[1-e^{-u^2\tau}\right]}{u^3\Delta(u)} du \tag{A.2}$$

where $\Delta(u) = \left[uJo(u)-(\alpha_1-hu^2)J_1(u)\right]^2 + \left[uYo(u)-(\alpha_1-hu^2)Y_1(u)\right]^2$ and Jo and J_1 are Bessel functions of the first kind of order 0 and 1, while Yo and Y_1 are of the second kind.

As noted in Section 4.3, the function G has not been tabulated[1], an impediment to performing calculations. However, for the physical properties and dimensions selected, Q = 50.0 Btu/ft-hr, r_o = 0.076 ft, k_e = 1.00 Btu/ft-hr-°F, $C\rho$ = 30.0 Btu/ft^3-°F, and $\alpha = k_e/C\rho \approx 0.033$ ft^2/hr, over the range of times of interest (t > 10 hours), the dimensionless time τ is large (e.g. for t = 10 hours, $\tau \approx 57.71$). This permits the use of a large τ approximation for G, giving[1]:

$$T(t) = \frac{Q}{4\pi k_e} \left\{2h + \ln\left(\frac{4\tau}{c}\right) - \frac{(4h-\alpha_1)}{2\alpha_1\tau} + \frac{\alpha_1-2}{2\alpha_1\tau} \ln\left(\frac{4\tau}{c}\right) + \ldots\right\} \tag{A.3}$$

where $c \equiv e^\gamma \approx 1.7811$, and $\gamma = 0.5772\ldots$ (Euler's Constant).

The pipe wall resistance is given by (see e.g. reference 2):

$$R_p = \frac{1}{2\pi k_p} \ln\left(\frac{r_o}{r_i}\right) \approx 0.07430 \text{ ft-hr-°F/Btu} \tag{A.4}$$

so that $h = 2\pi R_p k_e \approx 0.4668$, where k_p = pipe thermal conductivity (0.27 Btu/ft-hr-^oF), r_o = outer pipe radius (0.076 ft), and r_i = inner pipe radius (0.067 ft).

The fluid thermal capacity/unit length is given by:

$S_1 = \pi \times (0.067\ ft)^2 \times 1.00\ Btu/lb\text{-}^oF \times 62.4\ lb/ft^3 \approx 0.8800\ Btu/ft^oF$,

and

$\alpha_1 \approx 1.237$.

The large τ expression for T(t), Eq. (A.3) can be further approximated with little error. For example, for t = 10 hours, i.e., $\tau \approx 57.71$, the terms in the bracket on the right hand side of Eq. (A.3) are: $2h \approx 0.9336$, $\ln(4\tau/C) \approx 4.864$, $(4h-\alpha_1)/2\alpha_1\tau \approx 0.004414$, and $(\alpha_1-2)/2\alpha_1\tau\ \ln(4\tau/C) \approx -0.02599$. It can be seen that the last 2 terms are less than 1% of the first 2 terms. For larger times these terms can be seen to become even less important. Thus, to within 1%, for t > 10 hours, we can use:

$$T(t) = \frac{Q}{4\pi k_e}\left\{2h + \ln\left(\frac{4\tau}{c}\right)\right\} \tag{A.5}$$

This is Eq. (4.9) in the text.

A.2 Pulsed Heat Output

Since the unsteady heat conduction equation is linear, the pulsed solution may be generated from the constant heat output solution by the principle of superposition. First it is noted that the pulsed heat output may be expressed as a sum of constant heat outputs as illustrated in Figure A.1.

If $T_c(t)$ is the temperature of a conductor of radius r_o at time t with constant heat output as given by Eq. (A.1), by superposition the temperature of the same conductor after N+1 cycles of pulsed heat output may be written as:

$$\begin{aligned} T(t) &= T_c(t) - Tc(t-t_1) + T_c(t-t_2) - T_c(t-t_1-t_2) \\ &\quad + \cdots + T_c(t-Nt_2) - T(t-Nt_2-t_1) \\ &= \sum_{n=0}^{N} T_c(t-nt_2) - T_c(t-nt_2-t_1) \quad . \end{aligned} \tag{A.6}$$

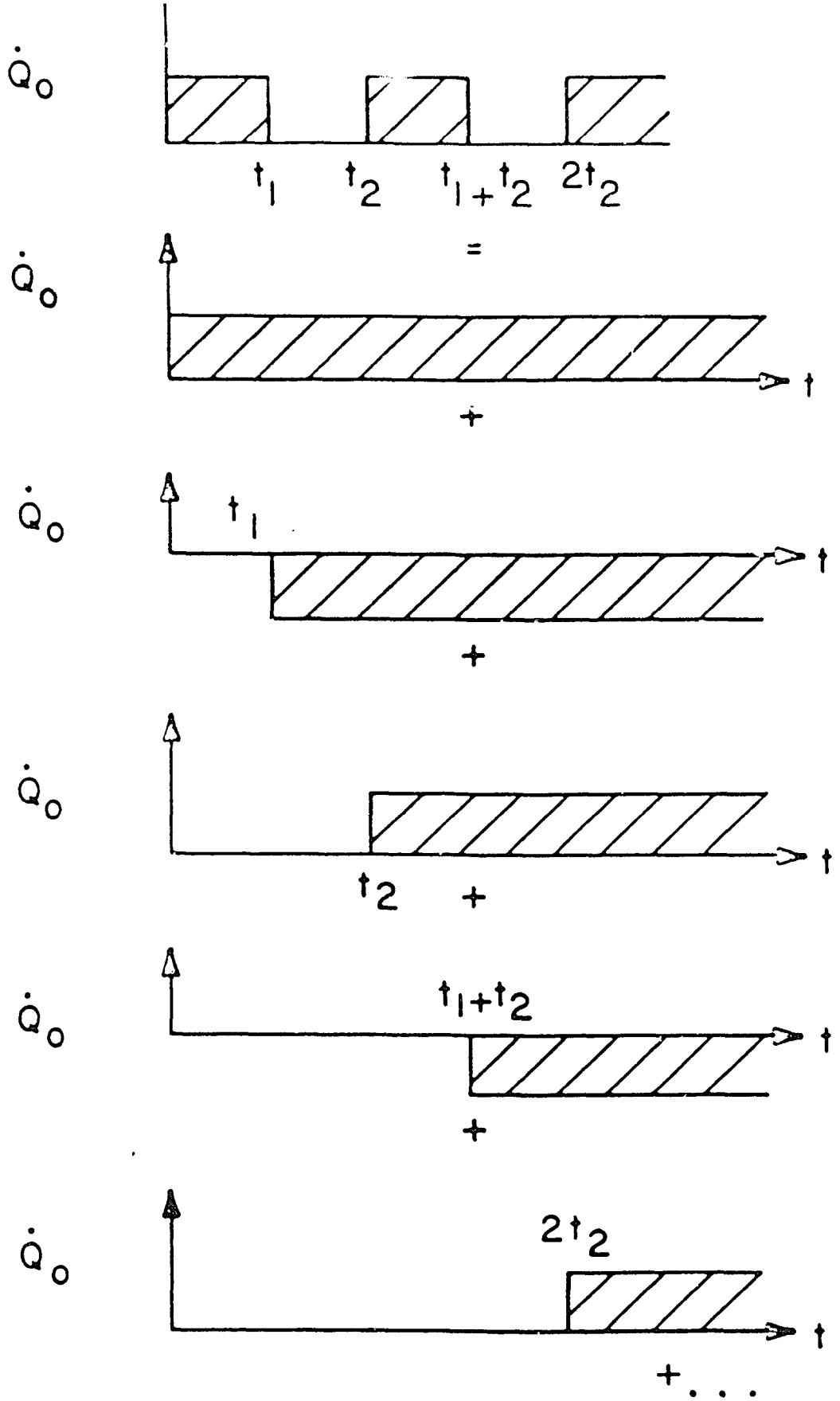

Figure A.1 Pulsed heat output can be represented as a sum of steady heat outputs.

Using Eq. (A.1), (A.2) and (A.6), and writing

$$\beta = \frac{\dot{Q}_o}{k_e}\frac{2\alpha_1^2}{\pi^3}$$

we have:

$$T = \beta\int_o^\infty \frac{1}{u^3\Delta(u)}\left\{\sum_{n=o}^{N} 1-\exp\left[-u^2(\tau-n\tau_2)\right] - \sum_{n=o}^{N} 1-\exp\left[-u^2(\tau-\tau_1-n\tau_2\right]\right\}du \tag{A.7}$$

$$= \beta\int_o^\infty \frac{1}{u^3\Delta(n)} \exp\left(-u^2\tau\right)\left[\exp(u^2\tau_1)-1\right]\sum_{n=o}^{N}\exp\left(u^2 n\tau_2\right)du \quad .$$

But since the series is a geometric progression:

$$\sum_{n=o}^{N}\exp(u^2 n\tau_2) = \sum_{n=o}^{N}\left[\exp(u^2\tau_2)\right]^n = \frac{1-\exp\left[u^2(N+1)\tau_2\right]}{1-\exp(u^2\tau_2)} \quad . \tag{A.8}$$

So we have

$$T = \beta\int_o^\infty \frac{1}{u^3\Delta(u)}\exp\left(-u^2\tau\right)\left[\exp(u^2\tau_1)-1\right]\left[\frac{1-\exp\left[u^2(N+1)\tau_2\right]}{1-\exp(u^2\tau_2)}\right]du \quad . \tag{A.9}$$

This represents the solution after N+1 pulses, but the on time temperatur during the N+2th cycle is desired, so $T_c(t-(N+1)t_2)$ is added to T. First, however, the solution is rewritten in terms of the variable $\theta = \tau-(N+1)\tau_2$. Substituting for τ, adding $T_c(t-(N+1)t_2)$ and rearranging gives:

$$T = \beta\int_o^\infty \frac{1}{u^3\Delta(u)}\left\{e^{-u^2\theta}\frac{\left[e^{-u^2\left[(N+2)\tau_2-\tau_1\right]}-e^{-u^2(\tau_2-\tau_1)}-e^{-u^2(N+2)\tau_2}+e^{-u^2\tau_2}\right]}{\exp(-u^2\tau_2)-1}\right.$$

$$\left. + \left(1-e^{-\theta u^2}\right)\right\}du \quad . \tag{A.10}$$

As a check, it can be shown that as $\tau_1 \to \tau_2$, $T(t) \to T_c(t)$ as it should.

Finally, to get the on time average temperature, take

$$\overline{T} = \frac{1}{t_1}\int_o^{t_1} T(\theta)\, d\theta \tag{A.11}$$

Eqs. (A.10) and (A.11) were successfully integrated on a CDC 7600 computer using subroutine DOIAMF from the Numerical Algorithms Group (NAG) Library. The results are presented in Figures 4.11. 4.12, and 4.13. The integration routine was checked by comparing the integration of Eq. (A.2) to the short and long time approximations as given in reference 1.

Note: A remaining approximation in the model should be noted. The fluid film resistance is neglected in comparison to the pipe wall resistance during pulsed operation, which is valid while the system is on. However, when the system is off and the flow stops, the fluid resistance may well be significant. Once a suitable approximation to this resistance is found, it can be incorporated into the program.

Appendix A - References

1. H.S. Carslaw and J.C. Jaeger, Conduction of Heat in Solids, 2nd ed., Oxford at the Clarendon Press, 1959.
2. S.S. Kutateladze, Fundamentals of Heat Transfer, Academic Press, NY, 1963.

APPENDIX B

MATHEMATICAL DEVELOPMENT OF R-C HEAT-FLOW MODEL

The governing differential equation for the R-C model shown in Figure 4.10 is:

$$Q = -C\dot{\theta} - 1/R\theta \tag{B.1}$$

or

$$Q + C\dot{\theta} + 1/R\theta = 0. \tag{B.2}$$

We write the solution for this differential equation in the regions $0 < t < t_1$ and $0 < t < t_2$ and assume continuity at the boundaries. The solutions for θ

$$\theta = K_1 e^{-t/\tau} + K_2 \tag{B.3}$$

$$\dot{\theta} = K_1/\tau \; e^{-t/\tau} \tag{B.4}$$

are substituted into (B.2), yielding $\tau = RC$ and $K_2 = -QR$. Then the continuity conditions

$$\begin{aligned} Q &= \dot{Q}_o \text{ and } \theta = \theta \quad \text{at } t = 0^+ \\ Q &= \dot{Q}_o \text{ and } \theta = \theta_i \text{ at } t = t_1^- \\ Q &= 0 \quad \text{and } \theta = \theta_1 \text{ at } t = t_1^+ \\ Q &= 0 \quad \text{and } \theta = \theta_o \text{ at } t = t_2^- \end{aligned} \tag{B.5}$$

are applied. This results in the equations:

$$\begin{aligned} \theta_o &= K_1 - \dot{Q}_o R \\ \theta_1 &= K_1 e^{-t_1/RC} - \dot{Q}_o R \\ \theta_1 &= K_1' e^{-t_1/RC} \\ \theta_o &= K_1' e^{-t_2/RC}. \end{aligned} \tag{B.6}$$

The solutions for K_1 and K_1' are

$$K_1 = \frac{\dot{Q}_o R(1-e^{-(t_2-t_1)/RC})}{1-e^{-t_2/RC}} \tag{B.7}$$

$$K_1' = \frac{\dot{Q}_o R(e^{-t_1/RC}-1)}{1-e^{-t_2/RC}} \tag{B.8}$$

Then, during heat extraction ($0 < t < t_1$),

$$\theta = -\dot{Q}_o R + \frac{\dot{Q}_o R(1-e^{-(t_2-t_1)/RC})e^{-t/RC})}{1-e^{-t_2/RC}} \tag{B.9}$$

During the off cycle ($t_1 < t < t_2$)

$$\theta = \frac{-\dot{Q}_o R(e^{(t_1/RC-1)}e^{-t/RC})}{1-e^{-t_2/RC}} \tag{B.10}$$

The time-average source temperature during heat extraction can be calculated:

$$\theta_I = 1/t_1 \int_0^{t_1} \theta dt$$

$$= -\dot{Q}_o R + \frac{\dot{Q}_o R^2 C(1-e^{-(t_2-t_1)/RC})(1-e^{-t_1/RC})}{t_1(1-e^{-t_2/RC})} \tag{B.11}$$

This is Eq. 4.14 in the text.

END
6/17/87